INVESTIGATING BISULFIDE SORPTION ONTO BENTONITE THROUGH LABORATORY EXPERIMENTS AND NUMERICAL MODELLING

SIFAT AZAD PAPRY

A DISSERTATION SUBMITTED TO
THE FACULTY OF GRADUATE STUDIES
IN PARTIAL FULFILLMENT OF THE REQUIREMENTS
FOR THE DEGREE OF DOCTOR OF PHILOSOPHY

GRADUATE PROGRAM IN CIVIL ENGINEERING
YORK UNIVERSITY
TORONTO, ONTARIO

June 2024

Investigating Bisulfide Sorption onto Bentonite through Laboratory Experiments and Numerical Modelling

Sifat Azad Papry

Doctor of Philosophy

Department of Civil Engineering
York University

June 2024

Abstract

The long-term performance evaluation of the Canadian deep geologic repository (DGR) relies significantly on bentonite clay, a crucial material in the engineered barrier system. One safety concern is microbiologically influenced corrosion of the used fuel containers (UFCs) which may occur if bisulfide (HS^-) transports through the bentonite buffer to the UFC surface. HS^- sorption onto bentonite can reduce the corrosion risk, but its dynamics are not yet well-understood, especially in DGR environments. Hence, this study offers a comprehensive insight into HS^- sorption process onto bentonite through extensive laboratory experiments and numerical modelling.

First, a robust methodology was developed to build confidence in the experimental procedure. Subsequently, six sets of batch experiments (including desorption tests) were performed as a function of temperature (10-40°C), contact time (1-120 hours), liquid to solid mass ratios (L:S) (100-1000), initial HS^- concentration (1-6 mg L^{-1}), pH (9-11), and ionic strength (0.01 M-1 M NaCl). The experimental results indicated that HS^- sorption onto bentonite occurred faster, and the equilibrium sorption capacity increased (by 3%) with increasing temperature. However, sorption decreased with increasing pH and ionic strength. Several established kinetic and

isotherm models were applied to the experimental data to provide insight into HS^- sorption dynamics onto bentonite.

In addition, desorption test results indicated that HS^- was irreversibly sorbed on bentonite. Surface analyses conducted using scanning electron microscopy along with energy dispersive spectroscopy, suggested that sorption might have occurred due to chemical reactions of HS^- with the iron (Fe) present in bentonite.

Lastly, a thermodynamic-based sorption model was developed in PHREEQC assuming that sorption was driven by three key processes: (i) redox reaction with the structural Fe^{3+} sites, (ii) surface precipitation as iron sulfide, FeS (likely mackinawite), and (iii) surface complexation reactions with surface hydroxyl group (OH) at the edge sites of montmorillonite. The model successfully described the experimental trends and provided valuable insights into the relative contribution of each process to the total sorption mechanism.

Altogether, this study provides novel insights from experimental and numerical modelling that enhance the understanding of HS^- sorption onto bentonite, which supports the Canadian DGR design and other nuclear repositories worldwide.

Acknowledgments

Pursuing a PhD has been one of the most fulfilling experiences of my life, and I am deeply thankful to Almighty Allah for granting me the opportunity to undertake this incredible journey. I cherished every moment of it.

During this time, I had the honor of encountering several exceptional people who offered their friendship, motivation, guidance, and support. Above all, my heartfelt thanks go to my supervisor, Professor Magdalena Krol, whose steadfast support and expertise were pivotal throughout my doctoral studies. Her valuable feedback and motivation have pushed me to exceed my own limits. I am truly appreciative of her mentorship and trust. I am also immensely grateful to my doctoral committee members, Professor Pulin Mondal, and Dr. Peter Keech. Their rigorous assessments and insightful suggestions significantly enhanced my dissertation.

My colleagues and fellow researchers at the York University, especially Dr. Tarek Rashwan, Farhana, Aditi, Reza, and Asad, provided a network of encouragement and enlightening interactions that significantly contributed to my personal and professional growth. Their steadfast friendship and confidence in my capabilities were a continuous source of inspiration and drive. My thanks also go to Dr. Magdalena Jaklewicz (York University) and Surface Science Western for their support in the surface analyses of the bentonite samples.

Further gratitude is due to Dr. Mehran Behazin and Dr. Peter Keech, who were instrumental in providing me industrial insight and develop experimental and numerical models. Additionally, I extend my appreciation to all the staff in the Department of Civil Engineering, including Sindy Mahal and Kunjan Rupakheti. The nurturing academic environment they fostered played a crucial role in my scholarly pursuits and greatly enriched my educational experience.

Lastly, to my spouse Dr. Sk Md Mashrur, beloved Muhtad baba, my parents, and in-laws, this achievement is for you. Words cannot adequately express my gratitude for your enduring love, support, and patience.

Table of Contents

List of Publications

The following chapters in this dissertation have been reproduced with modifications from previously published and presented materials:

Chapter 3: METHODOLOGY DEVELOPMENT AND PRELIMINARY EXPERIMENTS

* **Papry, S. A.**, Rashwan, T. L., Mondal, P., Behazin, M., Keech, P. G., & Krol, M. (2023). Investigating bisulfide sorption onto bentonite: methodology development and design of batch experiments, *Proceedings of CSCE 2023 Annual Conference*.

Papry, S. A., Rashwan, T. L., Mondal, P., Behazin, M., Keech, P. G., & Krol, M. (2022). Methodology development for Investigating bisulfide sorption onto bentonite through laboratory batch experiments. Presented at *Halifax 2022 – GAC-MAC-IAH-CNC-CSPG Joint Meeting, Canada*.

Chapter 4: FUNDAMENTALS OF BISULFIDE SORPTION DYNAMICS ONTO BENTONITE

*** Papry, S. A**., Rashwan, T. L., Mondal, P., Behazin, M., Keech, P. G., & Krol, M. (2023). Investigating bisulfide sorption onto bentonite through laboratory batch experiments, *Applied Geochemistry*, Volume 152, May 2023, 105626, DOI: https://doi.org/10.1016/j.apgeochem.2023.105626

Papry, S. A., Rashwan, T. L., Mondal, P., Behazin, M., Keech, P. G., & Krol, M. (2021). Investigating the effect of contact time and liquid-to-solid ratio on bisulfide sorption onto bentonite through laboratory batch experiments. Presented at *GeoNiagara 2021 Conference, Canada.*

Chapter 5: BISULFIDE SORPTION MECHANISMS ONTO BENTONITE: EFFECTS OF TEMPERATURE, pH, IONIC STRENGTH

Papry, S. A., Rashwan, T. L., Mondal, P., Behazin, M., Keech, P. G., & Krol, M. (2023). Exploring bisulfide sorption onto bentonite under deep geological repository (DGR) conditions, *5th Canadian Conference on Nuclear Waste Management, Decommissioning and Environmental Restoration, Canada*

Papry, S. A., Rashwan, T. L., Mondal, P., Behazin, M., Keech, P. G., & Krol, M. (2022). Investigating the effects of temperature, pH and ionic strength on bisulfide sorption onto bentonite. Presented at the *AGU Fall Meeting, Chicago, USA*

Chapter 6**: DEVELOPMENT OF THERMODYNAMIC SORPTION MODEL USING PHREEQC**

***Papry, S. A.,** Rahimi. R, Rashwan, T. L., Mondal, P., Behazin, M., Keech, P. G., & Krol, M. (2024). Exploring sorption mechanisms of bisulfide onto bentonite through laboratory experiments and numerical modelling *(submitted to Applied Clay Science Journal)*

Papers denoted by * are those that are directly used to reproduce chapters of this thesis.

All the research works presented in aforementioned papers are conducted by the first author under the direct supervision and guidance of Professor Magdalena Krol. The involvement of other co-authors to review the conducted research is greatly acknowledged.

List of Tables

List of Figures

Glossary

ANOVA	Analysis of Variance
Ca	Calcium
C_e	Aqueous phase concentration at equilibrium
C_i	Initial concentration
C_t	Aqueous phase concentration at time t
Cu	Copper
Cu_2S	Copper sulfide
DDL	Diffuse Double layer
DGR	Deep geologic repository
EBS	Engineered barrier system
EDZ	Excavation damaged zones
Fe	Iron
Fe^{2+}	Ferrous Iron
Fe^{3+}	Ferric Iron
Fe_3S_4	Gregite
FeS	Iron mono-sulfide (e.g mackinawite)
FeS_2	Pyrite
FESEM/EDS	Field emission scanning electron microscopy/energy dispersive spectroscopy
GCL	Geosynthetic clay liner
GFM	Gap-fill material
H_2S	Hydrogen sulfide gas
HCB	Highly compacted bentonite
HS^-	Bisulfide
IPD	Intraparticle diffusion model
L:S	Liquid to solid ratio
MDL	Method detection limit
MIC	Microbiologically-influenced corrosion
Na	Sodium
NWMO	Nuclear waste management organization

PFO	Pseudo–first-order
PHREEQC	PH REdox EQuilibrium in the language C
PSO	Pseudo–second-order
PTFE	polytetrafluoroethylene
q_e	Sorption capacity, i.e., mass of HS^- sorbed per unit mass of bentonite at equilibrium
q_t	Sorption capacity, i.e., mass of HS^- sorbed per unit mass of bentonite at any time t
RMSE	Root mean square error
S(0)	Elemental sulfur
SCM	Surface complexation model
SOH	Montmorillonite edge site
SRB	Sulfate reducing bacteria
TDB	Thermo-dynamic database
TDS	Total dissolved solids
T-O-T	Tetrahedral-octahedral-tetrahedral
TSM	Thermodynamic sorption model
UFC	Used fuel container

CHAPTER 1
INTRODUCTION

1 Chapter Overview

This chapter presents an outline of the research carried out in this thesis. First, the motivation for the study is presented in Section 1.1., followed by Section 1.2 highlighting the research objective. Finally, Section 1.3 outlines the dissertation structure.

1.1 Motivation

Due to the widespread use of nuclear power, used nuclear fuel management is a major challenge worldwide. The most preferred and internationally recognized approach for long-term storage of used nuclear fuel is isolation in deep geological repositories (DGRs) (J. Chen et al., 2018; Hall et al., 2021). Like many nuclear nations, Canada has been developing a national DGR strategy since the early 1970s (Baumgartner et al., 1996; Standish et al., 2016). The latest DGR concept proposed by the Nuclear Waste Management Organization (NWMO) is to encapsulate the used nuclear fuel in a steel container with an outer shell of copper and emplace these used fuel containers (UFCs) in either crystalline or sedimentary host rock at least 500 m below ground surface (Hall et al., 2021). In the host rock, the UFCs will be surrounded by highly compacted bentonite (HCB), which can suppress the migration of corrosive agents and prevent microbiological activity (J. Chen et al., 2018, 2019; Hall et al., 2021). Various additional bentonite components – such as spacer blocks, floor-leveling tiles, and gap-fill materials – are planned to seal gaps and ensure safe containment (Hall et al., 2021).

The use of bentonite – a swelling clay – in DGRs is widely favoured because of its low hydraulic conductivity, high sorption potential, self-sealing ability, and good durability (Kaufhold & Dohrmann, 2016; Sellin & Leupin, 2014). Bentonite material properties, thus, play a significant role in the long-term performance of the DGR. Moreover, to ensure that the bentonite buffer performs its safety functions properly over the repository lifetime, it is important to understand

the effects of the long-term geochemical evolution (e.g., temperature, pH, ionic strength, redox state) of the repository on the buffer properties.

Several countries have chosen copper (Cu) as the exterior of UFCs as it is thermodynamically immune to most corrosion processes that may occur within the anoxic conditions expected in the DGR (J. Chen et al., 2014; Martino et al., 2014). During the initial phase of the DGR life (i.e., within a few months or years), a limited quantity of trapped oxygen will be present due to repository excavation and emplacement. As such, the UFCs may undergo oxic corrosion over this initial period (King et al., 2017; Standish et al., 2016). Once all trapped O_2 is consumed by corrosion or other reduction processes, the repository environment is expected to remain anoxic for the remainder of its life (i.e., many millions of years) (King et al., 2017).

During this anoxic period, microbiologically-influenced corrosion (MIC) of Cu may occur due to bisulfide (HS^-) in the DGR, produced primarily by sulfate-reducing bacteria (SRB). HS^- may be generated in a DGR via 'far-field' production by SRB within the host rock or at the host rock/bentonite interface, particularly within the excavation-damaged zone or other cracks/fissures (Hall et al., 2021). The low water activity and high swelling pressure of bentonite with dry densities ≥ 1.6 g cm^{-3} have been proven to suppress microbial activity within the buffer material, including HS^- production from SRBs (Stroes-Gascoyne et al., 2010; Stroes-gascoyne et al., 2011). Anoxic UFC corrosion in the DGR is, therefore, expected to be governed by HS^- diffusion (no advection is expected given the low bentonite permeability and the low hydraulic gradient in the surrounding host rock) through the bentonite towards the UFC surface and subsequent formation of very porous copper sulfide (Cu_2S) films following Eq. (1.1) (Briggs et al., 2017; Hall et al., 2021):

$$2Cu_{(s)} + HS^-_{(aq)} + H^+_{(aq)} \rightarrow Cu_2S_{(s)} + H_{2(g)} \quad (1.1)$$

However, several studies suggest that bentonite has a retardation effect on HS^- transport (Bengtsson & Pedersen, 2016, 2017; Pedersen et al., 2017). Generally, any process that partitions the aqueous phase mass onto a solid phase surface (e.g., via adsorption, absorption, precipitation, or other chemical transformations) is described as *sorption* (Kaplan, 1999; Limousin, 2007; Vinšová et al., 2008). Therefore, HS^- sorption onto bentonite is expected to limit HS^- flux

towards the UFCs and minimize the risk of copper corrosion. A schematic illustration of HS^- sorption onto bentonite anticipated in the DGR is presented in Figure 1.1.

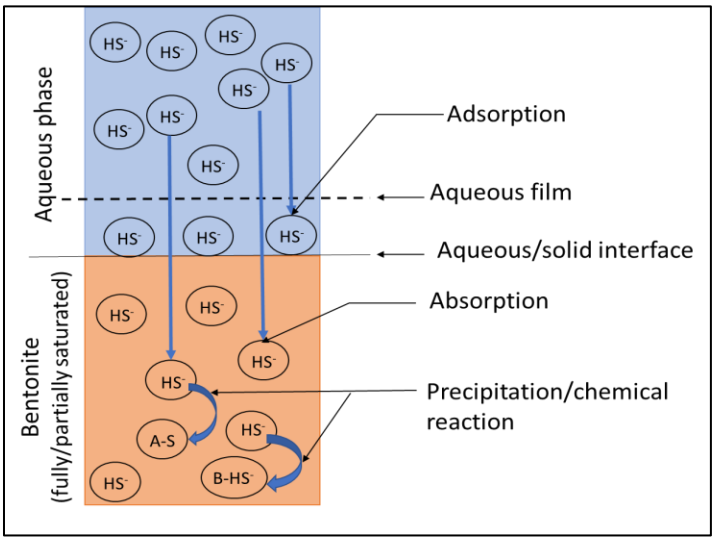

Figure 1.1 Schematic of HS^- sorption onto bentonite (A and B indicate different generic molecules)

Given this background, HS^- sorption onto bentonite could be an important aspect contributing additional DGR safety, but it is not well understood yet. As such, an in-depth investigation into bentonite's ability to sorb corrosive HS^- and retard its transport towards the UFC surface in the hydrogeochemical context of the DGR, is an important undertaking to ensure long-term safety of the repository.

1.2 Research Objective

Sorption capacity is an important characteristic for evaluating the contaminant retention in bentonite. Hence, a large number of studies have been conducted on the sorption mechanism of radionuclides (Hu et al., 2009; Kadoshnikov et al., n.d.; Khalili et al., 2013; Oscarson et al., 1994; Randall, 2012; Tran et al., 2018; Wu et al., 2009; Xu et al., 2008; S. Yang et al., 2009; Zhao et al., 2008), heavy metals (Liu & Zhou, 2010; M. K. Uddin, 2017; Verma et al., 2014; Xu et al., 2008) and several other organic and inorganic ions on bentonite. Although numerous bentonite sorption studies are available in the literature, only a few have investigated the processes controlling HS^- sorption dynamics onto bentonite (Hadi et al., 2023; Papry et al., 2023; Svensson & Wikberg, 2017). In general, there is a lack of systematic studies investigating the nature of HS^- sorption onto bentonite (i.e., whether it is a reversible or irreversible process or a

combination of both). In addition, the effect of various DGR conditions (e.g., temperature, pH, redox conditions, HS^- concentration) on the capacity of bentonite to sorb HS^- has not been thoroughly investigated. This knowledge gap hinders the development of a reactive transport model of HS^- in a DGR and predicting the transport of corrosive agents.

To address this knowledge gap, the overall objective of this research is to provide a micro-level insight into the sorption phenomenon of HS^- onto bentonite under various geochemical conditions. The specific objectives of this study include:

I. To develop a robust methodology for exploring HS^- sorption onto bentonite through laboratory experiments.
II. To investigate the fundamentals of HS^- sorption dynamics/mechanisms (including kinetics, isotherm, thermodynamics) through laboratory experiments and surface analysis.
III. To investigate the effects of critical geochemical factors (pH, ionic strength, and temperature) on HS^- sorption onto bentonite through laboratory experiments and statistical analysis.
IV. To develop a thermodynamic sorption model using the geochemical program PHREEQC to predict and interpret HS^- sorption mechanisms under the effect of changing system chemistry.

Having outlined the thesis objectives, a review of pertinent literature was first conducted to obtain insight into the general sorption phenomenon in bentonite and identify the key factors that influence its sorption capacity (Chapter 2). Later, a robust methodology was developed to build confidence in the experimental procedure, including selecting appropriate contact time, liquid to solid ratio (L:S), and initial HS^- concentration to conduct the laboratory batch experiments (Chapter 3). Based on the review of the literature and the preliminary experiments performed, six sets of batch experiments (including desorption tests) were designed and performed to investigate the fundamentals of HS^- sorption behaviour (e.g., kinetics, isotherm, thermodynamics) as well as to observe the effects of critical factors relevant to the DGR (e.g., temperature, pH, ionic strength) (Chapter 4 and Chapter 5). In addition, surface analyses (e.g., field emission scanning electron microscopy and energy dispersive spectroscopy (FESEM/EDS) analyses) were performed to obtain further insight into the HS^- interactions with bentonite (Chapter 5). Finally, a thermodynamic sorption model was developed (i.e., calibrated and

validated by experiment results) to understand the processes controlling HS^- sorption onto bentonite, including the contribution of each process to the total sorption (Chapter 6) Altogether, the study provides critical information on the underlying sorption phenomenon of HS^- onto bentonite, which can be useful for researchers and practitioners to understand how to maximize sorption to retard or decrease transport of corrosive compounds to the UFC and to accurately model the reactive transport of HS^- in the DGR environment. The outcomes of the study will ultimately contribute to the broader initiative for ensuring the long-term safety of the DGR system.

1.3 Dissertation Structure

Figure 1.2 illustrates the layout of the thesis.

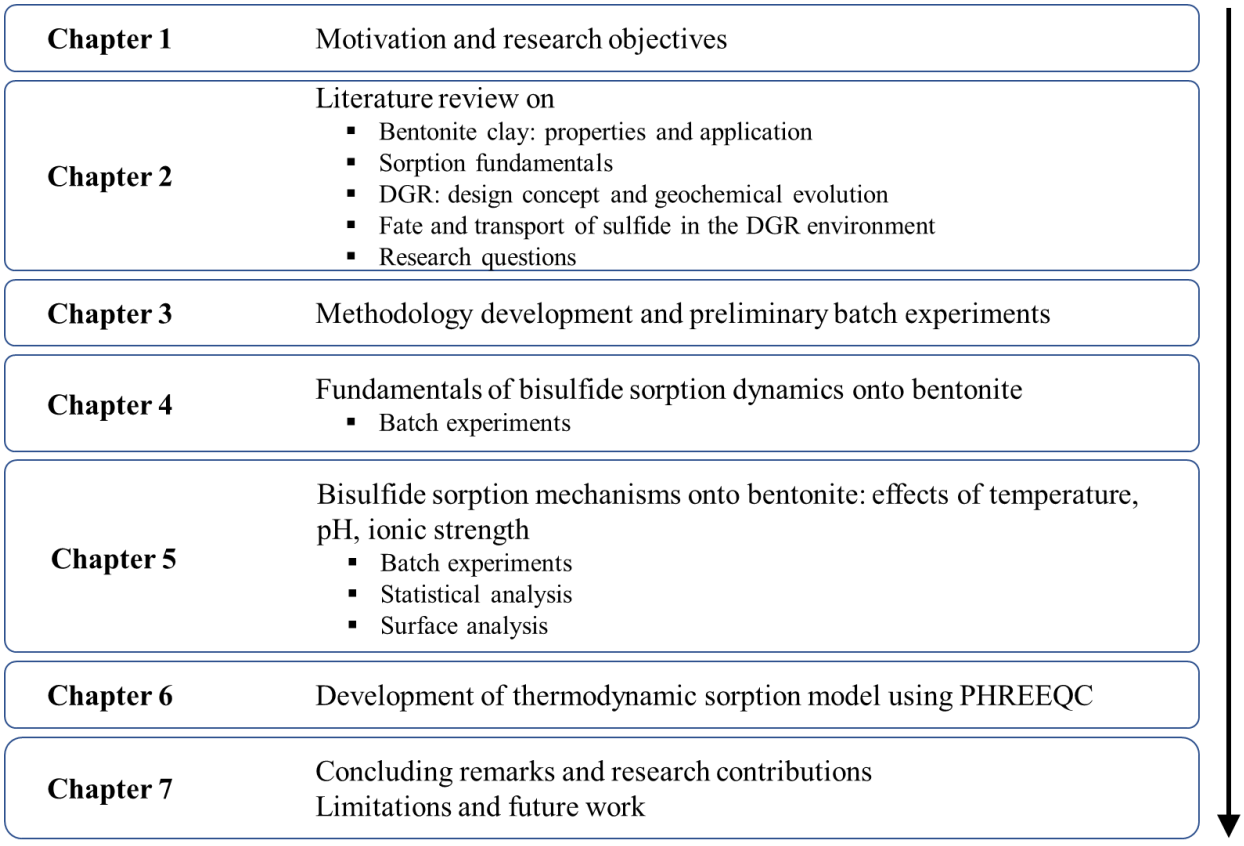

Figure 1.2 Dissertation layout.

Chapter 1 discusses the motivation and the objectives of the research. The chapter also briefly summarizes the research approaches followed, as well as presents a layout of the dissertation.

Chapter 2 includes a literature review of the critical components of the research topic. Firstly, the sorption fundamentals (e.g., definition, mechanisms, influencing factors, theory of the isotherm, and kinetic models) are discussed. Secondly, some important features of bentonite clay (e.g., mineralogy, environmental application) are highlighted. Thirdly, DGR geochemistry and the possible impacts on the transport of solutes are discussed, followed by a critical review of recent studies on bentonite-sulfide interaction.

Chapter 3 discusses the detailed methodology development work for exploring HS^- sorption onto bentonite through laboratory batch experiments. This includes the outcome of the preliminary experiments performed to select the appropriate range of critical conditions (e.g., L:S, contact time, initial HS^- concentration). Moreover, the quality control approaches implemented to increase confidence in the experimental procedure are discussed.

Chapter 4 discusses the outcomes of a series of batch experiments conducted to understand the sensitivity of various experimental conditions (i.e., contact time, temperature, L:S ratio, initial HS^- concentration) on HS^- sorption onto bentonite. The chapter also reveals the fundamental aspects of the sorption dynamics, including the kinetic rate-limiting processes, by applying various established kinetic, isotherm, and thermodynamic models to the experimental data.

Chapter 5 discusses the batch experiments performed to explore the effects of three critical geochemical parameters such as temperature, pH, and ionic strength, on HS^- sorption phenomenon onto bentonite. The trends observed in the experiments were further analyzed by 3 factor ANOVA (analysis of variance) tests. Furthermore, the desorption tests and surface analysis results documented in this chapter provide deeper insight into the key process(s) driving HS^- sorption onto bentonite. The findings helped to develop the hypothesis of the sorption model built in the following chapter.

Chapter 6 describes the thermodynamic sorption model development procedures, including calibration and validation of the unknown parameters. The model outcomes shed light on the fundamental processes governing HS^- sorption onto bentonite and how much each process may contribute to the overall sorption under the geochemical conditions investigated in the study.

Chapter 7 concludes the key research findings, highlights research limitations, and provides recommendations for future research directions.

CHAPTER 2
LITERATURE REVIEW

2 Chapter Overview

This chapter reviews relevant literature on important aspects of the research. First, it starts with highlighting the important features of bentonite clay (e.g., mineralogy, environmental application) (Section 2.1), followed by Section 2.2 discussing DGR geochemistry and the possible impacts on the transport of solutes. Later, a generic discussion of the sorption fundamentals (e.g., definition, mechanisms, influencing factors, isotherm, and kinetic models) is presented in Section 2.3, followed by a review of recent studies on the production and transport of sulfide in the repository environment in Section 2.4. Section 2.5 presents the state of the art of the study, highlighting the research gap in existing literature. Finally, Section 2.6 summarizes the chapter.

2.1 Bentonite Clay: Properties and Applications

As mentioned in the previous chapter, bentonite clay is the key component of the DGR engineered barrier. Hence, this section discusses some important features, including the properties, types, and applications of bentonite clay.

2.1.1 Bentonite Structure

Bentonite is a naturally swelling clay that occurs due to weathering through chemical transformation from acid volcanic glass tufa after it's been deposited in marine or freshwater environments. Clay mineralogists typically consider bentonite as an impure ore clay consisting of predominantly montmorillonite and small amounts of other minerals, such as quartz, feldspars, pyrite, organic carbon and other clay minerals. Bentonite is part of the smectite family of clays consisting primarily of montmorillonite which is a swelling clay. Montmorillonite has a 2:1 layer crystalline structure consisting of an octahedral aluminium-oxygen (Al_2 $(OH)_6$) sheet or magnesium-oxygen sheet ($Mg_3(OH)_6$) sandwiched between two opposing tetrahedral silica sheets. One tetrahedral silica sheet is connected to adjacent tetrahedra by sharing three corners

(i.e., forming a hexagonal network), and the remaining fourth corner to the adjacent octahedral sheet. The octahedral sheet is usually composed of aluminum (Al) and some magnesium (Mg) and/or iron (Fe(III)) in sixfold coordination with oxygen (i.e., from the tetrahedral sheet), and hydroxyl (OH) (Al-Ani & Sarapää, 2008; Mukherjee & Ghosh, 2013; F. Uddin, 2018).

Like any other clays of the smectite group, surfaces of montmorillonite carry a permanent negative charge, which mainly results from isomorphous substitution of lower-valency atoms for higher-valency atoms within the clay lattice. For example, the replacement of Al^{3+} by Fe^{2+} and Mg^{2+} can leave a net negative charge for the layer. Similarly, Si^{4+} can be replaced by Al^{3+} in the tetrahedral layer, which may also leave a charge imbalance. Further, the oxygen atoms on the surface of each clay crystals, and on their edges keep a net negative charge. The resulting charge imbalance at the clay surface, is satisfied by adsorbing exchangeable cations from pore waters and forming electric double layers at the water-solid interface (Yu & Neretnieks, 1997). Interlayers of the smectite are heterotopically occupied by Na^{+} and Ca^{2+} according to the formula (Xu et al., 2008):

$$Na_{0.18}Ca_{0.11}[Al_{1.52}Mg_{0.26}Fe(III)_{0.17}][Si_{3.96}Al_{0.04}]O_{10}(OH)_2$$

Each layer of the clay comprises a number of the above-mentioned molecular structures bonded to one another through the Van der Waals force, which is very weak and, thereby, permits water and exchangeable ions to enter through the pores within the clay lattice, leading to the development of swelling capacity (Ikpe & Okovido, 2018; M. K. Uddin, 2017; Yu & Neretnieks, 1997). Figure 2.1 represents a schematic illustration of montmorillonite crystalline structure indicating the tetrahedral-octahedral-tetrahedral (TOT) layers, the presence of silicon, aluminum, magnesium, and oxygen as well as the location of the exchangeable cations and absorbed water molecules.

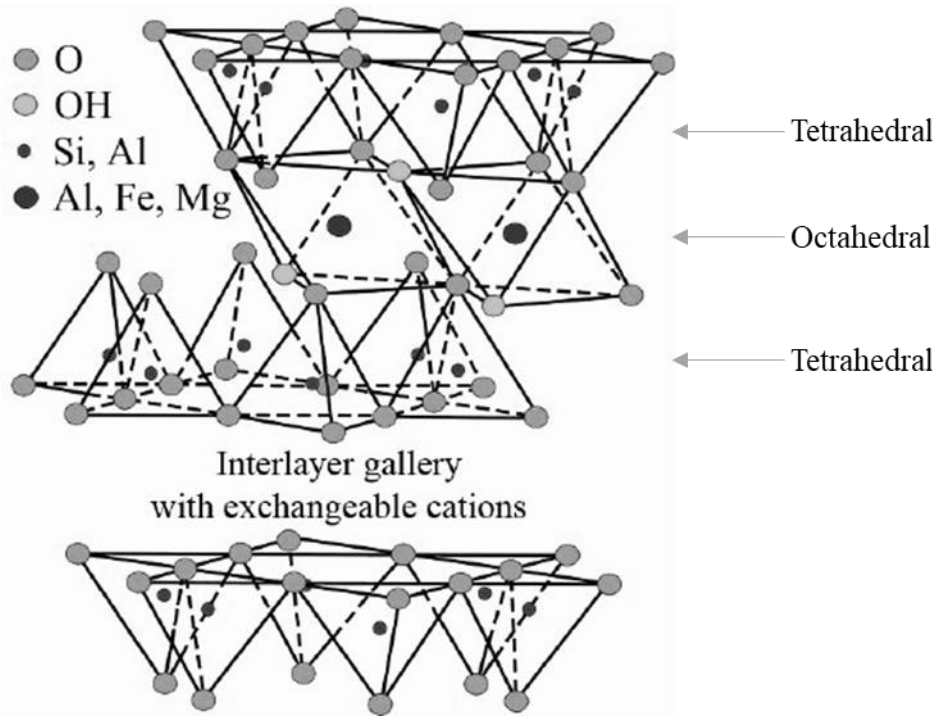

Figure 2.1 Schematic illustration of montmorillonite crystalline structure (adopted and modified from Steinmetz 2014)

Various conceptual models (e.g. multi-porosity model, Donnan equilibrium model) are found in the literature to interpret the pore structure and the properties of pore water in compacted bentonite (Idiart & Pękala, 2020). As per these models, the pore space of the compacted bentonite may contain 2 to 3 types of water (Idiart & Pękala, 2020):

(i) Interlayer water, which contains only water and cations balancing the charge of the tetrahedral-octahedral-tetrahedral (TOT) layers of montmorillonite.

(ii) Diffuse double layer (DDL) / Electrostatic double layer (EDL): the layer between the mineral surface and free water, which contains water, excess cations and a small number of anions.

(iii) Bulk/free pore water: charge balanced solution of cations and anions. The term "bentonite porewater" is usually indicated by the ''free water''.

A schematic representation of the pore water structure in compacted bentonite is presented in Figure 2.2. The amount of each type of water depends on several factors, such as the degree of compaction or the density of the bentonite, ionic strength of the pore water, the amount of accessory minerals, etc. (D. A. Dixon, 2019).

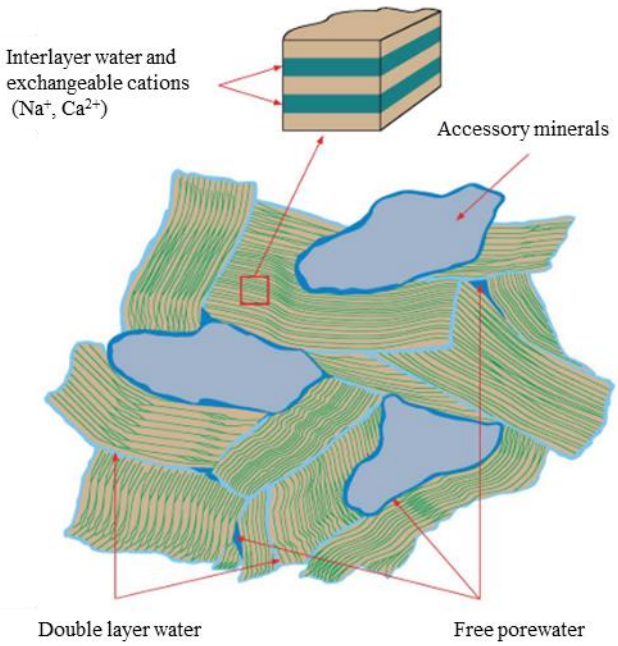

Figure 2.2 Schematic representation of the pore water structure in compacted bentonite (adapted from (Bradbury & Baeyens, 2003))

2.1.2 Bentonite Types and Physical Properties

Bentonite is typically identified based on the predominant cation in the interlayer position of montmorillonite (between the T-O-T layers), which can be easily replaced with other cations through ion exchange. The two most common types of bentonites are Na-bentonite and Ca-bentonite, with Na and Ca being the dominant interlayer cations, respectively.

The physical characteristics of bentonite are influenced by its type, whether Na or Ca. For example, Na-bentonite has higher zeta potential (-4.24 mV to -4.67 mV) than Ca-bentonite (-3.54 mV to -3.72 mV). This is because Na cations are loosely bound to the bentonite layers, primarily due to their higher mobility. In contact with water, Na ions easily get detached from the surface of the particle, leading to an increased zeta potential value due to higher potential difference between the negative particle surface and the liquid phase (Güngör & Dilmac, 1996). As a result, Na-bentonite has higher adsorption capacity for oppositely charged ions than Ca-bentonite. Moreover, the cation exchange capacity of Na-bentonite is higher (70 to 92 meq/100 g) than Ca-bentonite (27 to 46 meq/100 g) (Karakaya et al., 2011).

The degree of swelling, initiated by adsorbing water in the interlayer upon water addition, also depends on the type of major cations in the interlayer region (Dixon, 2019; Gleason et al., 1997; Karnland, 2010). The difference in the swelling behavior results from the hydration state of Na^+ and Ca^{2+} ions on the bentonite surface (Chen & Huang, 2013). Upon hydration, Na^+ ions form two solvation spheres in water and therefore, more water molecules can be contained in the interlayer position. As a result, Na-bentonite demonstrates higher swelling potential than Ca-bentonite. In contrast, Ca^{2+} ions forms hydrogen bonds to the exposed oxygen atoms in the bentonite. The hydrated Ca^{2+} ions, thus occupy the exchangeable sites on bentonite surface replacing the water molecules, leading to a lower hydration energy and thus lower swelling potential than Na-bentonite (Chen & Huang, 2013).

2.1.3 Environmental Application of Bentonite

A significant number of experimental and theoretical studies conducted over the past few decades have proved bentonite to be an efficient adsorbent for different types of heavy metals, organic and inorganic contaminants in soil, water, wastewater, sludge and synthesized contaminated solutions (Alshameri et al., 2019; Khalili et al., 2015; Otunola & Ololade, 2020; Sun et al., 2015; Uddin, 2017; Usman et al., 2010; Vhahangwele & Mugera, 2015). In recent years, the unique adsorption capacity of bentonite together with its low permeability, environmental compatibility, and ready availability, has increased its application as an affordable alternative to traditional remediation procedures such as excavation and dumping, soil washing/flushing, etc. which are often expensive and cause environmental disruptions (Yu et al., 2017; Xu et al., 2008). Apart from these applications, some other common uses of bentonite include landfill liners and covers (e.g. geosynthetic clay liner (GCL)), soil-bentonite slurry walls in excavated trenches, cement-bentonite grout-filled borings or holes etc. (Jankaite and Vasarevičius, 2010).

Na-bentonite, because of its higher degree swelling capacity associated with reduction in pore holes and thus, low hydraulic conductivity, is used more extensively than Ca-bentonite for various applications. One major application of Na-bentonite includes landfill liners such as: geosynthetic clay liner (GCL) to minimize the migration of toxic components out of landfills. The GCL usually consists of a thin (approximately 7–10 mm) layer of powdered or granular Na-

bentonite sandwiched between two layers of geotextiles or a bentonite layer glued to a geomembrane (Chai & Prongmanee, 2020).

Apart from liners and covers, bentonite is also used for cut-off walls around landfill sites to control the migration of contaminants. Soil–bentonite vertical cutoff wall installed with slurry trenching technology has attracted greater attention because of its limited hydraulic conductivity (typically ranges from 10^{-9} to 10^{-11} m/s) and cost-effectiveness. Soil–bentonite slurry walls usually comprise Na-bentonite and sandy soil. Some studies suggested using clayey soil mixed with Ca-bentonite as an alternative material, particularly in countries like China and India, where Na-bentonite is not readily available (Yang et al., 2017, 2019). However, these studies highlighted the necessity of amending Ca-bentonite before its use because it has a lower swelling capacity as compared to Na-bentonite and thus may result in the undesirably high hydraulic conductivity of the Ca-bentonite backfill.

Although Ca-bentonite has a lower swelling capacity, it is more resistant/stable and less susceptible than Na-bentonite to ion exchange when exposed to chemical constituents such as (Ca^{2+} or Mg^{2+}) in permeating fluids. In contact with fluids such as leachate from a landfill or contaminated groundwater, Na-bentonite can convert to Ca-bentonite by ion exchange, resulting in lowering of the diffused double layer and, therefore higher hydraulic conductivity (Villar, 2007). This type of cation exchange widens the distance between bentonite-layered structures, allowing more water to enter. Thus, for long-term bentonite stability in saline conditions, Ca or divalent bentonite is preferable over Na or monovalent bentonite (Koch, 2007). This phenomenon is also supported by another recent study (Jadda & Bag, 2020), which revealed that monovalent bentonite significantly modifies its morphology, microstructure and hydro-mechanical properties in contact with electrolyte, while the effect was observed to be negligible for divalent Ca-bentonite. Therefore, the authors suggested that divalent Ca-bentonite is more suitable in high electrolyte conditions whereas monovalent Na-bentonite is preferable for use in the low salinity conditions (Jadda & Bag, 2020). Despite this, Na-bentonite remains more commonly used than Ca-bentonite in various environmental applications, including geological repositories.

In addition to low permeability, Na-bentonite offers advantage of high cation-exchange capacity, enabling the immobilization of contaminants like metals through adsorption, thereby slowing

their migration into the surrounding environment. This is why compacted bentonite and sand–bentonite mixtures are attracting greater attention as buffer and backfill materials in geological repositories for the long-term management of radioactive wastes (Chen et al., 2019; Karnland et al., 2009; Lee et al., 2001; Tachi et al., 2001). The other key features of compacted bentonite that make it a suitable barrier in the DGR system include its large surface area, small pore size, and self-sealing ability (swelling capacity). The application of bentonite as an engineered barrier in the DGR is discussed at a greater length in the following section (Section 2.2.2).

2.2 DGR Design Concept and Geochemical Environment

Since radioactive wastes, including used nuclear fuel, are likely to remain hazardous for hundreds of thousands of years, the most preferred and internationally recognized option for long-term management of high-level radioactive wastes is a deep geologic repository (DGR) (Chen et al., 2018, Hall et al., 2021). Critical aspects of Canadian DGR, such as design concept, buffer properties, and geo-chemical evolution, are discussed in the following sub-sections.

2.2.1 Overview of the Canadian DGR Concept

Like other nuclear nations, the Canadian DGR design proposed by the Nuclear Waste Management Organization (NWMO) contains a multibarrier concept made up of natural and engineered barriers. According to the latest design concept of Canadian DGR, the natural barrier will comprise of the host rock (either sedimentary or crystalline) and surrounding geological formations (with site-specific hydrogeochemical characteristics) at a depth of about 500 m from the ground surface. The engineered barrier system (EBS) will include copper-coated used fuel containers (UFCs) encapsulated in a highly compacted bentonite (HCB) buffer box. The EBS will also include other highly compacted bentonite components, such as the spacer blocks floor-levelling tiles and gap-fill materials (GFM) to fill the remaining gaps between the walls and roof of the tunnel and the installed HCB/UFC components (Dixon, 2019). An illustration of the latest Canadian DGR design concept is presented in Figure 2.3.

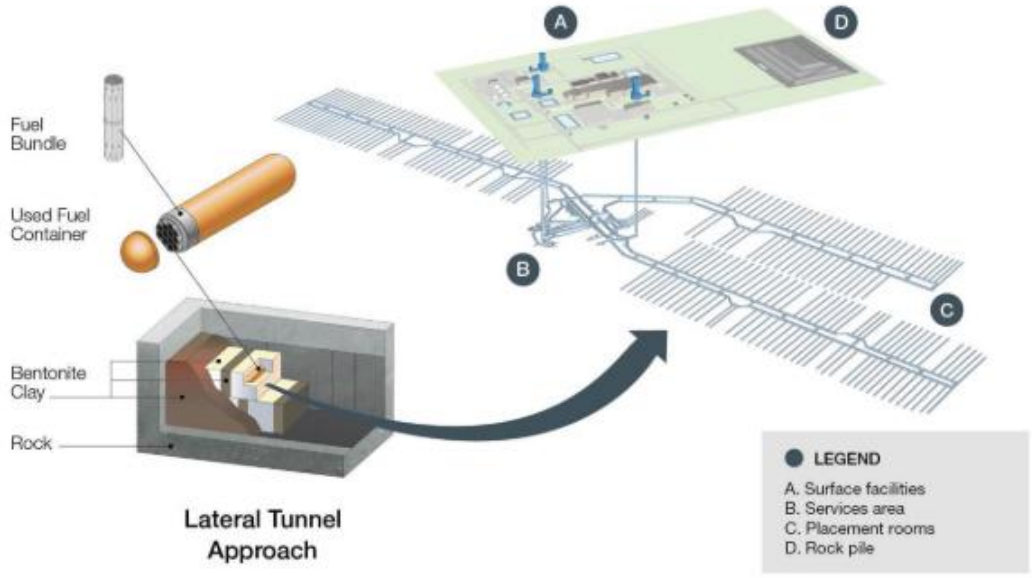

Figure 2.3 Conceptual design of Canadian DGR (adopted from (Dixon, 2019; Noronha, 2016))

2.2.2 Bentonite as an Engineered Barrier in the DGR

To contain the waste safely and comply with the prevailing safety principles, the principal requirements of a buffer material in the case of high-level used nuclear fuel disposal, regardless of the host rock, are (1) a low hydraulic permeability/conductivity; (2) a self-sealing ability; and (3) durability over the DGR life-time (Sellin & Leupin, 2014). Therefore, swelling clay, such as bentonite, has been selected as a viable barrier material in almost all national programs that are undertaking the option of disposing of high-level waste below the groundwater. Irrespective of the geosphere type (crystalline or sedimentary), NWMO has postulated some basic requirements of the bentonite-based sealing materials, which include but are not limited to: (i) to hold the UFCs in their location within the placement room; (ii) to restrict any physical and chemical deterioration of the UFCs by the host rock environment over the lifetime of the DGR; (iii) to restrict the movement of groundwater and contaminants (chemical or radioactive) into and through the placement rooms, etc. Apart from the basic requirements, NWMO has proposed some buffer design requirements to ensure the long-term effective performance of the buffer. The critical design requirements include (Dixon, 2019):

- 100% bentonite buffer and GFM with a minimum thickness of 300 mm

- Average dry density of bentonite-filled regions of ≥ 1600 kg/m^3 with a minimum swelling pressure of 100 kPa upon saturation and a maximum saturated hydraulic conductivity of 10^{-10} m/s.
- A maximum water activity of 0.96 to suppress microbial activity.
- UFC surface temperature to be less than 100 °C.

2.2.3 Thermo-Hydro-Geochemical Evolution of DGR

To aid in the development of the DGR design, a large number of experimental, theoretical, numerical and field studies have been performed over the past few decades addressing the key issues associated with the long-term performance assessment of the DGR system. Based on the investigation outcomes, it can be said that processes affecting the bentonite buffer behaviour in the near-field of a high-level waste repository include but are not limited to heat transport; radiation-related processes, freezing; water uptake (unsaturated conditions); evolution of swelling pressure, including hydro-mechanical interaction with liner, host rock, and canister; pore-water flow; diffusive transport of solutes; gas dissolution and transport; bentonite interaction with metal corrosion products; corrosion of the UFC; bentonite interaction with cementitious materials; thermal alteration of bentonite; colloid generation or erosion; and microbial effects (Sellin & Leupin, 2014).

In the DGR environment, the low hydraulic conductivity of the highly compacted bentonite (HCB) buffer combined with the low hydraulic gradient of the near-field and the host rock will limit the transport of solutes to a slow diffusive process. Different species, however, exhibit different diffusion behaviours. Several studies (Appelo et al., 2010; Glaus et al., 2017; Idiart & Pękala, 2020) have proven that cation diffusion through compacted bentonite is faster than anion diffusion. Various conceptual models of bentonite porosity have interpreted this phenomenon. One of the conceptions is that bentonite's negatively charged surface layer increases cation concentration in diffuse double layer compared to mobile free water. This effect leads to enhanced cation diffusion in the diffuse layer while partially or excluding anions from a fraction of the pores and interlayers depending on the degree of compaction/ dry density and the salinity/ionic strength of the solution. Due to this “anion exclusion” effect, the anion-accessible porosity is lower in compacted bentonite, leading to less diffusion of anions compared to cations and neutral species (Appelo et al., 2010; Glaus et al., 2017; Idiart & Pękala, 2020).

Another important feature that influences the diffusive transport of species in the bentonite buffer is the elements' strong sorption/geochemical reaction. Sorption onto bentonite can either occur by cation exchange method at the permanently charged layer surface of the clay mineral or by surface complexation (inner and outer sphere complexes) process at the variably charged edge surface. Ion exchange is the sorption mechanism for positive cations at low pH values. In contrast, surface complexation is a more common process for all reactive ions, such as transition metals, actinides, lanthanides, and reactive anions. The sorption behaviour of different elements onto bentonite has been reported to be influenced by environmental conditions such as pH, temperature, ionic strength, etc. Sorption is discussed in detail in Section 2.3.

Some key aspects of the long-term evolution expected for the near-field environment of Canadian DGR and subsequent effects of repository conditions on the diffusive transport of contaminants and the sorption ability of bentonite are discussed in the following sub-sections.

2.2.3.1 Thermal evolution and heat transport

High-level used nuclear fuel stored in the used fuel containers (UFCs) produce high heat (1000-2000 W) as a result of the radioactive decay processes (Sellin & Leupin, 2014). Heating from the used fuel containers establishes a thermal gradient across the EBS due to high temperature near the UFC and low temperature near the host rock (Cloet et al., 2017; Hall et al., 2020; King et al., 2017; Sena et al., 2010). The bentonite buffer is predicted to reach the highest temperature at the early stage of the repository lifetime (when the buffer will be in unsaturated or only partially saturated condition) and then gradually return to ambient temperature again (King et al., 2017, 2017). King et al. (2008) indicates that the temperature within the Canadian DGR will gradually rise due to the heat generated by the used fuel, reaching a peak temperature exceeding 80˚C after 10 years, and then gradually decreasing to around 20˚C over a span of 10,000 years (King et al., 2008). Rashwan et al. (2022) states that the thermal decay of used nuclear fuel may lead to the UFC surface heating up to approximately 80 °C after 50 years in the crystalline host rock and 40 years in the sedimentary host rock.

In the early phase, the heat transport will occur by conduction and limited convection process through the gaps at the rock interface, bentonite and UFCs. When the buffer becomes fully saturated and completely swelled, all gaps and joints will be filled, and the heat transport will occur by conduction through the water-saturated bentonite (Sellin & Leupin, 2014).

Based on experimental results, Bradbury et al. (Bradbury et al., 2014) suggested that the maximum temperature of the unsaturated bentonite (in the inner half of the bentonite) will not reach above 100°C. The chemical changes expected at this condition may include the possibility of dissolution/precipitation of amorphous silica, sulfates and to some extent carbonates close to the UFCs. This type of change may impact the mechanical properties (i.e., swelling) and diffusion characteristics of the buffer, but no significant changes are expected to occur in the montmorillonite component at a temperature <100°C. In addition, this study noted that no noticeable changes in the bentonite are expected under saturated conditions at temperatures ≤ 120°C. The general conclusion of the experimental findings is that the post-emplacement temperature evolution is not likely to have any significant detrimental influence on the properties of the outer half of the bentonite, which can perform its buffer function fully, particularly in terms of sorption (Bradbury et al., 2014). However, temperature variations may impact bentonite saturation and the diffusion of solutes through the bentonite, as solute diffusion rates are temperature-dependent (Rashwan et al., 2022).

2.2.3.2 Saturation of highly compacted bentonite

According to the latest design concept of Canadian DGR, the initial saturation of the buffer and backfill materials will be between 65–90% (HCB) and 6% (bentonite pellet gap fill) (King et al., 2017). Because of the high thermal gradient in the initial stage, water will move away from the container surface, leading to the drying of the bentonite buffer. When the repository temperature decreases, and hydro-static pressure develops between the host rock and the buffer, moisture will move back toward the buffer, and thus, the process of saturation will begin in the opposite direction of heat transport. In the context of Canadian DGR, the estimated timeline for full saturation of the near field is ~50 years (crystalline host rock) or ~5000 years (sedimentary host rock) as the time to saturation is dependent on the host rock's permeability (King et al., 2017). According to Rashwan et al. (2022), the saturation behaviour of the DGR depends on the host rock permeability and also on initial bentonite saturation. With an initial bentonite saturation ranging from 45% to 89%, it may take 10 to 80 years for crystalline host rock and 35 to 120 years for sedimentary rock to fully saturate.

The rate of buffer saturation will affect the rate of mass transport through the buffer since diffusion of dissolved species will be slow in the unsaturated buffer due to the low

interconnectivity of water-filled pores. However, species capable of partitioning into the gaseous phase may diffuse faster through partially saturated pores (King et al., 2017).

2.2.3.3 pH and redox condition

Immediately after excavation and placement, oxygen and moisture will be trapped in the repository. The initial level of O_2 is predicted to be 1–10 mol per m^2 of the UFC surface (King et al., 2017). Due to this small quantity of oxidants, the UFC may undergo negligible oxic corrosion over the early lifetime (Standish et al., 2016). In addition to Cu corrosion, O_2 may be consumed by other processes, such as aerobic microbial activity and the oxidation of bentonite and host rock minerals. The current estimated timeline for the oxic phase of the repository is between 0.5 and 1.5 years (King et al., 2017). Once all trapped O_2 is consumed, the repository environment will become anaerobic and remain so for > 99.9% of its lifetime (King et al., 2017).

The Canadian groundwater composition data reported by NWMO (Hall et al. 2020) indicates the pH of crystalline (CR-10) and sedimentary (SR-270-PW) host rocks to be 7.1 and 5.88, respectively. However, the repository pH might be buffered above 7 by the dissolution of carbonaceous minerals (e.g., calcite).

2.2.3.4 Bentonite pore water chemistry

As reported in the study of King et al. (2017), deep groundwater in crystalline and sedimentary host rocks in Canada tends to be saline with chloride concentration ranging between 0.1-5 mol/L and with the presence of Na^+ and Ca^{2+} as the dominant cations. However, the UFCs will not be in direct contact with groundwater but with bentonite pore water. Therefore, groundwater composition is of secondary importance to influence the bentonite pore water composition in the repository's early transient oxic phase but may impact the long-term corrosive conditions. The cation and anion concentration of bentonite pore water is also reported in the study, which suggests that MX-80 bentonite to be used in Canadian DGR contains 80% sodium montmorillonite. Due to the dissolution of gypsum and calcite from the buffer, part of these Na^+ ions will be exchanged for Ca^{2+} and thus will increase the initial pore water [Na^+]. In terms of anions, King et al., (2017) reports that the initial pore-water of bentonite is predicted to contain 0.03 mol/L Cl^-, 0.014 mol/L SO^{2-} and 0.00068 mol/L HCO^{3-}. With the rise of surface temperature and subsequent drying out of HCB, the pore water [Cl^-] will increase. Then it will decrease (after achieving a peak concentration of 0.066 mol/L) as the buffer re-saturates and

finally will reach equilibrium with the saline groundwater. At all times, Cl^- is expected to be the predominant anion in the pore water, at least two times higher than SO_4^{2-} and HCO^{3-}. The pH of bentonite pore water may vary between 8-10 whereas, the Eh levels may vary between -183 mV to -366 mV (Muurinen & Carlsson, 2010).

Bentonite porosity depends upon the degree of compaction, particle charges, the type of cations initially present in the interlayer and free porewater regions, as well as the ionic strength of the free pore water (Chowdhury et al., 2024). In cases of low cationic concentration of the free pore water, the thickness of the DDL is significant enough to keep the surrounding water molecules strongly associated with the clay particles, thus constraining the ability to transmit water through this part of the porosity. Therefore, in a high surface charge and a low salinity environment, the development of an extensive hydration layer surrounding the clay particles results in a high swelling capacity and a reduction in the macro-pore volume available for water movement. In contrast, with the increasing pore water salinity, the thickness of DDL will reduce, and the porosity available for flow will increase, resulting in higher hydraulic conductivity and lower swelling capacity. Moreover, the increasing cationic concentration in the DDL substituting the water molecules will reduce cation diffusion. Still, it will enhance the anion diffusion as more anions will pass with water through the increased interparticle pore space (Loon et al., 2003, 2007).

The negative effect of salinity on swelling pressure is noticeable only at a lower density of the bentonite (Chowdhury et al., 2024). The study of Dixon (2019) reports that even a modest total dissolved solids (TDS) (5-10 g/L) in the pore fluid results in a significant decrease in the swelling pressure at lower density (< 1 Mg/m^3), which becomes less evident with increasing density due to proximity of the clay particles to one another and the strong interaction of the pore fluid with the clay particle surfaces. According to the report, given the very high bentonite density (1440-1700 Kg/m^3), the pattern of decreasing swelling pressure with increasing TDS might not be noticeable for NWMO DGR option even in sedimentary rock formation, with TDS expected to be in the range of 200-350 g/L (Dixon, 2019).

2.2.3.5 Effect of bentonite interaction with iron corrosion products

A prominent effect on the bentonite sorption property might result from the interaction of bentonite with iron corrosion products. Several studies suggest that ferrous iron (Fe^{2+}) released

from the corrosion of steel containers can destabilize and alter montmorillonite at temperatures below 100°C. As a result of the alteration 3 types of swelling or non-swelling clay minerals may form, such as (i) Fe-rich smectites, (ii) 1:1 phyllosilicates belonging to the 7Å kaolinite/serpentinite group, and (iii) non-swelling clays and chlorites. Since the Fe-smectites have similar properties to the Na-montmorillonite, the formation of Fe-rich smectites (e.g.: dioctahedral saponite) will not significantly influence the barrier function concerning sorption and swelling. However, if 7Å clay minerals (e.g. berthierine) and chlorites are formed, noticeable changes in the pore structure may occur, resulting in a reduced swelling capacity and reduced sorption ability in the bentonite (Lanson et al., 2005).

2.2.3.6 Effect of bentonite interaction with cementitious materials

In most DGR designs, concrete is incorporated as structural support for galleries and sealing of the canister/bentonite packages, tunnels and shafts (Kaufhold and Dohrmann 2016, González-Santamaría et al. 2020). Geochemical processes within the concrete/clay interface may include decalcification of concrete; dissolution of montmorillonite; precipitation of calcium or magnesium silicate hydrates, chloride or sulphate; cation exchange in montmorillonite etc. (González-Ssantamaría et al., 2020). All these reactions are likely to cause pore clogging at the clay interface. Moreover, the dissolution of cementitious materials may increase bentonite pore fluid pH from almost neutral up to 13.5 (Fern et al. 2020., González-Santamaría et al. 2020) and thus may influence the diffusion and sorption behaviour of the solutes. However, the degree and location of these chemical alterations are conditioned by the type and composition of the cementitious materials. In this context, Fern et al. (2020) and González-Santamaría et al. (2020) suggested using low-pH cements (pH < 11) to lower the influence of alkaline dissolution of clays. On the contrary, high-pH cement materials (pH > 13) perform better in reducing the decalcification process (Fern et al., 2020.; González-Santamaría et al., 2020). However, under these uncertainties, a suitable bentonite should be as stable as possible against the chemical alteration induced by cementitious materials (Kaufhold & Dohrmann, 2016).

2.2.3.7 Copper corrosion of UFCs

Initially, the redox conditions in the DGR will be oxic because of the trapped air remaining from DGR construction and operation. This oxygen presence may lead to oxic corrosion of the copper

surface, such as uniform copper corrosion (UC) and stress corrosion cracking (SCC), although copper is generally not highly susceptible to SCC (Rashwan et al., 2022).

Once the initially trapped oxygen is consumed, anoxic conditions will prevail in the subsurface. Under anoxic conditions, microbiologically influenced corrosion (MIC) of UFC may occur if bisulfides (HS^-) are present or produced within the DGR. As discussed in Chapter 1, HS^- may be generated at the rock-bentonite interface through sulfate reduction by sulfate-reducing bacteria (SRB). If HS^- migrates through the bentonite to reach the UFC, it can corrode the copper barrier via the simplified reaction involving aqueous HS^- (refer to Eq. (1.1) in Chapter 1). As such, aqueous HS^- is likely the major contributor to long-term copper corrosion in the DGR (Hall et al., 2021).

Although the high-density bentonite used in the Canadian DGR will inhibit microbial activity near the container by reducing water activity, SRB may still be active at or beyond the bentonite-rock interface, driving HS^- production. Because this condition persists over an extended period, previous studies have estimated that MIC will be the primary contributor to UFC corrosion compared to other types, such as UC and SCC. Although extensive research has explored the chemical aspects of MIC, far less attention has been paid to the transport processes (i.e., diffusion and sorption) of HS^- specific to the Canadian DGR layout (Rashwan et al., 2022).

It is anticipated that "sorption" onto bentonite may limit HS^- flux to the UFC and thus, may minimize the extent of MIC. Hence, this research aims to investigate the sorption phenomenon of HS^- onto bentonite under various geochemical conditions. As a critical component of the research topic, the following section presents a comprehensive discussion on "sorption".

2.3 Sorption Fundamentals

2.3.1 Sorption Definition

In soil chemistry, sorption defines the interaction of solutes and contaminants with mineral and organic surfaces (Randall 2012)**.** When a substance comes in contact with the solid phase, it may undergo certain physical and chemical processes such as (i) adsorption onto the surface of a solid (physical adsorption), (ii) absorption into the structure of the solid, (iii) precipitation as a 3-dimensional molecular structure on the surface of the solid, (iv) chemical transformation and/ or (v) partitioning into the organic matter (Kaplan, 1999). Sorption is the generic term that includes

all these processes. Regardless of the mechanism, sorption describes the partitioning of the solute particles from an aqueous to a solid phase (Kaplan, 1999; Limousin, 2007). Sorption is considered a universal phenomenon governing the mobility of contaminants in subsurface porous media and aquatic environments (Limousin, 2007).

2.3.2 Sorption Mechanisms

Adsorption and precipitation are considered the most important sorption processes influencing the fate and transport of solutes within subsurface environments (Kaplan, 1999). As such, these two processes are discussed in the following sub-sections.

2.3.2.1 Adsorption

The term adsorption refers to the physical attachment or bonding of ions and molecules onto the surface of another solid or liquid phase. Adsorption is different from absorption, in which a substance penetrates the interior structure of the solid or liquid. It also differs from precipitation because precipitation is a 3-dimensional process whereas adsorption is a 2-dimensional process, where the solids used to adsorb gases or dissolved substances are called adsorbents; the adsorbed molecules are called adsorbate (Kaplan, 1999).

The adsorption mechanism involves two primary processes: physisorption and chemisorption.

(i) Physisorption

Physisorption (i.e., physical adsorption) occurs when the species attach to the mineral surfaces by van der waals forces (Clark, 2009). Since van der waals interactions are weak, physisorption is rapid, reversible, and exothermic, with a low adsorption enthalpy, nearly 20 to 40 kJ/mol. Since the energy released during physical sorption is small (i.e., insufficient for bond breaking), physically adsorbed species do not change chemically (Yu & Neretnieks, 1997).

(ii) Chemisorption

Chemisorption is also known as chemical adsorption, in which adsorption takes place onto the adsorbent surface by chemical bonds. Chemisorption is irreversible and endothermic, and owing to chemical bonding, the enthalpy of chemisorption is high, nearly 80 to 240 kJ/mol. In addition, chemisorption depends on the surface area (e.g., with an increase in surface area, chemisorption

increases) (Vilks, 2014; Yu & Neretnieks, 1997). The two major types of chemical sorption include (i) ion exchange and (ii) surface complexation.

a) Ion exchange

Ion exchange involves the reversible exchange of cations between water and the surface of a solid. The surfaces of clay minerals usually carry a permanent negative charge, mainly resulting from the isomorphous substitution of lower-valency atoms for higher-valency atoms within the clay lattice. For example, in montmorillonite, replacing Al^{3+} with Fe^{2+} or Mg^{2+} can leave a net negative charge for the layer. Similarly, Si^{4+}can be replaced by Al^{3+} in the tetrahedral layer, leaving a charge imbalance. Further, the oxygen atoms on the surface of each clay crystal and their edges keep a net negative charge. The resulting charge deficiency manifested at the clay surface can be satisfied by adsorbing exchangeable cations from pore waters and forming electric double layers at the water-solid interface. In the absence of other cations, negative charges can be neutralized by protons, H^+, which adsorb and desorb from surface charge sites. Therefore, the pH of the pore waters potentially influences the net surface charge of the clay and, thus, its exchange capacity. Cation exchange reactions are typically formulated by the equation as follows (Wang et al., 2001a):

$$nZNa + M^{n+} \rightarrow Z_n \mathrm{M} + nNa^+ \qquad (2.1)$$

Where Z^- is a negatively charged cation exchange site and M^{n+} is a cation of valency +n and Na^+ indicates the sodium ion.

b) Surface Complexation

Two standard terms involved with surface complexation are “inner-sphere complex” and “outer-sphere complex”. Both cation and anion sorption may occur on the variably charged surface sites (i.e., the edge sites) of minerals by inner and/or outer sphere surface complex formation. An inner-sphere complex refers to a case where a chemical bond (either ionic or covalent, although predominantly covalent) is formed between the molecule and the oxygen or hydroxyl ion. The inner-sphere complex is formed in direct contact with the clay surface, and there is no water molecule between the surface functional group and the bound molecule. On the other hand, outer-sphere complexes refer to cases where the functional group and the bound molecule are held by coulombic attraction and separated by one or two water molecules. Outer-spheres are

less stable than inner-sphere surface complexes, as the ionic or covalent bonds are much stronger than coulombic forces.

While ion-exchange sorption is mainly associated with cations, surface complexation reactions can be associated with both cations and anions (Wang et al., 2001b). The surface complex reaction of a cation M^{n+} and an anion A^{z-} on a neutral surface site ($\equiv SOH$) can be represented by the reactions as follows (Wang et al., 2001a):

$$\equiv SOH + M^{n+} \rightarrow \equiv SOM^{n-1} + H^{+} \text{ (cation)} \quad (2.2)$$

$$\equiv SOH + A^{z-} + H^{+} \rightarrow \equiv SA^{-z+1} + H_2O \text{ (anion)} \quad (2.3)$$

A review of relevant literature on various anion sorption (e.g., sulfate (SO_4^{2-}), phosphate (PO_4^{3-}), radionuclide anions) is included in Chapter 5 (Section 5.3.1) to help interpret the HS^- sorption mechanism onto bentonite.

2.3.2.2 Precipitation

Precipitation is a special type of complexation reaction in which two or more aqueous species form a structure on the surface of the solid. Precipitation as a new insoluble solid phase is a common phenomenon of solute (e.g., heavy metals, radionuclides) transport in subsurface media. For example, a bivalent cation (M^{2+}) may form a sulfide precipitate by the following equation:

$$M^{2+} + 2HS^{-} \rightarrow M(HS)_2 \quad (2.4)$$

Precipitation reactions can result in a uniform solid layer on the mineral surface or involve a solid mixture containing either a coprecipitate or a multi-nuclear precipitate that may involve ions from the solid surface. When ions from the soil mineral surface become part of the new solid on the surface, the outcome is a surface precipitate.

2.3.3 Factors Influencing Sorption Capacity

Table 2.1 presents several factors reported in several studies to control the sorption processes of the studied elements onto solid surfaces. Although different elements showed different sorption behaviour and the extent of influence of experimental conditions varied from one element to

another due to their variations in physicochemical properties, some common effects of these factors could be observed on the sorption capacity of bentonite.

Table 2.1 Influential factors of sorption capacity

Factors	Effects on the sorption capacity of bentonite	References
pH	Higher pH enhances the chances of negative surface charge in soil and increases the possibility of cation sorption, whereas anion sorption decreases with increasing pH	(Yu & Neretnieks, 1997, Vilks, 2014; Xu et al., 2008; Yang et al., 2009)
Ionic strength of background solution	Ion exchange or outer-sphere surface complexation is influenced by solution ionic strength. Usually, sorption (%) decreases with increasing ionic strengths.	(Verma et al., 2014; Xu et al., 2008; Yang et al., 2009; Zhao et al., 2008))
Contact time	Sorption increases with increasing contact /shaking time until equilibrium is reached	(Azizian, 2004; Jaafer, 2014; Xu et al., 2008; S. Yang et al., 2009)
Competing ions	Ions with higher ionic potential show higher sorption affinity. Among the competing ions, higher valance and lower radius ions tend to sorb more easily and strongly than others	(Verma et al., 2014; S. Yang et al., 2009)
Temperature	Depending upon the thermodynamic properties of ions, sorption capacity may either decrease (exothermic) or increase (endothermic) with increasing temperature	(Xu et al., 2008; S. Yang et al., 2009; Zhao et al., 2008)
Concentration of solid or liquid to solid ratio (L:S)	Sorption (%) increases with increasing solid content due to the increased availability of sorption sites. However, if the total concentration of available sorption sites is much higher in excess of the ion concentration, this effect might be negligible.	(Gupt et al., 2019; Tran et al., 2018; Xu et al., 2008; S. Yang et al., 2009, Wang et al., 2001a)
Type of bentonite	Soils with higher surface area, surface charge and cation exchange capacity have more sorption capacity. However, the surface charge of soil may vary with exchangeable cations (e.g. Na-bentonite has a higher sorption capacity than Ca-bentonite)	(Uddin, 2017; Yu & Neretnieks, 1997)
Density of bentonite	Sorption of Cs^+ on compacted bentonite was found to be about one-half to one-third the value of loose bentonite	(Oscarson et al., 1994)
Presence of organics	Presence of organics (e.g. resins, plastic, rubber, cellulose) causes a decrease in sorption as the organic cations also compete for adsorption sites on the clay mineral surfaces.	(Yu & Neretnieks, 1997; Uddin, 2017)

Considering the most important geochemical factors relevant to the DGR, the effects of temperature, pH and co-existing ions are discussed in the following sub-sections.

2.3.3.1 Effect of temperature

The influence of temperature on sorption reactions is evaluated based on the changes of energy between reactants and products, expressed as Gibbs-free energy. In sorption experiments, the thermodynamic parameters are calculated by using the equation (Edet & Ifelebuegu, 2020; Xu et al., 2008; Zhao et al., 2008):

$$lnK_0 = \frac{\Delta S^0}{R} - \frac{\Delta H^0}{RT} \tag{2.5}$$

Where K_0 is the thermodynamic equilibrium constant and ΔH^0, ΔS^0, and T are the enthalpy, entropy, and temperature in Kelvin, respectively. R is the gas constant. The enthalpy (ΔH^0) and entropy (ΔS^0) values can be obtained from the slope and intercept of $\ln K_0$ vs. 1/T plots. The following equation calculates the Gibbs free energy (ΔG^0) of specific adsorption:

$$\Delta G^0 = \Delta H^0 - T\Delta S^0 \tag{2.6}$$

Xu et al., (2008) investigated the adsorption of Pb (II) on MX-80 bentonite under three different temperatures: 291K, 308K and 328K. The study observed that Pb(II) adsorption decreases with the rise in temperature. In addition, the calculated thermodynamic parameters in this study revealed that ΔG^0 values are negative at all temperatures, indicating the spontaneity of the adsorption processes. Moreover, the negative value of enthalpy change, ΔH^0, indicated an exothermic Pb(II) sorption process, whereas the negative value of ΔS^0 indicated an ordered Pb(II) arrangement on the bentonite surface. The negative value of ΔH^0 and the increase in ΔG^0 (less negative) with an increase in temperature indicated that the Pb(II) sorption reaction with bentonite was less favourable at higher temperatures.

A similar phenomenon was observed in the study of Zhao et al., (2008), who investigated the adsorption process of Thorium (Th (IV)) on MX-80 bentonite. The study also found negative values of ΔH^0 and ΔG^0, indicating that the adsorption process of Th (IV) on MX-80 bentonite is exothermic and spontaneous. The study suggested that the exothermicity was observed as the adsorption of Th(IV) ions on MX-80 bentonite exceeded the dehydration energy of Th(IV),

whereas the positive values of the entropy ΔS^0 demonstrated the affinity of MX-80 bentonite toward Th(IV) ions. Also, the decrease in ΔG^0 with the decrease in temperature suggested more efficient adsorption at lower temperatures.

However, a positive value of the standard enthalpy change ΔH^0 was observed in the Ni(II) adsorption on GMZ bentonite by Yang et al., (2009), indicating that the sorption was endothermic. The study suggested one possible explanation for this positive entropy is that Ni(II) is dissolved well in water, and the associated dehydration energy exceeds the exothermicity of cations to attach to the solid surface. However, the Gibbs free energy change (ΔG^0) was negative, indicating a spontaneous process. Under the experimental conditions applied, the value of ΔG^0 became more negative with the increase in temperature, representing more efficient sorption at high temperatures. This phenomenon is also supported by the fact that the dehydration process needs energy, and cations are readily desolvated at high temperatures; the sorption process was favoured at higher temperatures.

According to Rani & Mahajan (2016), most adsorption is exothermic; thus, the adsorption capacity of adsorbents is expected to decrease with an increase in temperature. However, the endothermic phenomenon (i.e. increase of sorption capacity with increasing temperature) is observed when the sorption process is controlled by chemisorption involving the breaking of hydration bonds and formation of new bonds with the active sorbent sites (Saeed & Ahmed, 2006). Moreover, endothermicity may indicate the involvement of the intra-particle transport diffusion process, which becomes faster with the rise of temperature due to increased mobility of the sorbates and reduction in the retarding forces acting on the sorbent surfaces (Rani & Mahajan, 2016).

2.3.3.2 Effect of pH

Since the magnitude and polarity of the net surface charge of a mineral change with pH, the sorption phenomenon of dissolved ions is highly dependent on pH. The pH at which the overall charge of a surface is zero is known as its zero point of charge or ZPC. As pH increases from the ZPC, the mineral surfaces become more negatively charged due to the acidic dissociation of surface hydroxyl groups. Therefore, cation adsorption is favoured at higher pH ($pH > pH_{ZPC}$) and decreases with decreasing pH. In contrast, at $pH < pH_{ZPC}$, the surface becomes positively charged

due to protonation, thus favours the adsorption of negatively charged anions. Therefore, anion sorption is higher at low pH and decreases with increasing pH (Kaplan, 1999).

Another phenomenon associated with the effect of pH is its influence on species distribution, which in turn is reflected in the sorption behaviour. Xu et al. (Xu et al., 2008) found that Pb (II) adsorption on bentonite increases with increasing pH till pH 9 and starts decreasing as the pH value increases above 9. The study explained this behaviour by the distribution of Pb(II) species as a function of pH, indicating that at pH 9, the positively charged Pb^{2+} begins to transform to negatively charged $Pb(OH)^{3-}$, which is the predominating species at pH >11. Thus, adsorption of Pb(II) decreases at pH> 9 due to electrostatic repulsion.

2.3.3.3 Effect of co-existing ions

The presence of solutes or co-existing ions influences the sorption based on their relative affinity towards the charged surface of the solid. Generally, ions with higher ionic potential show a higher tendency to form inner-sphere surface complexes. Xu et al. (Xu et al., 2008) investigated the adsorption of Pb(II) on bentonite under the competition of Pb(II) with Li^+, Na^+ and K^+ on the bentonite surfaces. The study identified that as the radius of K^+ is smaller than the other two cations, the influence of K^+ on Pb(II) adsorption was more prominent than that of Na^+ and Li^+.

The study of Yang et al. (Yang et al., 2009) found that the sorption of Ni(II) on bentonite is the highest in 0.01M $NaClO_4$ and is the lowest in 0.01M $Ca(ClO_4)_2$ at pH 8. The study interpreted this by the competitive adsorptive capacity of the positive ions with Ni(II). Na^+ has a lower sorption ability, so it has a lower influence on Ni sorption than Ca^{2+} cations.

Previous sorption studies suggested that ion exchange or outer-sphere surface complexation is influenced by ionic strength, whereas inner-sphere surface complexation is affected by pH values (Miraoui & Amine, 2015; Vilks, 2014; Wu et al., 2009; S. Yang et al., 2009). The inner-sphere complex is formed in direct contact with the pH-dependent variable charge surface sites of the clay surface (resulting from protonation and deprotonation reactions as a function of the solution pH), and there is no water molecule between the surface functional group and the bound molecules (in the stern layer). On the other hand, outer-sphere surface complexes are formed containing water molecules between the functional group and the bound molecules. With the increasing solution ionic strength, more exchange sites at the diffuse double layer (DDL) get

occupied by cations instead of water molecules, leading to shrinkage of the DDL (Tang et al., 2014). Thus, outer sphere surface complexation decreases with increasing ionic strength. (S. Yang et al., 2009) observed that the sorption of Ni(II) on bentonite is affected by $NaClO_4$ concentrations at pH<8, whereas the sorption was independent of ionic strength at pH >8. Therefore, the study concluded that sorption of Ni(II) on bentonite is mainly dominated by ion exchange or outer-sphere surface complexation at low pH values (i.e., pH<8) and by inner-sphere surface complexation at high pH values (i.e., pH >8).

2.3.4 Sorption Isotherm Models

"Sorption isotherm" refers to a graphical presentation of mass adsorbed per unit weight of the solute (q) as a function of the equilibrium concentration of solute remaining in the solution (C) at a constant temperature (Fetter, 2001). It is used to evaluate the effect of contaminant concentration on sorption while other parameters are held constant. Several isotherm equations are available for analyzing experimental sorption equilibrium parameters. The most used isotherm models are Linear, Freundlich and Langmuir isotherms.

2.3.4.1 Linear isotherm

The simplest method to represent sorption is a linear isotherm model in which the sorption equilibrium is described by a linear relation between the concentration in the sorbed phase (q) and the concentration in the solution phase (C), characterized with a constant partition/ distribution coefficient K_d, which is defined as (Kaplan, 1999; USEPA, 1999; Yu & Neretnieks, 1997):

$$K_d = \frac{q\ (\frac{mg}{g})}{C\ (\frac{mg}{L})} \tag{2.7}$$

This model is also termed as a constant K_d model or a single parameter K_d model (Kaplan, 1999). The underlying assumptions of this model are that the sorption process is reversible and independent of the sorbate concentration in the liquid phase (Kaplan, 1999; Yu & Neretnieks, 1997). At low concentrations of the solutes in solution, this linear approximation has been found to describe the sorption equilibrium satisfactorily (Yu & Neretnieks, 1997). However, the greatest limitation of the constant K_d model is that it represents the sorption phenomenon as a

function of only one experimental condition and does not incorporate the sensitivity to changing conditions. Such homogeneity is not typical and, therefore, undermines the usefulness of the constant K_d (Kaplan, 1999). Nonetheless due to its simplicity, the linear isotherm is widely used to estimate sorption, and can be accurate at early times when contaminant load does not surpass the number of available sorption sites (see section 2.3.4.4).

In situations where the amount of contaminant loaded on the available sorption sites is increased enough to impact the linear relationship, the isotherm follows a concave shape, indicating a progressive saturation of the solid (Ayawei et al., 2017; Kaplan, 1999; Limousin, 2007; Yu & Neretnieks, 1997). In such cases, using non-linear multiparameter isotherm models is the best practice to describe the sorption relationship. The most popular non-linear isotherm models are the Langmuir and Freundlich models, which evaluate the effect of contaminant concentration on sorption while other physicochemical parameters are held constant. A brief discussion on the Langmuir and Freundlich isotherm models is presented in the following sub-sections.

2.3.4.2 Langmuir isotherm

The Langmuir isotherm model describes monolayer sorption occurring on distinct localized sorption sites with uniform energies (Edet & Ifelebuegu, 2020). The equation of Langmuir isotherm is:

$$q_e = \frac{k_L\, Q C_e}{1 + k_L\, C_e} \tag{2.8}$$

Eq. 2.8 can be expressed in the linearized form:

$$\frac{C_e}{q_e} = \frac{1}{k_L Q} + \frac{C_e}{Q} \tag{2.9}$$

where, k_L (L mg^{-1}) and Q (mg g^{-1}) are the Langmuir isotherm constants. Q indicates the maximum monolayer coverage capacity (mg g^{-1}) and k_L is associated with the energy (heat) of adsorption (A.O, 2012). The Langmuir constants Q and k_L are determined from the slope and intercept of the linear plot of C_e/q_e vs C_e, respectively.

2.3.4.3 Freundlich isotherm

The Freundlich isotherm describes multilayer sorption occurring on heterogeneous surfaces and active sites with different energies (Edet & Ifelebuegu, 2020). The equations of Freundlich isotherm are as follows:

$$q_e = k_f {C_e}^{1/n} \tag{2.10}$$

The linearized form of Eq. 2.10 is:

$$log q_e = log k_f + \frac{1}{n} log C_e \tag{2.11}$$

k_f ($mg^{1-n}\, g^{-1}\, L^n$) and n are the constants representing the relative sorption capacity of the sorbent and intensity of sorption, respectively, which are determined from the intercept and slope of the plot of $log q_e$ against $log C_e$, respectively. The "n" value describes the heterogeneity of the surface; a smaller $1/n$ value implies a more heterogeneous surface, and an n value between 1 and 10 indicates a favourable process (A.O, 2012; Edet & Ifelebuegu, 2020).

2.3.4.4 Applicability of the sorption isotherm models

The liner isotherm best describes the sorption phenomenon for low-concentration solutes (i.e., when most sorption sites are unoccupied). In such a case, using the linear isotherm is a good choice because it is easy to solve and understand. However, while dealing with concentrated sources or limited sorption sites where the amount of contaminant on the available adsorption sites is large enough, sorption relationships deviate from linearity and give rise to the need for non-linear isotherms (i.e. Langmuir and Freundlich) (Yu & Neretnieks, 1997). The fundamental difference between these two models is that Langmuir's model is theoretical, while the Freundlich model is empirical. In the Langmuir model, it is assumed that there is only a monomolecular layer on the surface at maximum coverage, indicating no stacking or layering of adsorbed molecules.

On the other hand, the Freundlich isotherm does not impose this restriction and considers multilayer coverage. Moreover, Freundlich constant "*n"* is a material-specific constant describing the adsorption surface's heterogeneity. Thus, Freundlich isotherm is closer to reality

than the Langmuir assumption and is more appropriate when the sorption is not limited to only physical sorption (A.O, 2012; Edet & Ifelebuegu, 2020; Yu & Neretnieks, 1997).

2.3.5 Sorption Kinetic Models

The models described in the previous section assume steady state conditions, when all processes have come to equilibrium. Kinetic models are critical in sorption studies to examine the rate of the process and the possible rate-controlling mechanism, i.e. mass transfer or chemical reaction (Kocer et al., 2008).

As suggested in the literature (Kajjumba et al., 2018; Sahoo & Prelot, 2020), sorption kinetics may involve several processes at the solid–liquid interface, such as (i) bulk diffusion of the solute from the solution to the liquid film/boundary layer around the solid (ii) external or film diffusion of the solutes across the liquid film to the external surface of the solid particles (ii) intraparticle diffusion or internal diffusion of the solutes into the interior of the sorbent by pore diffusion and surface diffusion (iv) interaction with the solid surface sites, either by physisorption or chemisorption. Since the first and fourth processes are relatively fast, the overall rate of the sorption ultimately depends on the second and/or the third step (i.e., film and/or intraparticle diffusion), which occurs slowly.

To understand the dynamics of the sorption process, various kinetic models have been applied in literature such as pseudo–first-order, pseudo–second–order, Elovich, and Weber's intraparticle diffusion model.

2.3.5.1 Pseudo-first-order kinetic model

The pseudo-first-order kinetic model assumes that the solute uptake rate is directly proportional to the number of unoccupied sites of the solid (Tsibranska & Hristova, 2011). This relation is defined using the Lagergren equation as follows (Ho & Mckay, 1998):

$$\frac{dq}{dt} = k_1(q_e - q_t) \tag{2.12}$$

After integration, the non-linear form of Eq. 2.12 results to:

$$q_t = q_e(1 - e^{-k_1 t}) \tag{2.13}$$

Eq. 2.13 can be expressed in linearized form:

$$\ln(q_e - q_t) = lnq_e - k_1 t \tag{2.14}$$

Where q_e and q_t are the amounts sorbed at equilibrium and at time t, respectively (mg g^{-1}), and k_1 is the rate constant of pseudo-first order sorption reaction constant ($time^{-1}$), determined from the slope and intercept of the linear plot of $ln\ (q_e - \ q_t\ )$ against t.

Several studies (Edet & Ifelebuegu, 2020; Ho & Mckay, 1998; Tsibranska & Hristova, 2011) suggested that the Lagergren pseudo–first-order kinetic model is generally applicable over the initial stage (initial 20-30 mins) of the sorption process and does not fit well for the entire range of reaction time. Additionally, the equilibrium sorption capacity q_e needs to be experimentally derived or, it might be necessary to extrapolate the experimental data to infinite time to obtain q_e (Ho & Mckay, 1998; Rani & Mahajan, 2016).

2.3.5.2 Pseudo-second-order kinetic model

The pseudo–second-order kinetic model considers chemisorption as the rate-limiting step and predicts the behaviour over the entire range of sorption (Edet & Ifelebuegu, 2020). The inherent assumption is that the sorption rate depends on sorption capacity instead of the sorbate concentration. The model is more advantageous over pseudo-first-order model in the sense that the equilibrium sorption capacity (q_e) can be directly calculated from the model; therefore, determining q_e from the experiment is not necessary (Edet & Ifelebuegu, 2020; Ho & Mckay, 1998).

$$\frac{dq}{dt} = k_2\ (q_e - q_t)^2 \tag{2.15}$$

After integration, the non-linear form of 2.15 results to:

$$q_t = \frac{tk_2q_e^2}{1 + tk_2q_e} \tag{2.16}$$

Eq. 2.16 can be expressed in linearized form:

$$\frac{t}{q_t} = \frac{1}{k_2\ {q_e}^2} + \frac{t}{q_e} \tag{2.17}$$

where k_2 is the pseudo-second-order rate constant (g mg^{-1} min^{-1}), determined from the slope and intercept of the linear plot of t/q_t versus t.

2.3.5.3 Elovich kinetic model

The Elovich equation describes second order chemical adsorption processes and has been found suitable for solid systems with heterogeneous surfaces (Edet & Ifelebuegu, 2020; Ho & Mckay, 1998; Kocer et al., 2008; Rani & Mahajan, 2016). The following equations represent the model:

$$\frac{dq}{dt} = \alpha exp k_1(-\beta q_t) \tag{2.18}$$

The linear form of the model:

$$q_t = \frac{1}{\beta}\ln(\alpha\beta) + \frac{1}{\beta} lnt \tag{2.19}$$

where q_t is the sorption capacity at time t (mg/g), α is the initial sorption rate (mg/g/min) and β is the desorption constant (g/mg) (Ho & Mckay, 1998).

2.3.5.4 Weber and Morris kinetic model

Weber and Morris kinetic model is applicable if there is intraparticle diffusion mechanism involved in the sorption process (Rani & Mahajan, 2016; Tsibranska & Hristova, 2011).

$$q_t = k_{inp} t^{0.5} + C_{inp} \tag{2.20}$$

where k_{inp} is the intraparticle diffusion rate (mg/g/$min^{0.5}$) and C_{inp} indicates the thickness of the boundary layer. The larger C_{inp} indicates the larger effect of the boundary layer (Tsibranska & Hristova, 2011). The k_{inp} and C_{inp} are determined from the slope and intercept of the regression line of the model equation. Sometimes, the weber model may exhibit multilinear plots indicating that more than one process is controlling sorption over time (Kajjumba et al., 2018; Li et al., 2007; Saeed & Ahmed, 2006; Sahoo & Prelot, 2020).

2.4 Production and Transport of Sulfide in the Repository

As discussed in Section 2.2.3.7, HS^- is expected to be a primary factor in long-term copper corrosion attributed to microbial activity. Because HS^- is a form of sulfide, which predominates at pH levels above 9, investigating the transport of HS^- necessitates an understanding of the sources and transport of sulfide within the repository environment. To this end, this section presents a review of relevant studies on the potential sources of sulfide and its fate and transport in the context of Canadian DGR.

2.4.1 Sources of Sulfide in the Repository

The potential sources of sulfide in the repository environment may include (i) groundwater, (ii) microbial activity, and (iii) minerals in the buffer and host rock.

2.4.1.1 Groundwater

In contrast to Sweden and Finland, the groundwater sulfide concentration in potential Canadian DGR locations is considerably low (King et al., 2017). The current reference base value for the dissolved sulfide content in crystalline or sedimentary rock formation (under consideration for Canadian DGR) is 34 ppb, or 1 μmol/L, respectively, with 88 ppb being the highest value observed (Hall et al., 2020).

2.4.1.2 Microbial activity

Given the negligible sulfide concentration in the groundwater, the principal source of sulfide in the Canadian DGR would be the activity of sulfate-reducing bacteria (SRB) (Hall et al., 2020). Under anaerobic conditions, which are expected in the late stage of the DGR, SRBs can contribute to the microbiologically-influenced corrosion (MIC) of the UFC copper surface in two ways: i) ‘near-field’ production of sulfide (i.e. within a biofilm at the copper/bentonite interface or within the bentonite and ii) ‘far-field’ production of sulfide within the rock mass or at the rock/bentonite interface (Hall et al., 2020).

A sufficiently high concentration of dissolved sulfate anions has been found in Canadian groundwater in crystalline (1243 mg/L) and sedimentary host rocks (440 mg/L) (Hall et al., 2020). In addition, the host rock may contain sulfate minerals, such as: gypsum ($CaSO_4$), celestite ($SrSO_4$) etc. SRBs use the sulfate anions as electron acceptors, and the nutrients

available from the organic matter in the clay/rock, methane, higher alkanes and hydrogen gas as electron donors (Cloet et al., 2017; Wersin et al., 2014). Under favourable conditions, the SRBs will reduce the dissolved sulfate, and as a result, bisulfide (HS^-) may be produced as shown in the following equation (considering H_2 as an electron donor) (Cloet et al., 2017).

$$SO_4^{2-}(aq) + 4H_2(aq) + H^+(aq) \rightarrow HS^-(aq) + 4H_2O \quad (2.21)$$

The metabolic activity of the SRBs and subsequent production of HS^- in the buffer or the host rock is governed by the availability of nutrients (electron acceptors and electron donors), adequate pore space, and water activity (Cloet et al., 2017). If any of these conditions are prohibited, microbial activity will likely cease. During the transient unsaturated phase of the repository, the water activity in the buffer will be too low to sustain microbial activity. In addition, when the HCB is fully saturated, the resulting swelling pressure will reduce the pore size and thus restrict microbial activity (Cloet et al., 2017). Based on experimental studies, the HCB buffer in Canadian DGR is designed with an average dry density ≥ 1.6 g/cm^3 so that its low water activity (< 0.96) and high swelling pressure (> 2.0 Mpa) will suppress microbial activity and thereby, no sulfide production due to microbial activity is likely to occur within the HCB buffer material (Hall et al., 2020). However, some SRB activity may still occur at the rock/bentonite interface, in the excavation damaged zones (EDZs) of the host rock, and in the rough floors, walls, and ceilings of the repository, as there will be enough water activity, pore spaces and nutrients available for microbial growth. In addition, the SRB activity in remote cracks and fissures of the host rock may also introduce dissolved sulfide into the system. (Hall et al., 2020).

2.4.1.3 Minerals in the buffer

Several studies have suggested that the MX-80 bentonite buffer contains traces (0.5-0.6 %) of sulfide, mainly in the form of pyrite (FeS_2). This iron-sulfide mineral is very stable under anoxic conditions but may still introduce low concentrations of dissolved sulfide (< 10^{-8} M) into the system (Wersin et al., 2014). The buffer also contains low concentration (0.5 – 1.3 %) of sulfate mineral, mainly gypsum ($CaSO_4$). Owing to the high solubility of gypsum, sulfate may readily be released into the buffer pore water and may diffuse into the rock (Wersin et al., 2014). Since the microbial activity within the HCB buffer is highly constrained (see section above), the possibility of microbial reduction of the sulfate while transporting to the rock is negligible. However, under

suitable conditions in the host rock near the buffer/rock interface, the sulfate may be microbially reduced to sulfide, which may diffuse back into the buffer (Wersin et al., 2014). Hence, the sulfate inventory in the bentonite buffer should also be considered as a possible source of sulfide in the DGR environment.

2.4.2 Fate and Transport of Sulfide in the Repository

The transport of dissolved sulfide species toward the UFC surface will be diffusion-dominated because of the low hydraulic conductivity of the highly compacted bentonite buffer. However, hydrogen sulfide is a highly reactive compound. Therefore, during diffusion, chemical reactions can partly immobilize it in the buffer, which may limit the sulfide flux towards the UFC. According to literature (Cloet et al., 2017; Pedersen et al., 2017; Rickard & Luther, 2007; Wersin et al., 2014), the key immobilization mechanism will be the oxidation-reduction (redox) reaction of HS^- with the ferric iron (Fe^{3+}) or ferrous iron (Fe^{2+}) present in the buffer, and the resulting precipitation of ferrous sulfide (FeS) and elemental sulfur (S(0)) by the following reactions (Hansel et al., 2015; Pedersen et al., 2017):

$$HS^- + 2Fe^{3+} \rightarrow 2Fe^{2+} + \mathrm{S}(0) + H^+ \quad (2.22)$$

$$HS^- + Fe^{2+} \rightarrow FeS + H^+ \quad (2.23)$$

Overall reaction, $2HS^- + 2Fe^{3+} \rightarrow Fe^{2+} + \mathrm{S}(0) + FeS + 2H^+$ (2.24)

The concentration of sulfide reaching the UFC will, therefore, depend on sulfate reduction rate by the SRBs, geochemical conditions (e.g. pH), the availability of Fe(II) from the dissolution of Fe-containing minerals (e.g. Fe oxyhydroxides, siderite, chlorite, biotite) and the solubility of iron sulfides. In aqueous solutions at ambient temperature, iron sulfide precipitation first occurs in the form of a brownish, tetragonal-shaped, iron (II) monosulfide known as mackinawite (FeS), which is subsequently transformed to more insoluble compounds such as Greigite (Fe_3S_4), and pyrite (FeS_2) (Cloet et al., 2017). Greigite (Fe_3S_4) is a tetrahedral and octahedral mixed sulfide which forms from mackinawite and can subsequently convert to pyrite (Rickard & Luther, 2007). Because of their similar structures, mackinawite can convert into greigite via a solid-state mechanism depending on geochemical conditions such as pH and polysulfide concentration. Pyrite (FeS_2) is, the most stable iron sulfide formation with a NaCl type cubic structure, which

may form from mackinawite and greigite via a dissolution/ precipitation process instead of a solid-state process (Cloet et al., 2017). The polysulfide reaction pathway of pyrite formation from mackinawite is as follows:

$$FeS + S(0) \rightarrow FeS_2$$

From the kinetic assessment of the dissolution-precipitation reaction, the study of (Benning et al., 2000) suggests that the precipitation of mackinawite is fast with an estimated rate of 7×10^{-9} mol/(L·s) or 0.22 mol/(L·year). Depending on the concentrations of mackinawite and H_2S or HS^- (in cases where S(0) is very small), precipitation of pyrite may proceed with estimated formation rates in marine sediments of $10^{-8} – 10^{-3}$ mol/(L year) or $3 \times 10^{-10} – 3 \times 10^{-5}$ mol/(g dry sediment year) (Cloet et al., 2017). However, the above mentioned solubility constants and kinetic rates are usually complex to apply in modelling of sulfide transport because it requires knowledge of pH, redox condition, FeS and S(0) concentrations in the repository context. The parameters can be estimated, but their actual values might be subject to change over the geochemical evolution of the near-field (Cloet et al., 2017).

Retention of sulfide onto bentonite is expected to reduce its migration toward the UFC canisters. However, the reduction of structural Fe^{3+} to Fe^{2+} may present challenges, as Fe^{2+} can have a destabilizing effect on montmorillonite. While the extent of montmorillonite alteration may not seriously affect the safety-relevant features of the bentonite backfill, it is rational to consider the extreme case of a complete transformation of montmorillonite to Fe-rich smectites, 7Å-minerals, or chlorite, which may impact the properties of the buffer (Lanson et al., 2005). As a replacement for montmorillonite, Fe-smectites can either increase or decrease hydraulic conductivity. The swelling capacity may also decrease, making it challenging to close cracks in the buffer through self-sealing. Although, negligible change in sorption capacity is expected due to alteration of montmorillonite, radionuclide retention may be reduced by sorption competition with Fe. Also, cation exchange capacity could reduce (Lanson et al., 2005). Montmorillonite transforming into Fe-smectites will not affect buffer density or colloid transport. But, if it transforms into minerals such as 7Å and chlorite, it may change the pore structure and harm the buffer's colloid prevention capacity.

2.5 Research Questions

MIC is an important component of possible corrosion processes that could occur in the DGR. As bentonite is the main component of the EBS, the role of bentonite as a sink to immobilize the sulfide as solid iron sulfides has been the subject of several studies (Maanoja et al., 2020; Miettinen et al., 2022; Wersin et al., 2014) as discussed in the previous section. However, only a few studies have quantified the capacity of bentonite to sorb HS^-. It has been found that bentonite exhibits significant adsorption capacity for hydrogen sulfide (H_2S) gas, particularly when bentonite was modified with iron (Fe) and copper chloride (Nguyen-Thanh et al., 2005; Stepova et al., 2009). In addition, Pedersen et al. (2017) reported the sulfide immobilization capacity of different types of bentonite clays (i.e., Wyoming MX-80, Asha, and Calcigel) was in the range of 40–90 μmole H_2S g^{-1} clay. However, the capacity was determined within a pH range of 1 to 7, where the sulfide was present in the form of H_2S. As such, a knowledge gap remains in estimating the sorption capacity of bentonite when HS^- becomes the dominant sulfide species (i.e., above pH 7). Another experimental study on MX-80 bentonite and sulfide solutions conducted by Swedish Nuclear Fuel and Waste Management Company observed a decrease in concentration of the sulfide added to the solution due to presence of bentonite (Svensson & Wikberg, 2017). That study suggested that sulfide-bentonite interaction seemed to proceed quickly (within 1–2 hours), and sulfide seemed to be removed in the range of 1–10 kg per 1000 kg of bentonite (Svensson & Wikberg, 2017). However, this study did not provide insight into the sulfide loss mechanism (e.g., absorption/transformation/reaction), and a key knowledge gap persists. While the reactions with Fe could be the dominant mechanism driving HS^- sorption onto bentonite, Hadi et al. (2023) revealed that only these reactions (i.e. Eqs. (2.22-2.24) did not account for all sulfide sorbed by bentonite in their study. Hadi et al. (2023), therefore, suggested that other concurrent processes should be considered to predict total HS^- sorption onto bentonite accurately. However, the other processes governing HS^- sorption onto bentonite have not yet been elucidated.

Based on the literature review conducted so far, it appears that there is a shortage of effective experimental procedures that can be directly applicable for studying the sorption of HS^- in the laboratory. These methods should have a suitable range of different conditions, such as contact time, L:S, and HS^- concentration, to allow for accurate exploration of HS^- sorption behaviour. To

this end, Chapter 3 of this study has addressed this concern and conducted several preliminary experiments to determine a workable range of the selected experimental conditions.

In addition, little is known about HS^- sorption dynamics such us, kinetics, isotherm, and thermodynamics as well as the sensitivity to various experimental conditions (e.g., temperature, contact time, L:S, HS^- concentration) on the sorption dynamics has not been thoroughly investigated. Chapter 4 has addressed this knowledge gap by performing a series of batch experiments and interpreting the results by various established kinetic and isotherm models.

Although surface complexation formation (i.e., inner and outer-sphere complexations, discussed in Section 2.3.2) is widely used to describe the pH and ionic strength effects on anion adsorption onto bentonite, no such study has yet investigated the possibility of HS^- adsorption by surface complex formation on the edge sites of montmorillonite. More broadly, the influences of pH and ionic strength on HS^- sorption onto bentonite are not thoroughly understood. Moreover, there is a knowledge gap in understating the nature of HS^- sorption onto bentonite (i.e., whether it is a reversible physisorption or, irreversible chemisorption or a combination of both). Chapter 5 of the study addresses this lack of knowledge by performing sorption-desorption experiments and surface analysis as a function of crucial geochemical factors of the DGR, including pH and ionic strength.

Quantifying and predicting the sorption processes by experimental methods are challenging because, in most cases, the sorbed chemicals represent only a negligible fraction of the total soil mass. Moreover, as soils contain several different surfaces and solid mineral phases, multiple sorption processes may co-occur. Therefore, mechanistic sorption models (e.g., thermodynamic sorption model) are often used to explain sorption experiment results and provide insight into the processes occurring at the solid-solution interface (Strawn, 2021). However, no numerical models have yet been developed that can be used to interpret and predict HS^- sorption mechanisms onto bentonite under a wide range of geochemical conditions. Chapter 6 of the study bridges this critical knowledge gap.

2.6 Summary

This chapter reviewed pertinent literature on four critical components of the research. (i) the mineralogy, physical properties and application of "**bentonite clay,"** an essential component of

the engineered barrier in the DGR, (ii) the design concept of "**DGR,"** its geochemical evolution and the expected impacts on the contaminant transport, (iii) "**sorption**" and the crucial factors influencing the sorption capacity and (iv) "**sulfide**" source and transport in the DGR environment. This chapter also highlighted the existing research gaps, which are addressed in the subsequent chapters of the thesis. Overall, this chapter is an essential guide for comprehending the critical aspects of the research and its significance.

CHAPTER 3
METHODOLOGY DEVELOPMENT AND PRELIMINARY EXPERIMENTS

3 Chapter Overview

The chapter is organized into seven sections. Section 3.1 highlights the study objective, followed by Sections 3.2 and 3.3 briefly discussing the experimental method and material selected for the study. Section 3.4 details the methodology development work, followed by Section 3.5 discussing the quality control approaches followed in the study. Section 3.6 discusses the outcome of the preliminary experiments conducted to select the suitable experimental conditions. Finally, Section 3.7 concludes the chapter.

3.1 Study Objective

The main goal of this chapter is to establish the most suitable practices for investigating HS^- sorption through laboratory experiments. As a part of the study, preliminary experiments were conducted to determine the ideal range of experimental conditions, which greatly helped in building confidence in the experimental procedure and design experiments that met the overall research objectives. The chapter's findings provide essential information on the sorption experimental process, which could be helpful for other environmental research inquiries.

3.2 Selection of Experimental Method

The conventional batch experiment was selected for the study since it is an established method for assessing the sorption capacity of soils used by others (Gupt, Yamsani, Prakash, et al., 2019; Xu et al., 2008; S. Yang et al., 2009; Zhao et al., 2008) and can be performed under a wide variety of experimental conditions. The simple methodology, low cost, and time requirements in the batch experiments allows for the inclusion of more than one variable in the experiments and to observe the simultaneous influence of these variables on the sorption phenomenon. Therefore, batch experiments may give insight into the sensitivity of the measured sorption parameters (e.g., sorption%, sorption capacity, kinetics) to the changing experimental conditions, which in turn, provides useful information on how the sorption capacity of bentonite buffer may change in

response to the changing DGR conditions. Although the fundamental design of batch experiments requires the use of dispersed bentonite, which may not provide a realistic simulation of the compacted system of the DGR condition, it may indicate the maximum extent of sorption achievable onto bentonite. Furthermore, batch test results can be incorporated to develop a mechanistic sorption model (e.g. a thermodynamic sorption model) which can then be used to interpret the sorption process and extrapolate the limited data set to a wide variety of chemical conditions.

3.3 Study Material

Wyoming MX-80 bentonite, supplied by NWMO, was used for performing the batch experiments. NWMO has chosen this type of bentonite, produced by Colloid Environmental Technologies Company (CETCO), to be used for the buffer and gap fill materials in the DGR due to its swelling potential and low hydraulic conductivity. Table 3.1 presents some important mineralogical and physical properties of MX-80 bentonite adopted from NWMO technical reports (D. Dixon et al., 2018; D. A. Dixon, 2019) .

Table 3.1 Mineralogy and physical properties of MX-80 bentonite (D. Dixon et al., 2018; D. A. Dixon, 2019)

Characteristics of smectite					
Amount of smectite (wt %)	**Interlayer cation**	**Cation exchange capacity (meq/100 g)**	**Surface area (m^2/g)**	**Layer charge**	
~85-90% montmorillonite	Na	69.6	30.03	0.28	
Accessory minerals (wt %)					
Mica	**Feldspar**	**Quartz**	**Calcite**	**Pyrite**	**Gypsum**
2.8-3.8	4.5	5-6	0.3-1.4	0.6	0.4

3.4 Methodology Development

A batch experiment is a commonly used method for estimating sorption. However, limited research has been conducted to explore HS^- sorption using this method. As a result, several challenges were faced while applying this method in the laboratory. The study adhered to the conventional steps in a batch experiment yet made some improvements in every step, aiming to

identify the most effective approach for achieving creditable results. The experimental procedures developed in the laboratory setup are discussed in this section.

3.4.1 Bentonite Stock Solution Preparation

In batch experiments, the first step generally is to prepare the sample by dispersing a required amount of soil in a solution containing the analytes of interest. Liquid to solid ratio (L:S) is thus an important parameter for batch experiments to measure the sorption capacity. For this study, 50 mL centrifuge tubes were chosen to prepare the samples. However, accurately weighing bentonite powder for each 50 mL sample was difficult and time-consuming, especially when a large number of samples needed to be prepared. To speed up the sample preparation process, a high-concentration bentonite slurry was prepared beforehand, from which the samples could be prepared easily by pipetting the required amount of bentonite solution into the centrifuge tubes and diluting to the intended L:S.

In this study, the bentonite slurry was prepared by mixing MX-80 powder bentonite (supplied by NWMO) in deoxygenated water at L:S = 20 (this ratio was found suitable for preparing the slurry based on trial experiments using L:S=10 and 20 in the laboratory). However, preparing this high-concentration bentonite slurry was challenging because of the high swelling capacity of bentonite (i.e., it adsorbs a high amount of liquid upon dispersion). In addition, breaking bentonite agglomerates uniformly required highly intense mixing forces, owing to the powerful bonding and van der Waals forces involved. Initially, bath sonication (using VWR Symphony 97043-936 Ultrasonic Cleaner) was applied to prepare the bentonite slurry. However, this process did not ensure homogenous dispersion of bentonite. Instead, conglomerated lumps and precipitation of bentonite were observed (as shown in Figure 3.1(a)).

To overcome this challenge, ultrasound probe sonication (using Qsonica Q700, 700 watts) was used. Applying the probe sonication for 1 hour at 40% amplitude helped deagglomerate the bentonite particles and thus, prepare a homogenously dispersed bentonite slurry with no lumps and precipitation (Figure 3.1(b)). This way, the samples could be prepared easily by pipetting the required amount of bentonite solution into the centrifuge tubes and diluting to the intended L:S.

(a)

(b)

Figure 3.1 Bentonite slurry preparation (a) after bath sonication: lumps and precipitation of bentonite were observed (b) after ultrasound probe sonication: no lumps and precipitation of bentonite were observed.

3.4.1.1 Checking and adjusting L:S:

To ensure consistency during the tests, extra attention was paid to maintaining a consistent L:S during sample preparation. Although the stock bentonite solution (as mentioned earlier) was prepared targeting a particular L:S, it was necessary to check if the actual L:S was the same or close to the value as intended. To do this, two to three aluminum dishes were filled with 10 mL of bentonite solution (pipetted from the stock solution) and kept in an oven for 24 hours to completely dry at 100°C (see Figure 3.2 (a) and (b)). The amount of solid bentonite in each 10 mL solution was then determined by subtracting the weight of the empty dishes from the weight measured after the oven-dry of the bentonite solution. The average of two/three measurements

was then used to determine the actual L:S ratio. For example, if the average oven-dried weight of bentonite measured from three 10 mL solutions was found to be 0.48 g, then the actual L:S would be = $\frac{10}{0.48} = 20.83 \approx 21$ instead of the desired L:S=20. It was assumed that the density of the solution was that of water and as such, the mass of 1 mL solution was assumed to be 1 g.

The process of estimating the actual L:S was followed every time the bentonite stock solution was prepared for any experiment. Based on the actual L:S, the amount of bentonite solution required to pipette from the stock during sample preparation was calculated (sample preparation procedure is discussed in Section 3.4.3).

(a) **(b)**

Figure 3.2 Estimating L:S of the bentonite stock solution (a) before oven-drying (b) after oven-drying.

3.4.2 HS^- Stock and Standard Solutions Preparation

All HS^- stock and standard solutions were prepared following the standard method 4500-S^{2-} A (APHA, 2017), by dissolving sodium sulfide nonahydrate ($Na_2S \cdot 9H_2O$, MilliporeSigma, ≥ 99.99% purity) salt in deoxygenated water (dissolved oxygen removed by N_2 infusion) at the desired concentration. The standard procedure for deoxygenating the water is described in APPENDIX A.

3.4.3 Sample Preparation

After preparing the stock solutions, all samples were prepared in 50 ml glass centrifuge tubes by filling half of the tube (25 ml) with bentonite solution (pipetted from the L:S=20 stock and diluted with deoxygenated water to double the required sample concentration) and the remaining

volume was filled with the HS^- solution of double the required HS^- concentration. An example sample preparation for achieving a L:S of 100 and HS^- concentration of 1 mg/L is illustrated in Figure 3.3.

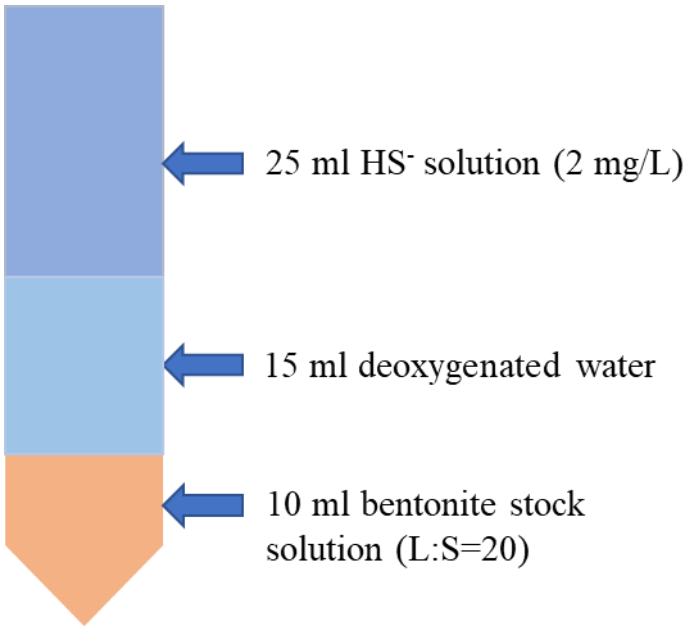

Figure 3.3 Example sample preparation to obtain L:S=100 and HS^- concentration = 1 mg/L

3.4.4 Shaking

After sample preparation, the centrifuge tubes were shaken until the sorption equilibrium (i.e., an equilibrium between the sorbed phase and aqueous phase concentration) was reached (time to equilibrium varied, see Section 3.6.3). A rotary shaker (MX-RD-Pro, SCILOGEX) was chosen, which achieved uniform mixing of bentonite with the HS^- solution without any settling.

3.4.5 Centrifugation

After shaking, the solid and aqueous phases required to be separated by centrifuging the solutions. For this purpose, the ALLEGRA X-14 SERIES centrifugation machine was used. Several trials were done to find the appropriate centrifugation speed and time and it was found that centrifuging for 30-90 minutes at 3500 rpm resulted in an effective separation of the solid bentonite from the solution prepared at various L:S values (e.g., 50-1000). Samples with lower L:S values required longer centrifugation time due to higher bentonite content (e.g., samples with L:S of 50 required 90 minutes whereas L:S of 1000 required 30 minutes). In addition, best practices for the safe and efficient operation of the centrifugation machine were followed

including (i) balancing the tubes by mass, not volume (ii) loading tubes symmetrically across the pivotal axis of the machine, and (iii) using “dummy” tubes if necessary for balancing loads.

3.4.6 Filtration

After centrifugation, the aqueous phases were filtered to minimize the interference from the colloidal bentonite. Among various filters available, hydrophilic polytetrafluoroethylene (PTFE) syringe filters (Fisher Scientific) were found chemically compatible with HS^- and therefore, were selected for the study. A 25 mm diameter filter size was selected based on the solution volume of 50 mL. Initially 0.2 um pore-sized filters were tried, however, this size proved to be difficult and inefficient as it required a long time, high pressure and frequent filter changing. The process was optimized by filtering in two stages, i.e., first with 1.2 µm and then with 0.2 µm filters. This two-stage filtration method made the process faster and more efficient.

3.4.7 Determining HS^- Concentration

The study measured the HS^- concentration in the aqueous phase using the standard methylene blue method (4500-S^{2-} D) with a spectrophotometer (Hach DR 3900, Hach) at a wavelength of 665 nm (APHA, 2017). The colorimetric method was chosen because it is a well-established, and low-cost method that can be applied across a wide range of sulfide concentrations.

Following standard procedures (USEPA, 2016) the method detection limit (MDL) (i.e., the minimum concentration measured with 99% confidence) was determined, and calibration of the spectrophotometer was performed. The estimated MDL for HS^- was 0.02 mg/L. Figure 3.4 presents a sample calibration plot prepared for the spectrophotometer used in the study.

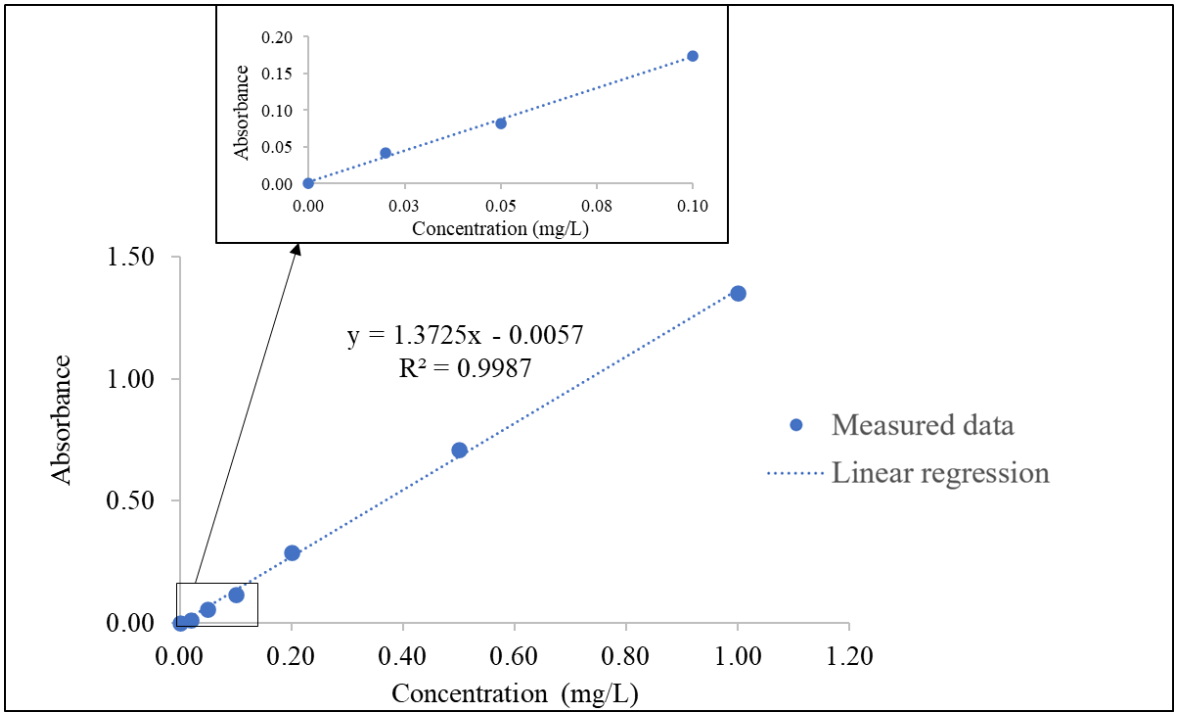

Figure 3.4 Calibration plot for the spectrophotometer (Hach DR 3900, Hach) used for methylene blue analysis

The coefficient of linear regression (R^2) demonstrated a high confidence level in the calibration process. The inset emphasizes the reliable performance at low HS^- concentrations (< 0.1 mg L-1). All data points presented are the average of two repeated measurements, with error bars indicating the range (error bars are not visible due to minimal difference).

The standard procedures of the methylene blue method and MDL calculation are briefly described in APPENDIX A.

3.5 Quality Assurance and Quality Control (QA/QC)

Quality assurance and quality control (QA/QC) measures are essential components of experimentation that are widely used for determining the precision and accuracy of experiment results and controlling data quality within acceptable limits.

As discussed in the previous section, the methodology of the batch experiments includes some steps for sample preparation and analytical measurement, such as weight and volume measurement for preparation of HS^- and bentonite stock solution, pH measurement, HS^- concentration measurement by spectrophotometry (methylene blue method) etc. This section discusses essential QA/QC activities

that were performed to achieve reproducible and acceptable results from the experiments. The procedures discussed were adopted from published literature (Bell, 2004; Krechmer, 2016; Taylor, 1981; Vardeman, 2005).

3.5.1 QA/QC Approaches Relevant to Experiments

To meet the criteria of data quality prescribed in the approved methods and to ensure the consistency of the data generated, the following QC procedures were applied in each experiment:

3.5.1.1 Blank analysis:

(i) Method blank/reagent blanks

Method blanks/reagent blanks are analyte-free samples that were prepared using the same reagents, glassware, and instrumentation but without any HS^- and bentonite. Analysis of the method blanks allowed for detecting and correcting systematic errors due to impurities in the reagents, contaminated glassware, etc. Method blanks were used to zero the measuring instruments (e.g., the spectrophotometer), determine the method detection limit (MDL) and perform an internal quality control check.

(ii) Experiment blank analysis

For each experimental condition, two types of experimental blanks were analyzed: type (*i*) with HS^- but no bentonite and type (*ii*) with bentonite but no HS^-. Type (*i*) blanks were used to determine the loss of HS^- due to experimental effects other than sorption onto bentonite (e.g., adsorption of HS^- on the centrifuge tube walls). In addition, type (*ii*) blanks were used to measure the background absorbance resulting from the combined effect of bentonite particle (< 0.2 µm) interference and the presence of background HS^- in bentonite (type (*ii*) blank analyses are discussed in detail in Section 3.6.2). If the type *(ii)* blank value was detected at a value more than the MDL, it was subtracted from the concentration determined from test samples.

3.5.1.2 Triplicate and replicate analysis

To evaluate the precision of the experiment results, triplicate and replicate analysis was performed for all experiments. In triplicate analysis, three samples were prepared using the same procedures and tested separately, while in replicate analysis, a single sample was tested twice within the batch.

3.5.2 QA/QC Approaches in Sample Preparation and Analytical Measurements

- All glassware were acid-soaked and rinsed with deionized water before and after use.
- All sample preparation and analysis were performed following standard operating procedures (APPENDIX A).
- All the stock, sample, and blanks were prepared in an anaerobic glove box (Coy laboratory products) to simulate the anoxic conditions expected in the DGR and to minimize the loss of HS^- due to oxidation. In addition, filtration and methylene blue analysis were carried out inside the glove box.
- The oxygen level in the globe box was regularly monitored, and necessary maintenance work was performed, such as regularly changing the catalysts and replenishing the hydrogen level with a gas mix (5% hydrogen and 95% nitrogen) to maintain the anaerobic environment.
- The bentonite and HS-stock solutions were stored in the anaerobic glove box with minimum headspace for no longer than one week after preparation.
- To ensure the reliability and accuracy of the instrumental performance, all equipment (pH meter, weight balance, spectrophotometer, etc.) was regularly calibrated following standard calibration procedures.
- To check whether the HS^- concentration measurement process was under statistical control over time, a control chart with control limits set at +/- 3 standard deviation (σ) was used for each experiment. Figure 3.5 demonstrates a control chart developed using 1 mg/L standard HS^- solution data collected on 17 consecutive days. The use of the control chart during every experiment helped monitor whether a recalibration needed to be performed.

If any measured value was found above the upper control limit or below the lower control limit, it was discarded from the analysis, and necessary corrective actions (e.g., preparing a new sample, recalibration of the instruments) were taken to keep the process “in control.”

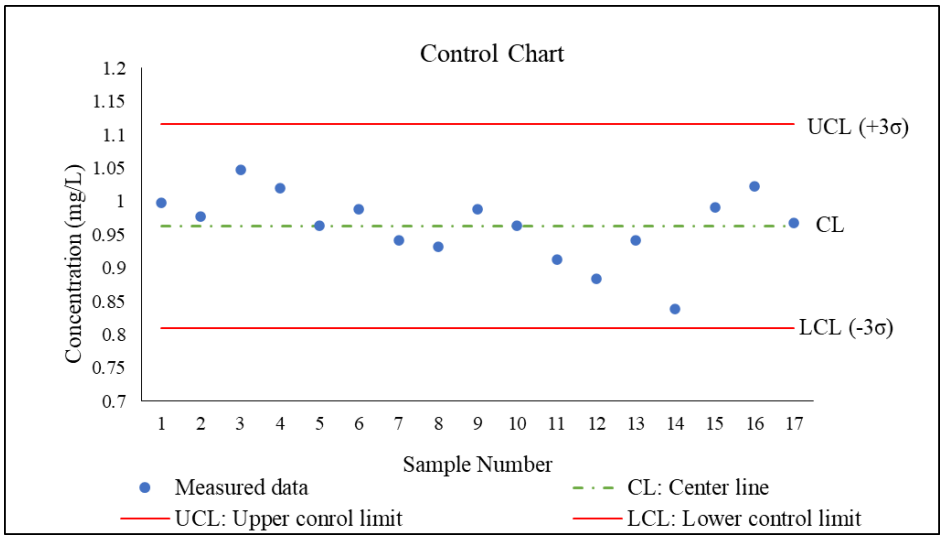

Figure 3.5 Control chart developed for monitoring the HS^- concentration measurement process.

3.6 Preliminary Experiments: Experimental Conditions Selection

Based on the review of literature (discussed in Section 2.3.3 in Chapter 2), six factors have been primarily selected for this study to explore HS^- sorption onto bentonite. The selected factors included: (i) contact time (ii) temperature (iii) L:S (iv) initial HS^- concentration (v) pH and (vi) ionic strength of background solution. While temperature, pH, and ionic strength were selected due to relevance with the key geochemical conditions of a DGR, the other factors (contact time, L:S and initial HS^- concentration) were selected to find the appropriate range to conduct the batch experiments under the laboratory setup to provide insight into HS^- sorption mechanism.

This section discusses the results of the preliminary experiments conducted to determine certain critical experimental conditions.

3.6.1 Centrifuge Tube Material Selection

To minimize HS^- experimental loss, which is highly reactive, it was essential to choose the right centrifuge tube material. To this end, two types of centrifuge tubes: Pyrex glass and polypropylene plastic tubes (Fisher Scientific) were tested with 1 ppm type (i) blanks (i.e., only sulfide but no bentonite) at laboratory temperature (22 ± 2°C) and 40°C. When shaken for a 1 hour at 22°C, both types of tubes demonstrated a loss of HS^- in the range of 2-4%. However, the results of long-term shaking (24 hours) were quite significant, revealing a clear distinction between the two materials. Plastic tubes showed a loss of almost 50% of HS^-, and increased to

nearly 85% at 40°C. In contrast, glass tubes exhibited a much lower HS^- loss rate of 6-8% (at 22°C) and 8-10% at 40°C. These findings demonstrate that the amount of HS^- loss increases with longer shaking time and higher temperatures, and that the centrifuge tube material significantly affects this process. Based on these results, glass centrifuge tubes were chosen for conducting the batch experiments, as they effectively minimized the HS^- loss due to reaction with the tube material.

3.6.2 Liquid to Solid Ratio and Initial HS^- Concentration Selection

In this study, the primary considerations regarding the L:S and initial HS^- concentration was to maintain detectable aqueous concentrations of HS^- (i.e., well-above the MDL). As such, initial L:S of 50, 100, and 200 were selected and 5 different initial HS^- concentrations (C_i) (0.2, 0.5, 1, 3, and 5 mg/L) were used for sample preparation. For each sample, the remaining HS^- concentration (C_t) was measured after 1 hour shaking. Figure 3.6 suggests that below a C_i value of 1 mg/L, the C_t values were very close to MDL at each of the L:S values studied. However, in the case of L:S =50, C_t was close to MDL over the whole range of C_i (i.e., 0.2-5 mg/L) whereas, for L:S=100 and 200, C_t values increased with increasing C_i from 1 mg/L to 5 mg/L and were much higher than the MDL. Based on this finding, it was suggested that a minimum: (i) L:S of 100:1 and (ii) initial HS^- concentration of 1 mg/L are required to obtain detectable amounts of aqueous HS^- (C_t) after bentonite sorption.

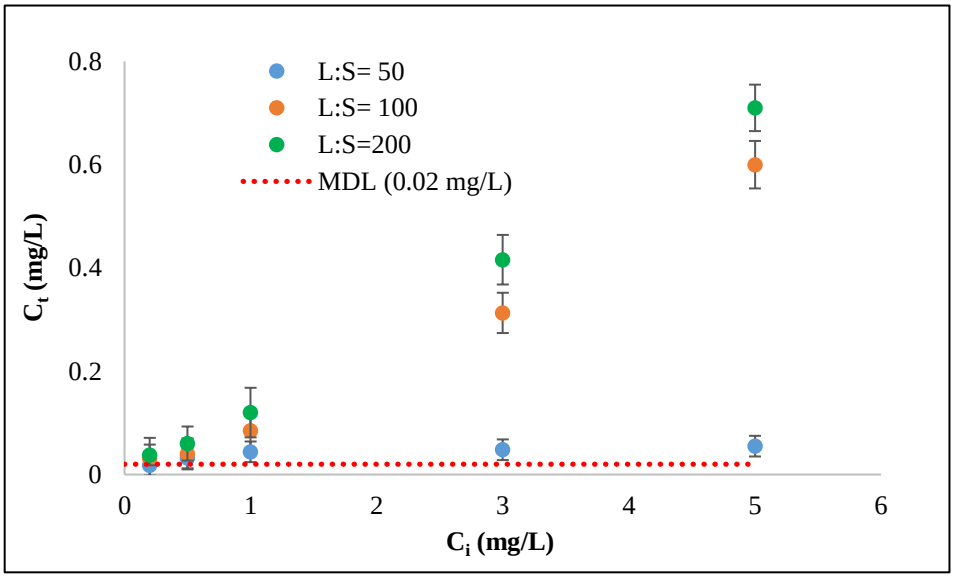

Figure 3.6 Effect of L:S (50-200) and C_i (0.2-5 mg/L) on HS^- concentration (C_t)

Another important factor to consider was the interference from bentonite particles and background HS^- with the colorimetric methylene blue (MB) analysis. To examine this interference, type (*ii*) blanks (i.e., only bentonite, no added HS^-) with different L:S (i.e., 50, 100, 200, 500, and 1000) were prepared and analyzed after centrifugation and filtration. Figure 3.7 shows that the small bentonite particles (< 0.2 µm, not removed by filtration) and background HS^- caused some interference (i.e., background absorbance), which decreased with increasing L:S. This interference from the type (*ii*) blanks was corrected for all subsequent analyses.

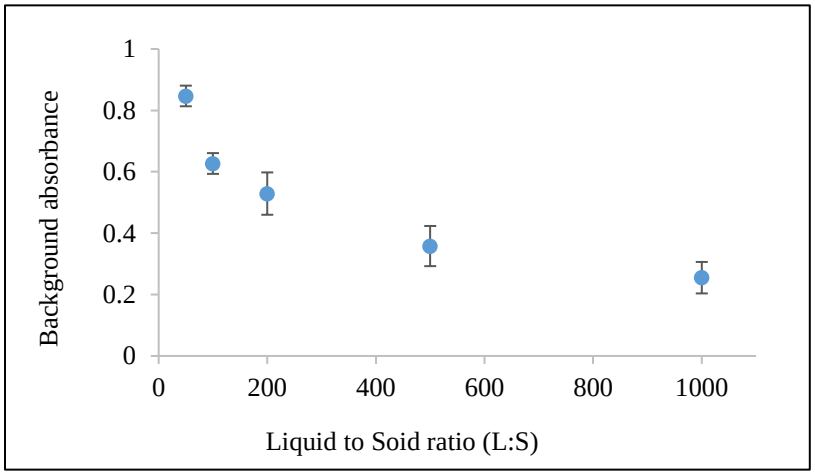

Figure 3.7 Effect of L:S on background absorbance from type (*ii*) blanks (i.e., only filtered bentonite and background HS^-). All data presented are the average of triplicate tests, with error bars showing the standard deviation.

It was also found that the type (*ii*) blank with L:S =50 developed a persistent pink colour upon adding the MB reagents after 5 minutes; in contrast, the type (*ii*) blanks with L:S = 100, 200, 500, and 1000 developed a light blue colour under the same conditions (see Figure 3.8). This distinction indicates that L:S = 50 exhibited the most incomplete reactions with the highest interference with MB analysis. However, the light blue colour observed upon adding the MB reagents in the type (*ii*) blanks (L:S = 100, 200, 500, and 1000), which progressively became lighter with increasing L:S, was a potential indication of background aqueous HS^- (see Figure 3.8). Based on these findings, L:S= 100 was chosen as the minimum ratio suitable for conducting sorption experiments to minimize all problems associated with maintaining HS^- concentrations above the detection limit and minimizing background interference.

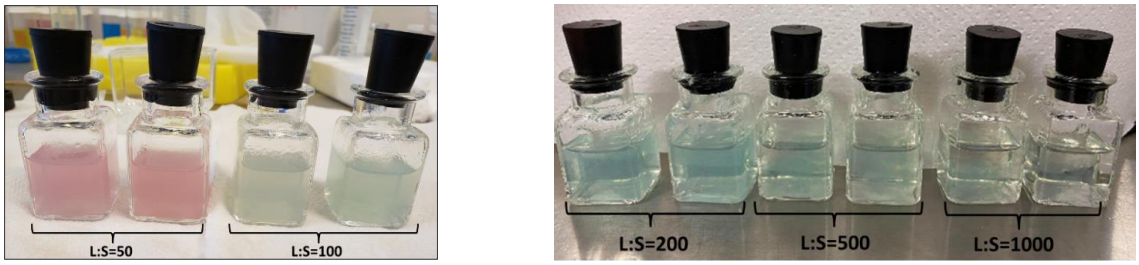

(a) (b)

Figure 3.8 Effect of L:S on color development in methylene blue analysis of blanks (only bentonite, no HS^-) (a) L:S=50 and 100; (b) L:S= 200, 500 and 1000

3.6.3 Contact Time Selection

To investigate the sorption behaviour throughout each batch experiment, it was important to identify when the process reached equilibrium. The experiment was initially conducted at room temperature (22 ±2 °C) varying the contact time over 2 hours at 15 minutes interval. The results (Figure 3.9(a)) suggest that significant sorption (around 85-90%) occurred within the first 2 hours of contact with bentonite. However, the fluctuating data points indicate that equilibrium was not reached in 2 hours and a longer time interval was required. Therefore, the contact time was increased, and data were taken after 1, 2, 4, 8, 16, 24, and 48 hours of shaking. From Figure 3.9(b), it is seen that there was a sharp rise in sorption % (85% to 94%) up to 4 hours, which gradually increased to 96% after 16 hours, and finally reached equilibrium after 24 hours (97% sorption). The results provide a preliminary estimation of the required contact time to reach sorption equilibrium at laboratory temperature (22 ± 2°C).

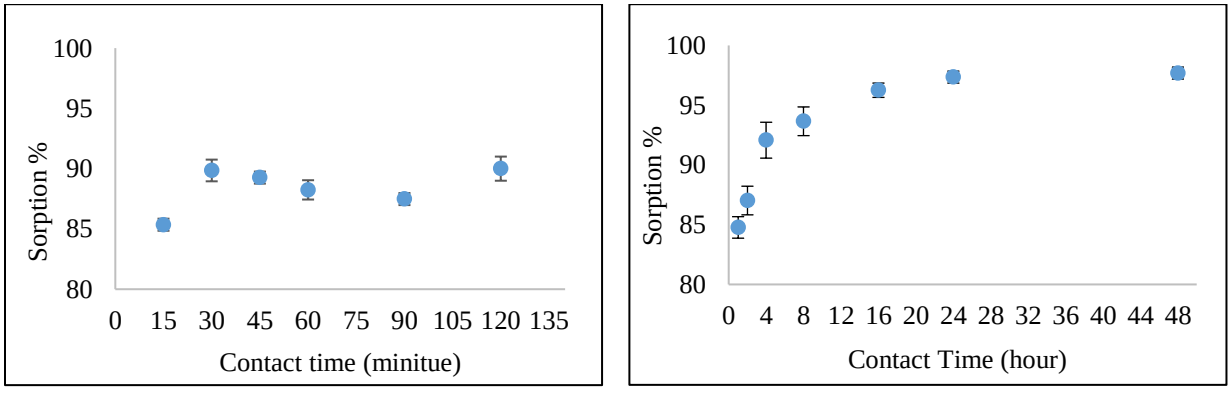

(a) (b)

Figure 3.9 Effect of contact time on sorption % using (a) up to 2 hours (b) 1 hour to 48 hours (L: S=100; Initial HS^- concentration = 5 mg/L, pH=9-9.5; Temperature= 22±2°C)

Apart from experiment results, visual observation of the MB colour changes also suggested a gradual increase in sorption with increasing contact time. Figure 3.10 shows the colour progression after 5 minutes of reaction time with MB reagents and variable hours of shaking. After 2 hours of shaking, the colour was dark blue and became lighter with increasing contact time. This colour almost faded after 24 hours of shaking (i.e., the sample and blank looked nearly the same). These visual observations support that sorption reached equilibrium after 24 hours.

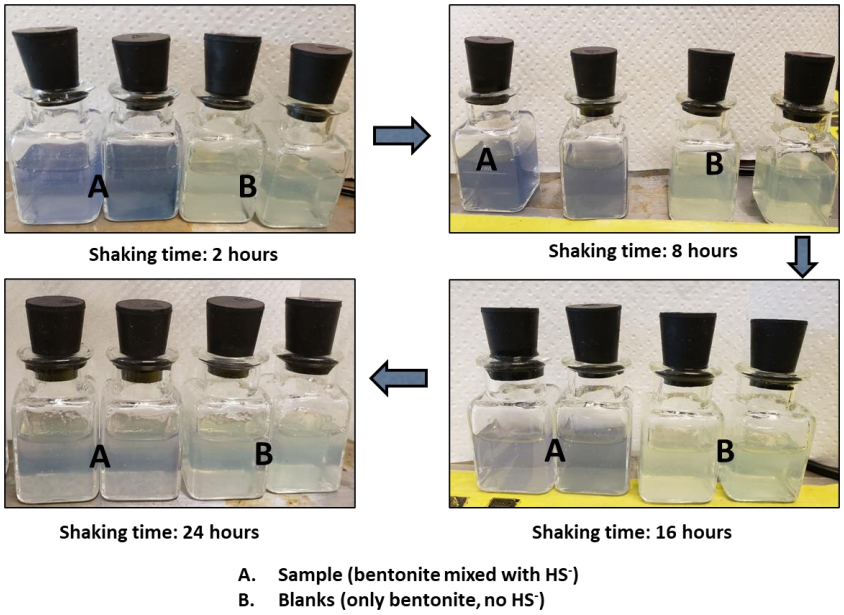

Figure 3.10 Effect of contact time on colour development in methylene blue analysis of samples (bentonite mixed with HS^-) and blanks (only bentonite, no HS^-); (L: S=100; Initial HS^- concentration= 5 mg/L, pH=9-9.5; Temperature= 22±2°C)

3.7 Summary

The chapter presented the rationale behind selecting the batch experiment and highlighted the procedures of batch and sample preparation. In addition, the methodology development work was discussed in detail, along with the QA/QC approaches followed to enhance confidence in the experimental procedure. The preliminary experiments performed indicated that experimental loss of HS^- can be minimized by using glass centrifuge tubes. In addition, a minimum (i) L:S of 100 and (ii) initial HS^- concentration of 1 mg/L is required to maintain detectable HS^- in the aqueous phase after sorption. The results also suggested that a minimum of 24 hours of shaking is required to ensure the sorption equilibrium. The study's findings were helpful in designing the batch experiments to meet research goals 2 and 3. The next chapter presents the batch experiments performed to understand the fundamentals of HS^- sorption dynamics onto bentonite.

CHAPTER 4

FUNDAMENTALS OF BISULFIDE SORPTION DYNAMICS ONTO BENTONITE

4 Chapter Overview

This chapter is divided into six sections. First, Section 4.1 highlights the study objective, followed by Section 4.2 providing an overview of the batch experiments conducted. Later, Section 4.3 discusses the experimental results, while Section 4.4 discusses possible consequences to Canadian DGR based on the experimental findings. Finally, Section 4.5 concludes the chapter.

4.1 Study Objective

Understanding the sorption behaviour of HS^- is critical in understanding the HS^- transport dynamics and in assessing the long-term safety of the DGR. As such, the study presented in this chapter investigated the sorption phenomenon of HS^- onto bentonite through laboratory batch experiments under the influence of various experimental conditions, such as contact time (1-120 hours), temperature (10-40°C), liquid to solid mass ratios (L:S) (100-1000), and initial HS^- concentration (1-6 mg L^{-1}). In addition, several established kinetic and isotherm models were applied to the experimental data to provide insight into the key processes driving HS^- sorption onto bentonite. Although the study does not aim to directly explore sorption in the compacted bentonite planned in a real DGR, it endeavours to provide key information on the fundamental aspects of HS^- sorption onto bentonite. Additionally, the sorption dynamics obtained from this study will allow researchers to accurately model the reactive transport of HS^- in the DGR.

4.2 Materials and Methods

This section provides a concise overview of the materials and methods employed in the batch experiments described in this chapter. For a more detailed account of the methodology, please refer to Chapter 3.

4.2.1 Materials

All the experiments were conducted using MX-80 powder bentonite supplied by NWMO. According to the X-ray diffraction (XRD) analysis results reported by (D. Dixon et al., 2018; D. A. Dixon, 2019), the MX-80 bentonite sample contains predominately montmorillonite (79-95%, with an average of 87%) and some other minerals such as Calcite (2.2-3.6%), Quartz (1.6-3.5%), Illite (0.3-7.1%), K-Feldspar (3-6.8%), Pyrite (0.6%), Gypsum (0.4%). In addition, some key minerology related characteristics of MX-80 include cation exchange capacity of >75 cmol(+) kg^{-1}, specific surface area of >500 m^2 g^{-1}, and specific gravity of 2.75 (D. Dixon et al., 2018; D. A. Dixon, 2019).

All solutions used in the study were prepared using ASTM Type 1 (18 MΩ-cm) ultrapure filtered and deionized (DI) water (Milli-Q® Direct 8/16, MilliporeSigma) deoxygenated by purging nitrogen gas. The water was kept for deoxygenation for 40 to 60 minutes or until the dissolved oxygen level came below 1 mg/L (See Section A 1.1 in APPENDIX A). All chemicals used, e.g., sodium sulfide salt ($Na_2S{\cdot}9H_2O$, ≥ 99.99% purity), bisulfide analysis reagents, sodium hydroxide salt (NaOH, 99.99% purity), hydrochloric acid (HCl, 36.5 to 38% assay) were analytical grade, purchased from Fisher Scientific and MilliporeSigma.

4.2.2 Sorption Experiments

As part of the literature review, four independent variables were identified by others as some of the key factors influencing the sorption dynamics on bentonite and as such, were selected for this study (Gupt, Yamsani, Prakash, et al., 2019; Xu et al., 2008; S. Yang et al., 2009; Zhao et al., 2008). These include i) contact time, (ii) temperature, (iii) liquid to solid mass ratio (L:S), and (iv) initial HS^- concentration. Table 4.1 presents an overview of three sets of batch experiments that were conducted to observe the effects of the selected factors on HS^- sorption onto bentonite and were used to determine the thermodynamic parameters. Temperature was selected as an important factor to help understand sorption kinetics and thermodynamics, and due to its relevance in the DGR. The other parameters, such as: contact time, liquid to solid mass ratio (L:S), and initial HS^- concentration were selected primarily as critical parameters to execute the batch experiments in the laboratory and to provide more information about sorption dynamics. The range of these factors were selected considering the experimental constraints and anticipated DGR conditions (see Table 4.1).

Table 4.1 Batch experiment overview

Experiment set no.	Objective(s)	Independent variables	Rationale for selecting the range of values	Constant experimental conditions
1.	▪ To observe the effect of temperature and contact time ▪ To investigate the sorption kinetics	▪ Contact time = 1-120 hours	▪ From experimental observation of the time required to reach equilibrium	▪ pH = 9.5-10 ▪ L:S = 100 ▪ Initial HS^- conc. = ▪ 5 mg L-1
		▪ Temperature = 10, 22, 30, 40˚C	▪ The Canadian DGR is anticipated to experience elevated temperatures (10-80°C) (Hall et al., 2021; King et al., 2017), which will affect sorption kinetics and thermodynamics. ▪ The range (10-40°C) was chosen based on equipment limitations.	
2.	▪ To observe the effect of L:S and initial concentration of HS^- ▪ To develop sorption isotherms (e.g., Langmuir and Freundlich isotherms)	▪ L:S = 200, 500, 1000	▪ Based on preliminary work performed to select the appropriate L:S for the study (discussed in detail in Section 3.6.2 in Chapter 3)	▪ pH = 9.5- ▪ Temp = 22±2°C ▪ Contact time = ▪ 28-30 hours
		▪ Initial HS^- Concentration = 1, 2, 3, 4, 5, 6 mg L^{-1}	▪ A minimum of 1 mg L^{-1} initial HS^- concentration was required to maintain detectable aqueous HS^- after sorption onto bentonite ▪ Samples with higher initial HS- concentration (> 6 mg L^{-1}) exhibited large measurement error.	
3.	▪ To determine thermodynamic parameters (e.g., enthalpy, entropy, Gibb's energy)	▪ Temperature = 10, 22, 30, 40˚C	As mentioned for experiment sets nos. 1 and 2	▪ pH = 9.5 ▪ L:S = 200 ▪ Contact time = 28-100 hours
		▪ Initial HS^- Concentration = 1, 2, 3, 4, 5, mg L^{-1}		

4.2.2.1 Stock solution preparation

Bentonite stock solutions were prepared for all experiments at a liquid to solid ratio (L:S) of 20 by adding required amount (12.5 g) of dried bentonite powder in deoxygenated water (250 ml) and mixing with a probe sonicator (Qsonica Q700, 700 watts) for 1 hour at 40% amplitude. The ultrasonication helped to deagglomerate the bentonite particles and to ensure a homogenously dispersed bentonite slurry.

HS^- stock solutions were prepared at desired HS^- concentrations by dissolving sodium sulfide nonahydrate ($Na_2S \cdot 9H_2O$, MilliporeSigma, ≥ 99.99% purity) salt in deoxygenated water following the standard method 4500-S^{2-} A (APHA, 2017).

4.2.2.2 Sample and blank preparation

Sample solutions were prepared in 50 mL Pyrex® glass centrifuge tubes (Fisher Scientific) by mixing the required amounts of bentonite and HS^- stock solutions and diluting with deoxygenated DI water to obtain the desired L:S and HS^- concentration (as shown in Table 4.1). The initial pH values of the samples were found in the range of 8-10. As HS^- is the dominant sulfide species at pH > 9 (Ahlatci et al., 2016; Lewis, 2010; Neto et al., 2018), the pH values of the samples were adjusted at ≈9.5 (by adding 0.1 M NaOH and/or 0.1 M HCl) to avoid loss of HS^- due to H_2S gas formation. To ensure quality of the data, all samples were prepared in triplicates.

In addition, two types of experimental blanks were prepared for each experimental conditions: type (i) with only HS^- and type (ii) with only bentonite. The blanks were used to measure and the experimental loss of HS^- other than sorption onto bentonite and background HS^- (i.e., released from the bentonite). Around 2-10% loss of HS^- was observed from type (*i*) blank analysis (type (*i*) and (*ii*) blank analyses are discussed in detail in Section 3.6 of Chapter 3).

The stock, sample, and blank solutions were prepared in an anaerobic chamber (Coy Laboratory Products) to minimize the loss of HS^- due to oxidation and to ensure anoxic conditions, as expected in the DGR.

4.2.2.3 Measuring the HS^- concentration (C_t)

After sample and blank preparation, the centrifuge tubes were placed in a tube rotator (MX-RD-Pro, SCILOGEX) and shaken at 60 rpm for the required contact time (as shown in Table 4.1). To vary the temperature, the rotary shaker was placed in a dual incubator/refrigerator (MaxQ 6000, Thermo Fisher Scientific) and the tubes were shaken at four different temperatures controlled at 10, 22, 30 and 40°C. After shaking, the solid and aqueous phases were separated by centrifuging the solutions at 3500 rpm for 30-90 minutes depending on the L:S values (see Section 3.4.5 in Chapter 3). After centrifugation, the aqueous phases were sequentially filtered with 1.2 and 0.2 µm hydrophilic polytetrafluoroethylene (PTFE) syringe filters (Fisher Scientific). Finally, the

HS^- aqueous concentration was measured using the standard methylene blue method (4500-S^{2-} D) with a spectrophotometer (Hach DR 3900, Hach) at a wavelength of 665 nm (APHA, 2017). The experiment blanks were analyzed using the same protocol followed for the test samples.

4.2.3 Determination of Sorption Parameters

4.2.3.1 Sorption% and Sorption Capacity

From the measured aqueous concentration of HS^- (C_t), the sorption percentage of initial HS^- concentration C_i (mg L^{-1}) was calculated using the following equation:

$$Sorption\% = \frac{C_{i,corr} - C_t}{C_{i,corr}} \times 100\% \tag{4.1}$$

where $C_{i,corr}$ is the corrected initial HS^- concentration (mg L^{-1}). In this study, the type (i) blank concentration at each experimental condition was used to determine $C_{i,corr}$ to account for the experimental losses of HS^- other than sorption on bentonite. C_t is the HS^- aqueous phase concentration at time t (mg L^{-1}). The absorbance from type (ii) blank was subtracted from C_t to account for the interference from small bentonite particulates and background HS^-.

In addition, sorption capacity, (i.e., mass of HS^- sorbed per unit mass of bentonite) at any time (t), q_t and at equilibrium, q_e were calculated using the following equations:

$$q_t = \frac{(C_{i,corr} - C_t)V}{m} \tag{4.2}$$

$$q_e = \frac{(C_{i,corr} - C_e)V}{m} \tag{4.3}$$

Where C_e is the HS^- aqueous phase concentration at equilibrium (mg L^{-1}). V is the solution volume (ml), and m is mass of bentonite (g). The masses of the liquid and bentonite define the liquid to solid mass ratio (L:S) in each experiment (as described in Chapter 3).

4.2.3.2 Kinetic, isotherm and thermodynamic parameters

To investigate the rate-limiting mechanisms and the nature of HS^- sorption onto bentonite, three different kinetic models were explored: (i) Pseudo–first-order (PFO), (ii) Pseudo–second-order (PSO), and (iii) Weber's intraparticle diffusion (IPD) model. While PFO and PSO models

assume chemisorption to be the rate-limiting mechanism, the Weber and Morris kinetic model is applicable if intraparticle diffusion limits the rate of the sorption (Ho & Mckay, 1998; Rani & Mahajan, 2016; Tsibranska & Hristova, 2011). In addition, two common isotherm models were explored: (i) Langmuir and (ii) Freundlich models. The Langmuir isotherm model describes monolayer sorption occurring on distinct localized sorption sites with uniform energies, whereas the Freundlich isotherm describes multilayer sorption occurring on heterogeneous surfaces and active sites with different energies (Edet & Ifelebuegu, 2020). The corresponding equations (Eqs. (2.7-2.13)) and implications of the kinetic and isotherm models are discussed in detail in Sections 2.3.4 and 2.3.5 of Chapter 2.

In addition, the thermodynamic parameters were determined following the Eqs. (2.5-2.6) as presented in Section 2.3.3 of Chapter 2.

4.3 Results and Discussion

4.3.1 Effect of Contact Time and Temperature

The resulting sensitivities in HS^- sorption capacity of bentonite with contact time and temperature from Experiment set 1 (Table 4.1) are presented in Figure 4.1. The sorption % results are presented in Figure A.1 in APPENDIX A.

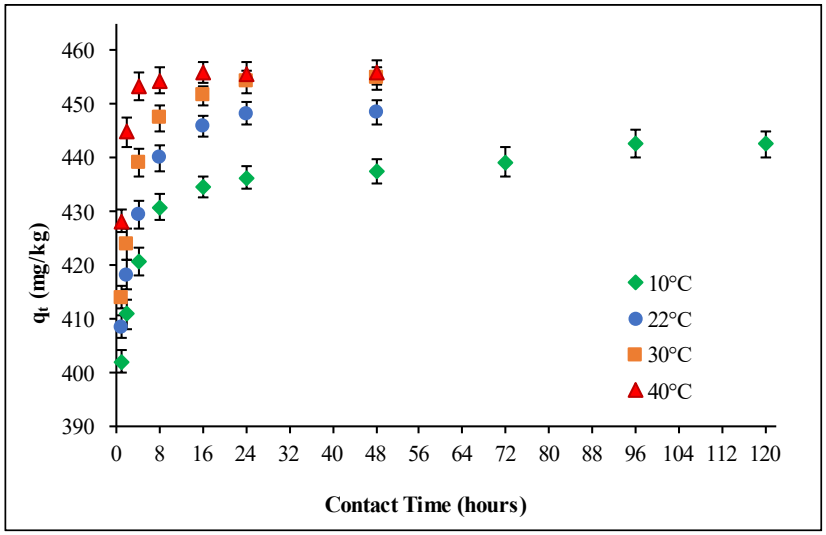

Figure 4.1 Effect of contact time and temperature on sorption capacity, q_t (mg kg^{-1}) related to HS^- sorption on bentonite (experimental conditions: L:S = 100, C_i = 5 mg L^{-1}, pH = 9.5). All data presented are the average of duplicate or triplicate tests, with error bars showing the standard deviation.

Figure 4.1 suggests that similar sorption behaviour was observed for temperatures of 22, 30, and 40°C. At these temperatures, the sorption capacity increased sharply until 8 hours, and then gradually approached equilibrium in 24 hours at 22 and 30°C, and in 16 hours at 40°C. In contrast, slower sorption was observed at 10°C and a much longer contact time (i.e., around 96 hours) was required to reach equilibrium at this lower temperature.

As shown in Figure 4.1, the sorption capacity values at equilibrium conditions slightly increased from 442.5±1.71 to 455.8±0.85 mg kg-1 (about 3% increment) with increasing temperature from 10 to 40°C. To investigate whether this variation is significant or not, a single factor ANOVA (analysis of variance) test was performed (using Microsoft Excel) on the equilibrium sorption capacity values (i.e., from triplicate measurements, Table A.1 in APPENDIX A). From the ANOVA analysis test results (Table A.2 presented in APPENDIX A), the F-Statistic value (85.57) was found higher than F-Critical value (7.59, at 99% level of confidence), which suggested this small increase in equilibrium sorption capacity with temperature was statistically significant (Kazerouni, 2009). Altogether, these findings show that HS^- sorption onto bentonite was faster and the equilibrium sorption capacity increased slightly with increasing temperature.

According to several studies (Boparai et al., 2011; Saeed & Ahmed, 2006) this type of sorption trend (i.e., increase in sorption capacity with increasing temperature) indicates an endothermic chemisorption process, which involves the breaking of hydration bonds and formation of new bonds with the active sorbent sites (Saeed & Ahmed, 2006). To investigate the rate limiting process of HS^- sorption onto bentonite three kinetic models were applied and discussed in the following section.

4.3.2 Sorption Kinetic Models

The linearized and non-linear forms of Pseudo-first-order (PFO), Pseudo-second-order (PSO) and Intraparticle diffusion (IPD) models were used to investigate the rate limiting mechanism of HS^- sorption on bentonite. While the sorption kinetics in these experiments are complicated because of various consecutive processes, e.g., film/external diffusion, intraparticle diffusion, surface interaction by physisorption or chemisorption (Can, 2015; González-lópez et al., 2022; Nguyen et al., 2017; Sahoo & Prelot, 2020), these simplified kinetic models are commonly used to initially understand sorption processes in various contexts – including bentonite sorption studies (Dada et al., 2019; Galambos et al., 2013; Gomdje et al., 2015; Pająk et al., 2019). Figure

4.2 and Table 4.2 presents the key results from comparing the non-linear plots of the applied kinetic models, as many recent studies recommend non-linear methods provide improved insight and reduced method bias than linearized methods (Bujdák, 2020; González-lópez et al., 2022; Moussout et al., 2018; Nguyen et al., 2017; Revellame et al., 2020; Simonin, 2016; Zafar et al., 2015). Moreover, as per the recommendations of these studies, the chi-squared (χ^2, Eq. (A.1), APPENDIX A) values were calculated alongside the coefficients of determination (R^2, Eq. (A.2), APPENDIX A) to evaluate the fit of each model (Table 4.2). The linearized plots of the sorption kinetic models and their associated parameter values are presented and discussed in Figure A.2 and Table A.3 in APPENDIX A.

Table 4.2 Kinetic parameter values obtained from non-linear fitting of kinetic models

Model	Parameters	Temperature (°C)			
		10	**22**	**30**	**40**
Pseudo-first- order model $q_t = q_e(1 - e^{-k_1 t})$	$q_{e,exp}$ (mg kg^{-1})	442.538	448.512	454.781	455.756
	$q_{e,cal}$ (mg kg^{-1})	431.831	439.223	446.074	453.851
	k_1 (h^{-1})	2.581	2.571	2.539	2.839
	R^2	0.551	0.566	0.604	0.891
	χ^2	1.332	0.196	0.170	0.008
Pseudo-second- order model $q_t = \frac{tk_2q_e^2}{1 + tk_2q_e}$	$q_{e,exp}$ (mg kg^{-1})	442.538	448.512	454.781	455.756
	$q_{e,cal}$ (mg kg^{-1})	440.231	446.798	453.678	456.610
	k_2 (kg mg^{-1} h^{-1})	0.019	0.021	0.023	0.033
	R^2	0.903	0.923	0.928	0.950
	χ^2	0.551	0.007	0.003	0.001
Intraparticle diffusion model $q_t = k_{inp}t^{0.5} + C_{inp}$	C_{inp} (mg kg^{-1})	413.237	412.612	417.804	439.287
	k_{inp} (mg kg^{-1} h$^{1/2}$)	3.099	6.494	6.399	3.360
	R^2	0.679	0.755	0.701	0.450

Figure 4.2 and Table 4.2 suggest that the PSO model showed a better fit (with higher R^2 [0.903-0.950] and lower χ^2 values [0.001-0.561]) to the experimental data than the PFO and IPD models at all temperatures studied. The PSO model derived q_e values were found to be close to the experimentally determined q_e values (442.5±1.71 to 455.8±0.85 mg kg^{-1}) and an increasing trend in second-order rate constants (k_2) values (from 0.019 to 0.032 kg mg^{-1} h^{-1}) was observed with increasing temperature from 10 to 40°C. In contrast, the non-linear PFO model provided lower R^2 (0.551-0.891) and higher χ^2 values (0.269-1.45), indicating a poorer fit to the experimental data

than the PSO Model. Furthermore, no trend in the first order rate constant (k_1) values was obtained from the PFO model.

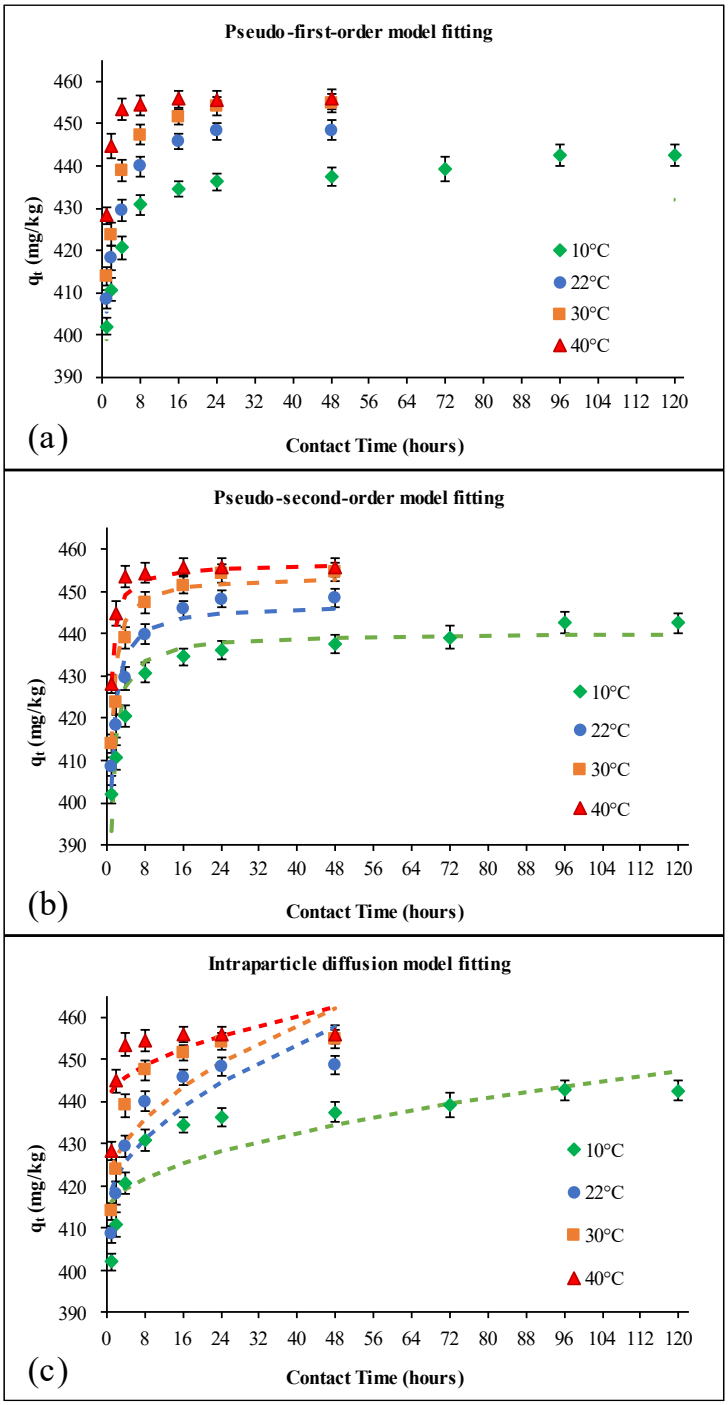

Figure 4.2 Non-linear plots of Pseudo-first-order, Pseudo-second-order, and Intraparticle diffusion models for HS^- sorption on bentonite (Experiment set 1 conditions: L:S = 100, initial HS^- concentration = 5 mg L^{-1}, pH = 9.5). Points represent experimental data and dotted lines represent non-linear fit of models to the experimental data.

Like the PFO model, the IPD model also showed a poorer fit (R^2 values [0.450-0.755]) to the experimental data than the PSO model. For all the temperatures, the IPD model plots did not pass through the origin (Figure 4.2); which indicates that intraparticle diffusion was not the only rate-limiting step, but some other sorption mechanisms likely occurred simultaneously (Crini et al., 2007; Li et al., 2007; Tsibranska & Hristova, 2011).

Overall, the model results in Figure 4.2 reveal that PSO kinetics best described the sorption dynamics, which suggests that chemisorption appears to be the principal rate-limiting process of HS^- sorption on bentonite (Boparai et al., 2011; Crini et al., 2007; Falahian et al., 2018; Ho & Mckay, 1999; Senthilkumaar et al., 2006; Zbair et al., 2019). However, due to the limitations of the applied kinetic models (Bujdák, 2020; Nguyen et al., 2017), the following sections provide additional analyses to better understand the underlying sorption mechanisms of HS^- onto bentonite.

4.3.3 Effect of L:S and Initial HS^- Concentration

To evaluate the effect of L:S and initial HS^- concentration on sorption, Experiment set 2 varied these parameters between 200 to 1000 and 1 to 6 mg L^{-1}, respectively. For these experiments, all samples and blanks were shaken at ambient temperature (22±2˚C) for more than 24 hours (28-30 hours) to ensure equilibrium (as found from Experiment set 1 results, discussed in Section 4.3.1). However, Experiment set 1 result show that L:S = 100 resulted in high sorption% at equilibrium (around 97-99%, Figure A.1 in APPENDIX A). As such, Experiment set 2 was conducted with higher L:S ratios (i.e., 200 to 1000) so the C_e values were well-above the method detection limit (0.02 mg L^{-1}).

Figure 4.3 presents the sorption capacity, q_e (mg kg^{-1}) sensitivities to L:S and initial HS^- concentration. In addition, the effects on sorption% are presented in Figure A.3 in APPENDIX A.

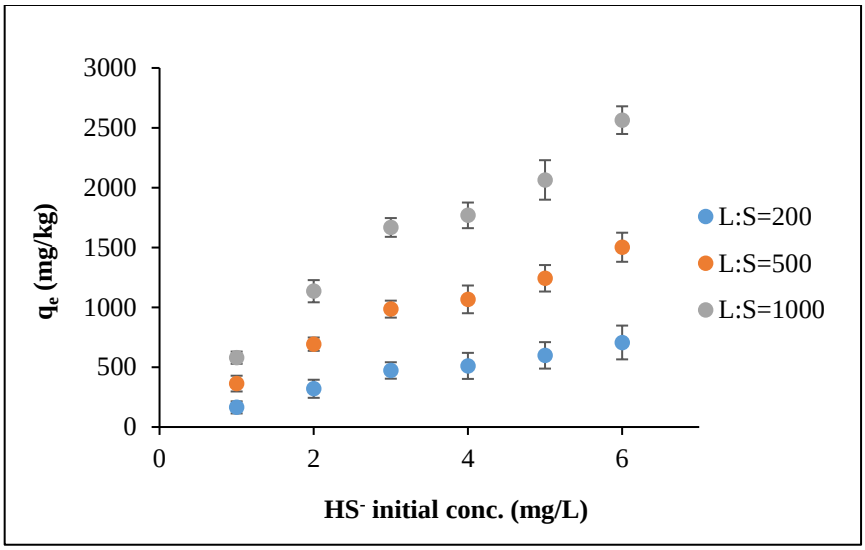

Figure 4.3 Effect of L:S and initial HS^- concentration on HS^- sorption capacity of bentonite (condition: pH = 9.5, temperature = 22±2°C, contact time = 28-30 hours). All data presented are the average of duplicate or triplicate tests, with error bars showing the standard deviation.

Figure 4.3 shows that the sorption capacity (mg kg^{-1}) increased with increasing L:S and initial HS^- concentration. These results are consistent with other sorption studies performed using bentonite (Gupt et al., 2019; Xu et al., 2008; S. Yang et al., 2009). Gupt et al. (2019) attributed the reason for the lower sorption capacity of bentonite at higher solid content to clay's expansive behaviour. The study reported that the expansiveness of bentonite results in gel-like consistency at low L:S values, which may inhibit interactions between the ions and adsorbent. However, this inhibition reduces considerably as the L:S is increased. Although no gel-like consistency was observed at the studied L:S values (i.e., 200 – 1000), the trend observed (i.e., increasing sorption capacity with increasing L:S) may be explained by the fact that increasing L:S induced better bentonite dispersion, which minimized the effects from bentonite expansion. Therefore, the experiments with L:S = 1000 exhibited the least interference due to bentonite expansion and facilitated better interaction of HS^- with bentonite surface resulting in higher HS^- sorption on per unit mass of bentonite than the experiments using L:S = 200 and 500. However, further study into this phenomenon would be valuable.

Under the combined effect of both L:S and initial HS^- concentration considered in Experiment set 2, the maximum sorption capacity was observed at around 2564 mg kg^{-1} at the highest L:S and initial HS^- concentration used (i.e., L:S of 1000 and HS^- initial concentration of 6 mg L^{-1}).

However, since the maximum capacity did not reach any plateau at the conditions investigated (see Figure 4.3), it might increase further if the initial conditions increased.

4.3.4 Sorption Isotherms

Many researchers have used Langmuir and Freundlich models to understand the adsorption of organic and inorganic substances onto clays like bentonite (Dawodu et al., 2012; Derakhshani et al., 2016; Emilio Alvarenga et al., 2016; Gupt et al., 2019; H. He et al., 2022; Shahmohammadi-Kalalagh et al., 2015; Xu et al., 2008; S. Yang et al., 2009; Zhao et al., 2008). At present, Langmuir and Freundlich models are the most extensively used models to analyze equilibrium sorption data. Therefore, the equilibrium data from Experiment set 2 were fitted to Langmuir and Freundlich isotherm models to obtain a preliminary understanding of the nature of HS^- sorption onto bentonite. The results are presented in Figure 4.4 and Table 4.3.

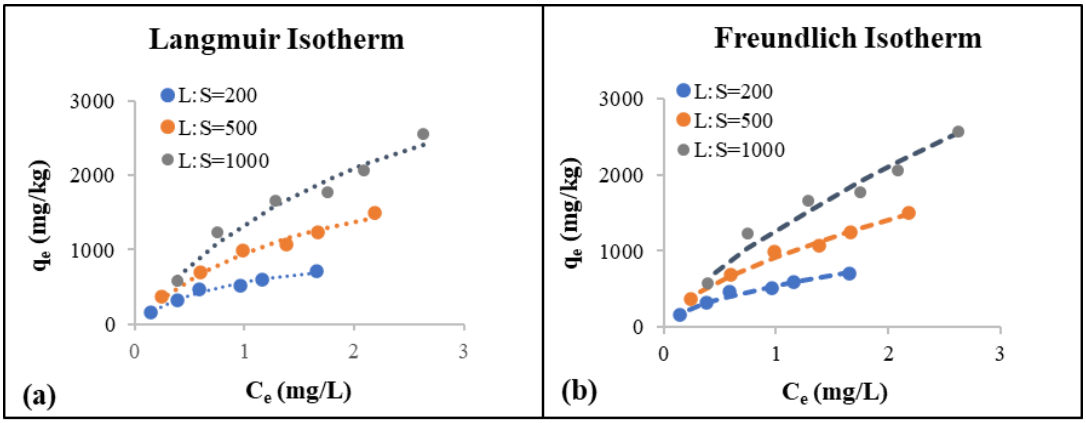

Figure 4.4 Isotherm models for HS^- sorption on bentonite (a) Langmuir and (b) Freundlich (experimental conditions: pH = 9.5, temperature = 22±2°C, contact time = 28-30 hours). Points represent experimental data and dotted lines represent non-linear fit of models to the experimental data.

Table 4.3 Parameter values obtained from non-linear fitting of isotherm models.

Liquid to solid ratio (L:S)	Langmuir Model $q_e = \frac{k_L Q C_e}{1 + k_L C_e}$				Freundlich Model $q_e = k_f C_e^{1/n}$			
	Q (mg kg^{-1})	k_L(L mg^{-1})	R^2	χ^2	k_f (mg^{1-n} kg^{-1} L^n)	n	R^2	χ^2
L:S=200	1018.019	1.251	0.977	8.666	546.350	1.874	0.970	14.797
L:S=500	2489.128	0.628	0.981	15.751	925.573	1.658	0.987	12.205
L:S=1000	7953.876	0.177	0.934	53.472	1272	1.38	0.960	67.062

Figure 4.4 (a) and (b) shows the non-linear fit of the data to the models. The good model fits in this figure shows that sorption over the experimental conditions investigated could be reasonably described by either Freundlich or Langmuir models. However, multiple features of HS^- sorption onto bentonite precludes the strict application of either model (see full discussion below). While neither model is suitable to fundamentally describe HS^- sorption onto bentonite, some observations from these models can provide helpful clues regarding the underlying sorption mechanisms. For example, the "n" values (> 1) from the Freundlich model (Table 4.3) indicate that the sorption process was favorable, and HS^- had a high sorption affinity towards bentonite (Boparai et al., 2011; Raihan Taha et al., 2004). However, the model results reported in Table 4.3 indicate that both models fitted the experimental data with high R^2 (0.96-0.99) at all L:S values studied. Therefore, it is not clear if the sorption was mono- or multi-layered, as similar R^2 values were observed for both models under the conditions investigated. Note that Langmuir and Freundlich describe sorption in a mono- and multi-layer domains, respectively (see additional discussion in Sections 2.3.4 in Chapter 2).

In terms of chi-squared (χ^2) test, the Langmuir model χ^2 value (8.666) at L: S=200 was found lower than the χ^2 critical value at a significance level of 0.05 and 5 degrees of freedom (11.071); while the Freundlich model χ^2 value was higher (14.797), indicating an acceptable and better fit of Langmuir model at L:S = 200. But for higher L:S ratios (i.e., 500 and 1000), both models had higher χ^2 values (15.751-67.062) than the tabulated value (11.071). These high χ^2 values indicate that, despite high R^2 values, the models did not robustly describe HS^- sorption onto bentonite, particularly at high L:S values. The L:S dependency, observed by other researchers (e.g., Gupt et al., 2019), ultimately invalidates the strict application of either model to predict sorption. Moreover, both models were developed assuming a reversible adsorption process (González-lópez et al., 2022; Nguyen et al., 2017), whereas HS^- sorption could be better described as chemisorption process, which would be irreversible. Therefore, the sorption results from Figure 4.4 might not be appropriate to use directly in predictive models – but may instead provide insight into the sorption mechanisms.

4.3.5 Thermodynamic Study

As discussed earlier in Section 4.1, the increase in HS^- sorption onto bentonite with increasing temperature indicates that sorption was endothermic (Figure 4.1). To further explore this result,

thermodynamic parameters for HS^- sorption onto bentonite were quantified from Experiment set 3 results (Table 4.1). In this study, the thermodynamic equilibrium constants (K_o) at different temperatures (10 to 40°C) were determined from the intercepts of the plots of $ln(q_e/C_e)$ versus C_e (Figure 4.5 (a) (Demirbas et al., 2006; Khan & R.P.Singh, 1987). The K_o values obtained were used to plot lnK_o vs $1/T$ (Figure 4.5 (b)), which was used to approximate ΔH^0, ΔS^0 and ΔG^0 following Eq. (2.5) and (2.6), Chapter 2. Negative values of ΔG^0 (Table 4.4) indicate that HS^- sorption onto bentonite was spontaneous, and the degree of spontaneity increased with increasing temperature (Boparai et al., 2011). In addition, the positive enthalpy change, ΔH^0 (2.6 kJ mol-1, Table 4.4) indicates that the sorption of HS^- on bentonite was endothermic, which agrees with the increased sorption observed with increasing temperature (see Figure 4.1). Moreover, the positive values of the entropy ΔS^0 (Table 4.4) indicates an increase in the system disorder, which may suggest the affinity of bentonite towards HS^- and some structure changes associated with the sorption (Boparai et al., 2011; S. Yang et al., 2009; Zhao et al., 2008).

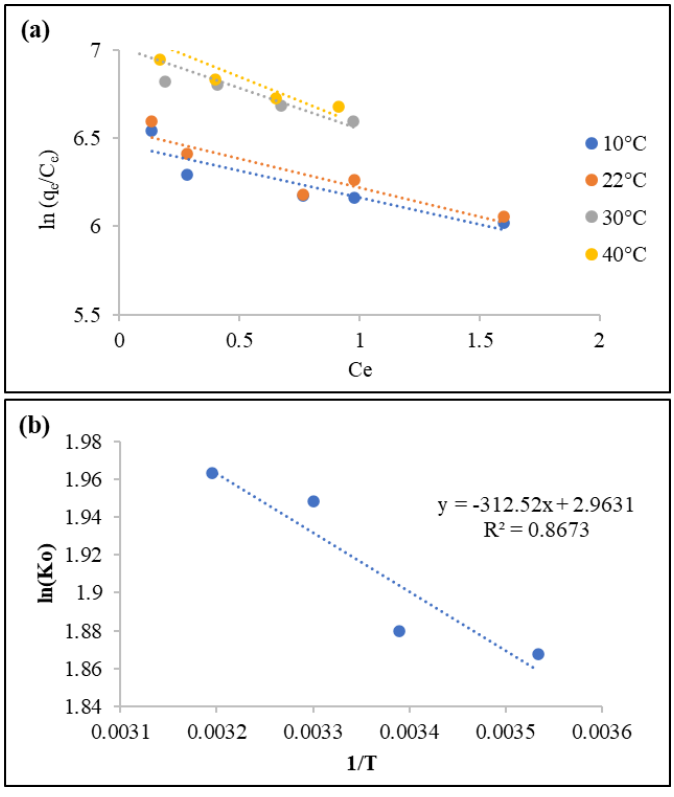

Figure 4.5 (a) Plot for determining thermodynamic equilibrium constant (K_o) (Experimental condition: L:S=200, HS^- initial concentration 1-5 mg L^{-1}; pH: 9.5-10; (b) Plot for determining thermodynamic parameters, enthalpy (ΔH) and entropy (ΔS). Dotted lines indicate the linear fit of the data.

Table 4.4 Thermodynamic parameters of HS^- sorption onto bentonite.

Thermodynamic parameters	Temperature(°C)			
	10	22	30	40
ΔG^0 (kJ mol^{-1})	-4.38	-4.67	-4.86	-5.11
ΔH^0(kJ mol^{-1})		2.60		
ΔS^0 (J mol^{-1})		24.63		

4.4 Consequences to the DGR

The above experimental observations indicate that HS^- sorbs/retains onto bentonite via a rapid and endothermic chemisorption process, which will prevent it from reaching the surface of the UFC and cause corrosion. From the maximum sorption capacity values determined from Experiment set 2 (580-2564 mg HS^-/kg bentonite, i.e., 0.018-0.078 moles HS^-/kg bentonite), preliminary estimates can be performed to quantify the implications of HS^- sorption on Cu corrosion reduction in a DGR. Since 1 mole HS^- reacts with 2 moles of Cu (as per Eq. (1.1) in Chapter 1), the amount of Cu corrosion reduction will be 0.035-0.155 mole Cu (equivalent to 2.23-9.85 g Cu). Dividing the amount of Cu corrosion reduction by the Cu density of 8.95 g/cm^3, the calculated volume of Cu corrosion reduction is $2.49*10^{-7}$ to $1.10*10^{-6}$ m^3. Considering a 1 m^2 area, the volume corresponds to a Cu corrosion reduction depth of 0.25-1.10 µm m^{-2}.

This preliminary estimation indicates the maximum possible Cu corrosion reduction per 1 kg of bentonite given a HS^- flux of 1-6 mg/L. As shown in Sections 4.3.1 and 4.3.3, the sorption capacity will depend on various geochemical conditions (e.g., temperature, HS^- concentration). In addition, other geochemical conditions in DGR may also impact HS^- sorption, such as groundwater composition (including pH and ionic strength). To offer a better understanding of the phenomenon, the next chapter will present the results of further batch experiments conducted under the combined effects of three crucial geochemical factors of the DGR, including temperature, pH and ionic strength.

4.5 Summary

This research conducted a series of laboratory batch experiments to understand the sensitivity of key parameters (i.e., contact time, temperature, liquid to solid ratio (L:S), initial HS^- concentration) on HS^- sorption onto bentonite. It was found that HS^- sorption on bentonite

increased with increasing contact time and occurred faster with increasing temperatures, where equilibrium was reached after 16 hours (at 40°C), 24 hours (at 22 and 30°C) and at 96 hours (at 10°C). In addition, the sorption capacity increased (by about 3%) with increasing temperature. Among the kinetic models studied, the pseudo-second-order model showed the best agreement with the experimental results, which implies that the rate of sorption might have been limited by chemical processes. The Freundlich isotherm constant $n > 1$ reflected that the sorption process was favorable, and that bentonite has a high sorption affinity towards HS^-. Under the experimental conditions investigated, both the Langmuir and Freundlich isotherm models fitted the data with high R^2 (> 0.9) values. However, high $\chi 2$ values indicated that these models might not reliably describe HS^- sorption onto bentonite – particularly at high liquid to solid ratios. Thermodynamic analysis results showed that the sorption process was endothermic and spontaneous in nature.

Altogether, this chapter serves as a foundation for comprehending the basic sorption behavior of HS^- onto bentonite. The subsequent chapter builds on these findings and conducts additional analyses to investigate the potential sorption mechanisms of HS^- onto bentonite. This helps to gain a better understanding of the fate of HS^- in bentonite.

CHAPTER 5
BISULFIDE SORPTION MECHANISMS ONTO BENTONITE: EFFECTS OF TEMPERATURE, pH, IONIC STRENGTH

5 Chapter Overview

This chapter is organized into five sections. First, Section 5.1 presents the study objective, followed by Section 5.2 describing the study methodology. Later, Section 5.3 discusses the results, while Section 5.4 discusses the possible sorption mechanism of HS^- onto bentonite based on the experimental findings. Finally, Section 5.5 summarizes the chapter.

5.1 Study Objective

Comprehending the sorption/retardation mechanisms of HS^- on bentonite is important for the prolonged safety of the DGR. The experimental findings documented in the previous chapter (Chapter 4) revealed that HS^- sorbs onto bentonite via an endothermic chemisorption process. In accordance with existing literature, the chemical sorption mechanisms onto soil include inner- and outer-sphere surface complexes formation and precipitation on soil particle surfaces as new solid phases (Kaplan, 1999; Strawn, 2021). Several studies have highlighted that HS^- reacts with the Fe in bentonite and precipitates as an iron-sulfide (FeS) mineral on the bentonite surface. However, a lingering question persists regarding whether HS^- sorption onto bentonite is exclusively governed by the FeS precipitation reaction or if other mechanisms, such as adsorption by surface complex formation, also contribute to the overall process.

Many studies (L. M. He et al., 1997; Wang et al., 2001b; Walker, 2018) have used the surface complexation model to describe anion adsorption onto mineral surfaces – including montmorillonite – which is the predominant smectite component of bentonite (85-90%). Anion adsorption may occur on variably charged surface sites of montmorillonite (i.e., the edge sites with hydroxyl functional groups) either by (i) inner-sphere complexes, forming in direct contact with the surface (i.e., no water molecule between the surface and the adsorbing ion), or (ii) outer-sphere complexes, containing at least one water molecule between the adsorbing ion and the surface functional group. Despite the prevalent use of diverse surface complexation models (e.g., diffuse layer model, constant capacitance model, charge distribution multi-site complexation

model) to elucidate the impacts of pH and ionic strength on anion adsorption, no research has explored the potential of HS^- adsorption through surface complex formation on the edge sites of montmorillonite. In a broader context, a comprehensive understanding of how pH and ionic strength influence HS^- sorption onto bentonite remains unexplored. While the preceding chapter suggested a rise in HS^- sorption with increasing temperature, it is also imperative to investigate whether this temperature effect exhibits a similar pattern under different pH levels and ionic strength conditions.

To gain a better understanding of the mechanisms involved in HS^- sorption onto bentonite, this study (as presented in this chapter) consisted of batch sorption experiments to explore HS^- sorption onto bentonite under the combined effects of three critical geochemical factors of the DGR, such as temperature, pH, and ionic strength. A 3-way ANOVA (analysis of variance) test was performed to assess whether the effects observed in the experiments were statistically significant and whether there was a significant interaction effect among the experimental variables. Desorption tests and field emission scanning electron microscopy/energy dispersive spectroscopy (FESEM/EDS) analyses were also performed to obtain further insight into the HS^- interactions with bentonite.

5.2 Methodology

This section presents the methodology followed for the batch sorption tests, desorption tests, statistical and surface analysis performed in this study.

5.2.1 Sorption Experiments

A total of nine batch experiments were performed under experiment set 4 to observe the effects of temperature, pH, and ionic strength on HS^- sorption onto bentonite.

Table 5.1 presents a brief overview of the experimental conditions and justifications regarding the selected ranges of the experimental conditions. Table B.4 in APPENDIX B presents a description of each test. The constant experimental conditions, such as liquid to solid mass ratio (L:S), HS^- initial concentration and contact time, were applied based on the experimental findings of the previous chapter.

Table 5.1 Batch experiment overview.

Experiment set no. (con't from Chapter 4)	Objective	Experimental conditions		Selection justification
4.	To observe the effects of temperature, pH, and ionic strength on HS^- sorption onto bentonite	Variable conditions	Temperature: 10, 25, and 40°C	• The anticipated temperature range of Canadian DGR is 10-80°C (King et al., 2017; Hall et al., 2021) • The temperature during the period where HS^- is present is generally expected to be after the peak temperature. • The range (10-40°C) was selected to reflect the long-term condition, and for practical equipment limitations
			pH: 9, 9.5, 10, 10.5, and 11	• HS^- is the dominant sulfide species over the pH range of 9-11 • To avoid H_2S gas formation (Ahlatci et al., 2016; House & Weiss, 2014; Lewis, 2010; Neto et al., 2018)
			Ionic strength: 0.01, 0.1, and 1 M NaCl	• Cl^- concentration of bentonite pore water may range between 0.03-0.07 M (King et al., 2017; Hall et al., 2021) • Cl^- concentration of Canadian groundwater in crystalline and sedimentary host rocks may range between 0.1-5.0 M, respectively (King et al., 2017; Hall et al., 2021)
		Constant conditions	Liquid to solid mass ratio (L:S) = 1000	• L:S = 1000 showed minimal interference from bentonite expansion, enhancing HS^- interaction with the bentonite surface (Papry et al., (2023) (see Section 4.3.3 in Chapter 4)
			HS^- initial concentration = 3 mg L^{-1}	• Samples with higher initial HS^- concentration (> 3 mg L^{-1}) previously exhibited a higher standard deviation (i.e., higher measurement error) (Papry et al., (2023) (see Figure 4.3 in Chapter 4)
			Contact time: 30 hours (at 25 and 40°C); 100 hours (at 10°C)	• HS^- sorption onto bentonite reached equilibrium at 16 hours (at 40°C), at 24 hours (at 22 and 30°C) and at 96 hours (at 10°C) (Papry et al., (2023). (see Section 4.3.1 in Chapter 4)

Similar to the previous experiments described in Chapter 4, these experiments were performed using powdered MX-80 bentonite obtained from the NWMO, Canada. Before each experiment, sodium chloride (NaCl), bentonite, and HS^- stock solutions were prepared and later used for sample preparation to maintain experimental consistency. NaCl stock solutions were prepared by dissolving NaCl salt (MilliporeSigma, ≥ 99.99% purity) in deoxygenated deionized water (Milli-Q® Direct 8/16, MilliporeSigma; deoxygenated by purging nitrogen gas). Three bentonite stock solutions were prepared by mixing dried bentonite powder in NaCl solution at the required background ionic strength (i.e., 0.01, 0.1 and 1 M) at a liquid to solid ratio (L:S) of 20. As followed in the previous experiments, the bentonite stock solutions were sonicated with a probe sonicator (Qsonica Q700, 700 watts) for 1 hour at 40% amplitude to ensure the bentonite was homogenously dispersed. Moreover, HS^- stock solutions were prepared following the standard method 4500-S^{2-} A (i.e., by dissolving sodium sulfide nonahydrate ($Na_2S \cdot 9H_2O$, MilliporeSigma, ≥ 99.99% purity) salt in deoxygenated water at desired HS^- concentrations) (APHA, 2017).

The previous experiment results discussed in Section 4.3.3 in Chapter 4 suggested that among the L:S values (200, 500, 1000) investigated, the maximum sorption capacity was observed for L:S= 1000. As such, for this study, the sample solutions for all the experiments were prepared in 50 mL Pyrex glass centrifuge tubes (Fisher Scientific) at an L:S of 1000 and HS^- initial concentration of 3 mg L^{-1}. In this regard, each sample was prepared by filling half of the tube (25 ml) with bentonite solution (pipetted from the L:S = 20 bentonite stock and diluted with NaCl solution at twice the required concentration) and the remaining volume with 6 mg L^{-1} of HS^- (also twice the concentration necessary).

The initial measured pH of all samples was between 8-10. Before the experiments, the pH values were adjusted to the desired levels (i.e., 9-11, Table 5.1) by adding 0.1 M NaOH dropwise and/or 0.1 M HCl. Following the quality control approaches, all test samples were prepared in triplicates. In addition, two different types of experimental blanks, i.e., (i) only HS^- without bentonite and (ii) only bentonite without HS^-, were prepared for each test condition to measure the background absorbance and to determine the experimental loss of HS^- other than sorption onto bentonite. All solutions used in the experiments (i.e., stock, sample, and blank) were prepared in an anaerobic chamber (Coy Laboratory Products). The total number of test samples and blanks prepared for each test condition is reported in Table B.4 in APPENDIX B.

After preparation, the centrifuge tubes containing samples and blanks were placed in a tube rotator (MX-RD-Pro, SCILOGEX). To control the temperature at the levels indicated in Table 5.1, the rotator was placed in a dual incubator/refrigerator (MaxQ 6000, Thermo Fisher Scientific), where the tubes were rotated at 60 rpm until sorption equilibrium was reached.

The kinetic study results presented in Section 4.3.1 in Chapter 4 revealed that the HS^- sorption onto bentonite reached equilibrium at 16 hours (at 40°C), at 24 hours (at 22 and 30°C) and at 96 hours (at 10°C). As such, the samples in this study were shaken for 30 hours at 25 and 40°C and for 100 hours at 10°C to ensure sorption equilibrium. After shaking, the solid and aqueous phases were separated by centrifuging the solutions at 3500 rpm for 1 hour. Afterwards, the samples were taken back into the anaerobic glovebox and the after-experiment pH of each sample was measured (see Table B.4 in APPENDIX B). The supernatant was then stage-filtrated with 1.2 and 0.2 μm hydrophilic polytetrafluoroethylene syringe filters (Fisher Scientific) and finally analyzed using the colorimetric methylene blue method (4500-S^{2-} D) (APHA, 2017). A similar procedure was followed to analyze the experiment blanks.

A flow chart summarizing the batch sorption experiments methodology is presented in Figure 5.1.

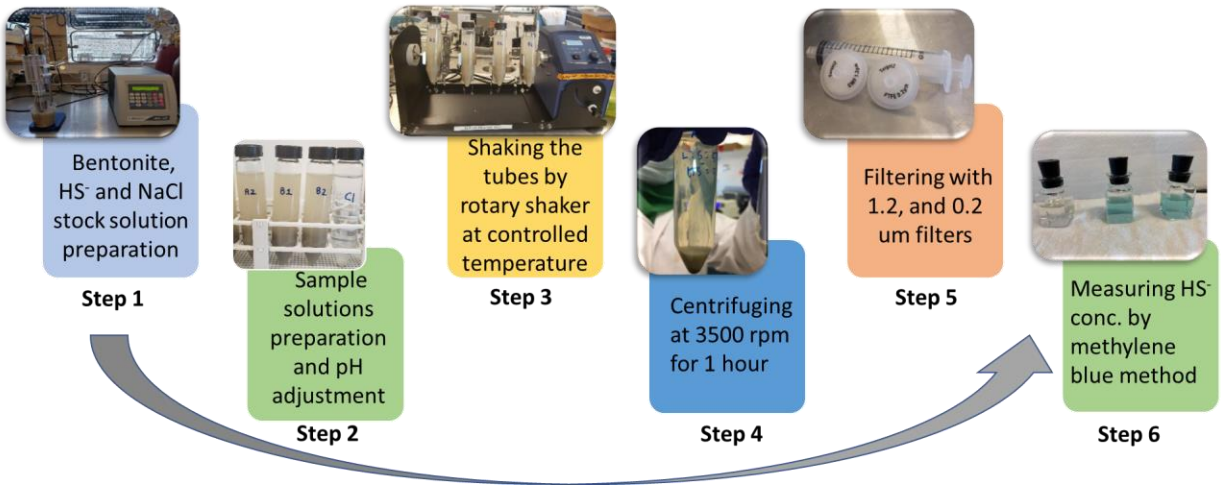

Figure 5.1 Flow chart illustrating the batch sorption experiments methodology.

From the measured HS^- concentration, the equilibrium sorption capacity, i.e., the mass of HS^- sorbed per unit mass of bentonite at equilibrium (q_e), was calculated using Eq. (4.3), Chapter 4. Each calculation took into account the corrected initial HS^- concentration determined from the

type (i) blank (i.e., only HS^-) at each experimental condition and the absorbance reading from type (ii) blank (i.e., only bentonite) to consider the interference from background HS^- and small bentonite particulates.

5.2.2 3-way ANOVA Analysis

A 3-factor ANOVA (analysis of variance, also referred to as F-tests) test was performed to investigate if the experimental effects were statistically significant and if there were interactions among the variables. ANOVA tests were performed because the study includes more than two groups of independent variables (i.e., five pHs, three ionic strengths, and three temperatures). Altogether, 45 observations, including experimental triplicates, were included in the ANOVA analysis. In the ANOVA test, the F-stat value (i.e., the ratio of "between-group variation" to "within-group variation") was determined and compared with the F-critical value (i.e., obtained from an F-table). In addition, P-values were determined to compare against the significance level (i.e., α values).

5.2.3 Desorption Tests

Following the batch sorption experiments, desorption tests were performed to investigate whether HS^- sorption onto bentonite is a reversible or an irreversible process or a combination of both. Desorption test samples were prepared with bentonite and HS^- solution at various L:S ratios, initial HS^- concentrations, pH levels and ionic strength conditions. An overview of the selected test conditions for desorption experiments is presented in Table 5.2.

Table 5.2 Desorption experiments conditions overview

Experiment set no.	Objective	Variable experimental conditions	Constant experimental conditions
5.	To investigate whether HS^- is reversibly or irreversibly sorbed onto bentonite under various conditions	L:S= 100,1000 Initial HS^- concentration= 3, 6 mg/L Temperature= 25, 40°C	pH = 9.5 Contact time =30 hours
6.		pH= 9, 9.5, 10, 10.5, 11 Ionic strength= 0.01 M, 1 M NaCl	L:S= 1000 Initial HS^- concentration= 3 mg/L Temperature= 25°C Contact time =30 hours

After preparation, the samples were shaken at room temperature (22±2°C) and 40°C for 30 hours to reach sorption equilibrium, (as determined from Experiment set 1 result discussed in Section 4.3.1 in Chapter 4). Then, the phases were separated by centrifugation, and the aqueous phase was removed as much as possible. The volume of solution removed was replaced by an equal volume of deoxygenated DI water without HS^- at a pH ≈ 9.5. The new mixtures were then shaken for 24, 48, 72, and 96 hours at 22 and 40°C, centrifuged, and filtered. The aqueous phase was then analyzed through the methylene blue method to determine whether any HS^- had been desorbed from the bentonite.

Figure 5.2 presents a flow chart summarizing the desorption experiments methodology.

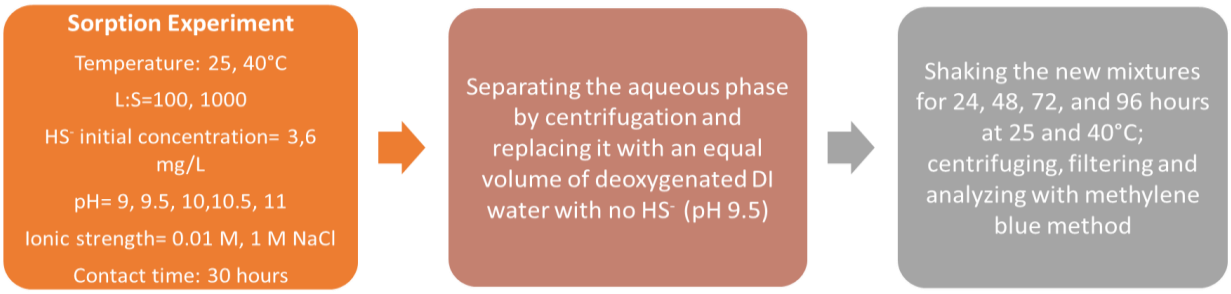

Figure 5.2 Flow chart illustrating the desorption experiments methodology.

5.2.4 Bentonite Surface Analysis

Surface analyses via field emission scanning electron microscopy (Thermo Fisher Scientific Quanta 3D 20KV voltage) coupled with energy dispersive spectroscopy were performed on selected test samples (bentonite with HS^- at L:S = 1000 and initial HS^- concentration 6 mg L^{-1}) and type (*ii*) blank samples (i.e., only bentonite, no HS^-). For FESEM/EDS analysis, the solid phase samples, which were separated via centrifugation, then dried in the anaerobic chamber upon a 2-3 cm bed of drierite. The samples were then crushed into a fine powder using a pestle and sieved through a 200 mesh (75 µm) USA Standard sieve. The samples were then mounted on aluminum stubs over carbon tape, followed by compressed air spraying (to obtain a bounded monolayer) and coated with 2-3 nm platinum plasma using a sputter coater.

5.3 Results and Discussion

5.3.1 Experiment Results

Figure 5.3 presents the experimental findings on HS^- sorption sensitivity to pH and ionic strength at various temperatures.

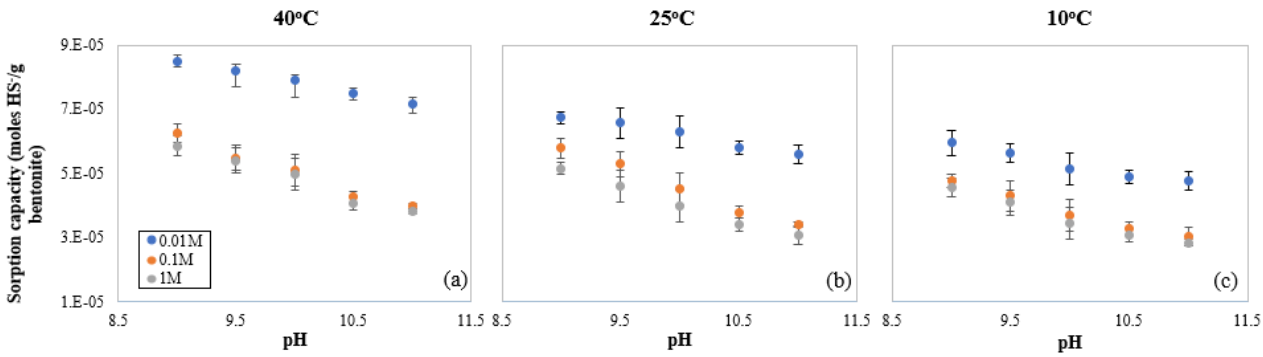

Figure 5.3 Effects of pH and ionic strength on HS^- sorption onto bentonite at various temperatures (a) 40°C (b) 25°C, and (c) 10°C. All data presented are the average of triplicate tests, with error bars showing the standard deviation. The pH values indicate the adjusted before-experiment pH levels.

5.3.1.1 Effect of temperature

Figure 5.3 reveals that the sorption capacity increased with increasing temperature from 10°C to 40°C at all ionic strength and pH values studied. This phenomenon is consistent with the findings of the previous chapter (Section 4.3.1 in Chapter 4) and supports the hypothesis that HS^- sorption onto bentonite is an endothermic chemisorption process. Since chemisorption involves the breaking of hydration bonds and the formation of new bonds with the active sorbent sites, chemisorption increases with increasing temperature up to a certain limit (Boparai et al., 2011; Saeed & Ahmed, 2006). As such, HS^- sorption onto bentonite was favoured at higher temperatures (Figure 5.3).

5.3.1.2 Effect of pH

Figure 5.3 suggests that at all temperatures and NaCl solutions studied, HS^- sorption decreases with increasing pH. This pH effect is consistent with other studies that applied surface complexation modelling to investigate anion sorption onto various mineral surfaces. For example, a decreasing sorption trend with increasing pH was reported for sulfate (SO_4^{2-}) and

phosphate (PO_4^{3-}) adsorption on alumina and kaolinite (He et al., 1997); radionuclide anions (I^-, IO^{3-}, SeO_3^{2-}, SeO_4^{2-}, and TcO_4^-) on various minerals (e.g., ferrihydrite, bentonite, montmorillonite, goethite, alumina) (Wang et al., 2001b); arsenite adsorption on iron oxide (Goldberg, 2014); sulfate (SO_4^{2-}) and selenate (SeO_4^{2-}) adsorption onto iron oxide (Fukushi and Sverjensky, 2007); selenium (HSe^-) sorption onto illite and bentonite (Walker, 2018). This pH dependence suggests that surface complexes with the surface OH groups may have influenced HS^- sorption onto bentonite.

The pH trend observed may be because, as the solution pH increased from the zero point of charge pH_{ZPC} of bentonite, i.e., between 6.5-8 – the pH at which the overall bentonite surface charge is zero (Wieland et al., 1994; Tertre, 2006), the bentonite edge surface became more negatively charged due to increasing deprotonation (i.e., acidic dissociation of surface hydroxyl groups). In all experiments, the after-experiment pH consistently measured lower than the before-experiment pH, suggesting the occurrence of deprotonation reactions (Table B.4 in APPENDIX B). As a result, HS^- sorption might have decreased with the increasing pH due to increasing electrostatic repulsion between the bentonite surface and negatively charged HS^-. Furthermore, the acid/base surface properties of montmorillonite and other oxide minerals reported in several studies suggest that the degree of deprotonation of surface OH groups (which drives the negative bentonite surface charge) increases with increasing ionic strength in the alkaline pH range (Wanner et al., 1994; Wieland et al., 1994; Bourg et al., 2007). Accordingly, a steeper drop in HS^- sorption with increasing pH was observed at increasing ionic strengths, i.e., with 0.1 and 1 M background NaCl in Figure 5.3 (b) and (c), respectively.

5.3.1.3 Effect of NaCl concentration

Figure 5.3 suggests that HS^- sorption onto bentonite decreased with increasing NaCl concentration from 0.01 to 0.1M. As NaCl is not reactive with bentonite or sodium sulfide, the NaCl concentration is being attributed to ionic strength of the solution. As such, the “ionic strength” term used in this chapter and Chapter 6 refers to the background NaCl solution concentration.

The decreasing HS^- sorption trends with increasing ionic strength may be due to multiple reasons, e.g., (i) increased amounts of NaCl occupied the surface of the clay at higher ionic strengths, which decreased HS^- anion access to the surface sites; or (ii) the higher ionic strength

increased bentonite particle aggregation, which limited the accessibility of sorption sites. It is beyond the scope of this study to resolve the magnitude of each effect. Regardless, in either case, HS^- sorption likely decreased with increasing ionic strength due to reduced accessibility of sorption sites.

In addition, the ionic strength dependence can be used to differentiate between inner- and outer-sphere sorption mechanisms, as outer-sphere complexes are likely to be more sensitive to ionic-strength variations than inner-sphere complexes (Goldberg, 2014). This difference is because the electrolyte ions are placed closest to the outer-sphere complexes (see an illustration in Figure 5.4). With the increasing solution ionic strength, more exchange sites at the diffuse double layer (DDL) become occupied by background electrolytes instead of water molecules, thereby leading to diffuse layer shrinkage (Hayes et al., 1988; Tang et al., 2014; Musso et al., 2019). This layer shrinkage causes increasing competition between the electrolyte ions and the adsorbing ions for available sorption sites (Hayes et al., 1988; Musso et al., 2019). As such, the number of ions adsorbed by weak outer-sphere complexes (e.g., sulfate, selenate, arsenate) decreases with increasing ionic strength (McBridge, 1997; Fukushi and Sverjensky, 2007; Wang et al., 2018).

On the other hand, since anion adsorption by inner-sphere complexes (i.e., by ligand exchange) involves direct coordination to the soil surface, i.e., far from the electrolyte ions, it is comparatively less sensitive to the ionic strength (Baeyens and Bradbury, 1997; McBridge, 1997; Yang et al., 2009; Goldberg, 2014). Therefore, anions (e.g, phosphate, borate) that are adsorbed by stronger inner-sphere surface complexes show little ionic strength dependence or increasing sorption with increasing ionic strength (Goldberg, 2014; L. M. He et al., 1997; McBridge, 1997). One possible explanation provided by McBridge (1997): with increasing ionic strength, the DDL contraction allows more anions to approach the surface, which increases the formation of inner-sphere complexes and thus, increases inner-sphere adsorption. Moreover, some ions may adsorb as both inner- and outer-sphere complexes. For example, Wang et al. (2018) reported that sulfate forms both outer- and inner-sphere complexes on hematite surfaces. However, one process was found to dominate over another at different adsorption stages (Wang et al., 2018).

Based on the above discussion, the decreased sorption of HS^- with increasing ionic strength could be evidence of outer-sphere complex formation with surface hydroxyl groups (Figure 5.4 illustrates the potential surface complexation formation of HS^- with surface OH group of

bentonite). However, little (at 22°C and 10°C) to no (at 40°C) effect was observed when the ionic strength was increased from 0.1 M to 1M (Figure 5.3). This insensitivity suggests that the ionic strength effect might have reached a maximum threshold at 0.1 M ionic strength, beyond which the contribution from outer-sphere complex formation to the sorption capacity was negligible.

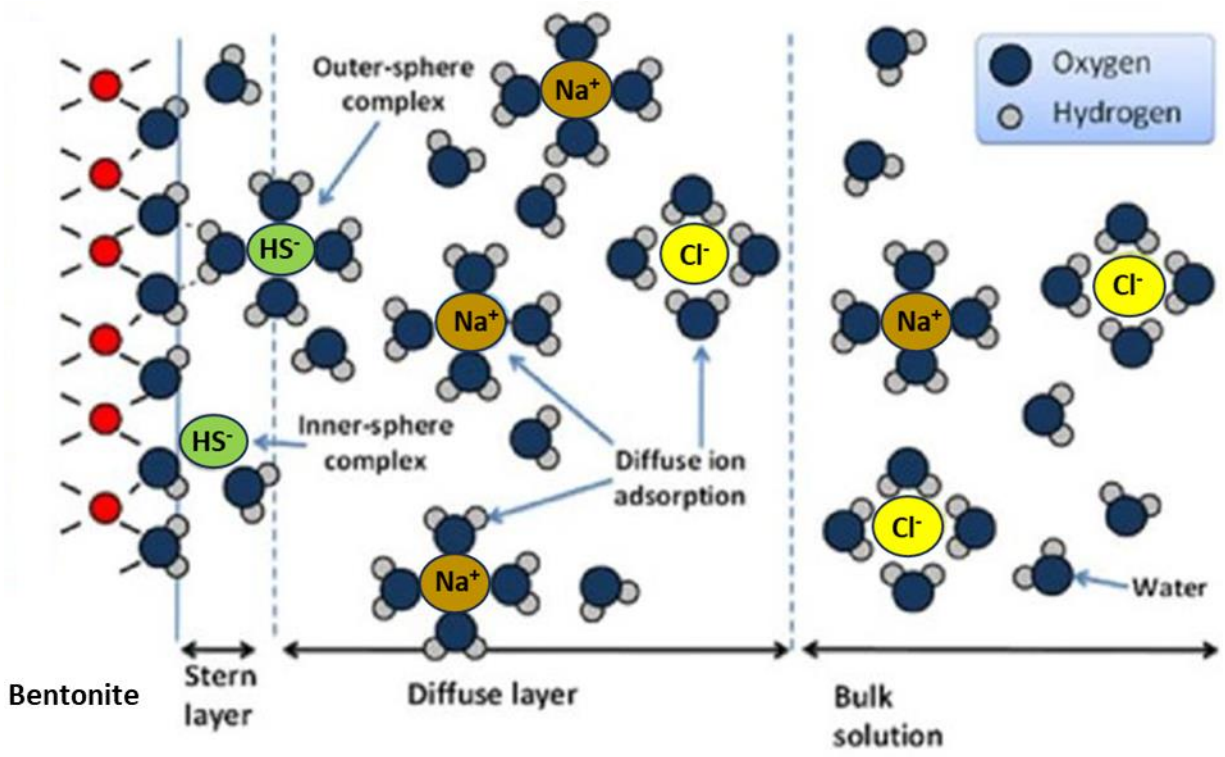

Figure 5.4 Schematic diagram of the potential surface complex formation of HS^- onto bentonite's edge surface with NaCl as the background electrolyte (adopted and modified from (Glocheux, Y., 2014)).

Overall, the experiment results suggested that HS^- sorption onto bentonite was favoured at high temperatures, low pHs (i.e. 9-9.5), and low ionic strengths. The estimated maximum sorption capacity (moles/g) from the experimental conditions investigated was 8.52×10^{-5} moles/g (at 40°C, pH 9, and 0.01 M ionic strength).

5.3.2 Statistical Analysis (3-way ANOVA)

The experimental results indicate some interaction effects of the variables, such as a more pronounced drop in HS^- sorption with increasing pH was observed at higher ionic strengths. As such, a 3-way ANOVA test was performed to explore whether the interaction effects between the

experimental variables – i.e., pH, temperature, and ionic strength- are statistically significant. The ANOVA test results are summarized in Table 5.3.

Table 5.3 Three- way ANOVA test results

Effects	Factors	P value	Significance
Individual	pH	$<2 \times 10^{-6}$	***
	Temperature	$<2 \times 10^{-6}$	***
	Ionic strength	$<2 \times 10^{-6}$	***
2-way interaction	pH & temperature	0.023	*
	pH & ionic strength	$<2 \times 10^{-6}$	***
	Temperature & ionic strength	0.025	*
3-way interaction	pH, temperature & ionic strength	0.423	

Notes: *** 99.99% level of significance (i.e., α= 0.001)
** 99 % level of confidence (i.e., α= 0.01)
* 95% level of confidence (i.e., α= 0.05)
The P-value is the probability of measuring the indication against the null hypothesis.

Table 5.3 indicates the following effects on HS^- sorption onto bentonite are statistically significant at the 99.99% level of confidence (i.e., $p < 0.001$): (i) individual effects of temperature, pH, and ionic strengths and (ii) the 2-way interaction effects between pH and ionic strength. In addition, the 2-way interaction effects between (i) pH and temperature and (ii) temperature and ionic strength are statistically significant at a 95% level of confidence (i.e., $p < 0.05$). However, no significant 3-way interaction effects were observed between the variables (i.e., $p > 0.05$). These results imply that the individual and 2-way interaction effects should be considered in understanding HS^- sorption mechanisms onto bentonite, e.g., in a geochemical model/reactive transport model of HS^- through bentonite in the evolving geochemical conditions of the DGR. The interaction effects of the variables could indicate the complex nature of the sorption, involving more than one simultaneous process.

5.3.3 Desorption Tests

No desorbed HS^- was detected in the aqueous phase at any of the applied test conditions (as described in Table 5.2). In other words, HS^- sorption onto bentonite was irreversible under the

conditions investigated. This finding further supports the hypothesis that HS^- was sorbed onto bentonite via chemical processes, which would likely be irreversible.

5.3.4 Surface Analysis

Figure 5.5 presents a comparison of SEM images from a test sample (L:S = 1000, initial HS^- concentration = 6 mg L^{-1}) and a blank sample (only bentonite at L: S = 1000, no HS^-). As shown in Figure 5.5 (a) and (b), some distinct crystal structures oriented together were identified in the blank and test samples. These structures were found in different shades (relatively brighter) than the bulk area of the bentonite, indicating the presence of different atoms with higher atomic mass and different chemical compositions. The EDS point analysis results indicate these structures contained iron (Fe) and sulfur (S) with an atomic% ratio of nearly 1:2 (EDS point analysis results shown in Figure B.4 (a) and (b) in APPENDIX B. This ratio indicates the presence of pyrite (FeS_2) (Rickard & Luther, 2007; Wen et al., 2017) in both the test and blank sample, which was expected as MX-80 bentonite often contains ~0.6 w% of pyrite ((D. Dixon et al., 2018; D. A. Dixon, 2019). In addition, Figure 5.5 (c) shows that relatively irregular shaped particles without sharp crystal edges were identified at some locations in the test sample. The atomic% ratio of Fe and S from EDS analyses at these locations were found to be very close to 1:1 (EDS point analysis results shown in Figure B.4 (c) in APPENDIX B). This observation indicates the presence of a newly formed FeS compound, likely amorphous FeS/mackinawite (Behazin et al., 2021; Bolney et al., 2021; Lemire et al., 2020; Marić et al., 2019; Szczepanik & Sawlowicz, 2010). The co-existence of Fe and S in the test sample (as shown in Figure 5.5 (c)) was also reflected in EDS mapping (i.e., the spatial distribution of Fe and S over the image area shown in Figure B.5 in APPENDIX B. However, no such FeS compounds (i.e., with Fe:S = 1:1) were identified in the blank sample. Altogether, this analysis shows that while Fe and S are present together in the initial sample as pyrite, it appears that new iron-sulfide minerals (possibly amorphous FeS/mackinawite) were formed from HS^- sorption experiments, which aligns with previous studies (Maanoja et al., 2020; Miettinen et al., 2022; Pedersen et al., 2017; Wersin et al., 2017).

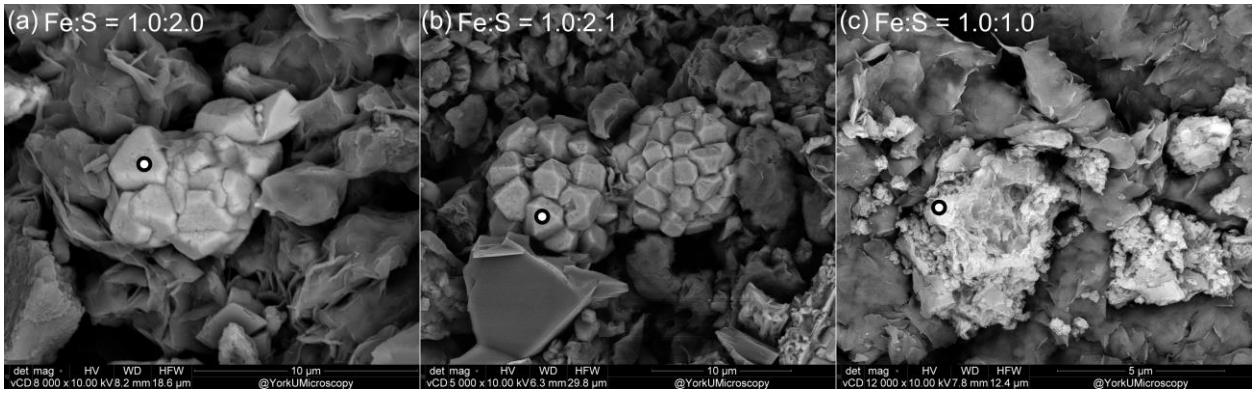

Figure 5.5 SEM (back-scattered) images of blank (only bentonite with L: S = 1000, no HS^-) and test sample (with L:S = 1000, initial HS^- concentration = 6 mg L^{-1}) (a) pyrite identified in the blank sample; (b) pyrite identified in the test sample and (c) FeS identified in the test sample. The circles denote the EDS point analysis locations, and the Fe:S atomic % ratios are also listed from these EDS analyses.

As reported in the literature, in aqueous solutions at ambient temperature, sulfide reacts rapidly with Fe(II) and first forms iron (II) mono-sulfide known as mackinawite (FeS), which is subsequently transformed into more insoluble compounds such as greigite (Fe_3S_4) and pyrite (FeS_2) depending on geochemical conditions such as pH and polysulfide concentration (Cloet et al., 2017; Rickard & Luther, 2007). According to literature (Szczepanik & Sawlowicz, 2010), pyrite is the most stable iron sulfide formation that is generally found in well-defined crystal shapes; conversely, greigite and mackinawite have less regular shapes and typically form smaller crystals than pyrite. Another study reported that at reducing conditions and low temperatures (i.e., below 100°C), the rate of pyrite formation from mackinawite is insignificant (Benning et al., 2000). As such, pyrite was probably not formed in the sorption experiments (i.e., conducted under anaerobic conditions and room temperature). Instead, the newly formed Fe and S structures observed in the test samples (Figure 5.5 (c)) suggest that HS^- sorption on bentonite might have been governed by chemical interactions with the Fe present in bentonite and subsequent formation of FeS compounds, e.g., amorphous FeS/mackinawite.

In addition, several other studies (Pedersen et al., 2017; Hadi et al., 2023) indicated that the governing process of HS^- immobilization by bentonite could be the redox reaction between the HS^- and structural Fe (III) of bentonite. In this process, the HS^- can act as an electron acceptor to reduce the Fe(III) to Fe(II) while being oxidized to elemental sulfur, S(0). In this study, EDS point analysis results on a few other locations of the test sample indicated a relatively higher percentage of S than typically expected in mackinawite (Fe:S = 1:1) and pyrite (Fe:S = 1:2). At

these locations, the atomic% ratio of Fe and S was found to be 1:3.03. (EDS point analysis results are shown in Figure B.4 (d) in APPENDIX B). This additional amount of S could indicate the presence of S(0) in the test sample as suggested by the literature. However, it is important to note that EDS is a semi-quantitative elemental analysis tool, which only provides the percentage data of the elements on the surface and not the chemical compounds and their various forms. Therefore, it was difficult to ascertain whether the additional S detected was in the elemental sulfur, S(0), form or a part of some other chemical compounds from the EDS data. Moreover, quantification of the sorption processes from EDS mapping was challenging because of the heterogenous bentonite surface and presence of high background S. Nevertheless, these SEM-EDS analyses results provided important evidence to support that HS^- sorption onto bentonite was driven via chemical reactions, particularly with Fe.

5.4 HS^- Sorption Mechanisms

Given that bentonite is a complex soil containing various solid mineral phases, the sorption of HS^- onto bentonite might not be a straightforward process; instead, multiple sorption mechanisms likely occurred concurrently. This study seeks to elucidate the potential sorption mechanisms of HS^- onto bentonite by employing sorption-desorption tests and conducting surface analyses on samples before and after experiments.

The irreversibility observed in the desorption test results suggests that chemical reactions (e.g., precipitation) and/or chemical adsorption (e.g., surface complexation) are the primary drivers of sorption. The surface analysis results align with prior research indicating that HS^- interacts with Fe in bentonite, leading to subsequent precipitation as FeS (likely mackinawite). Although direct evidence from the surface analysis is lacking, the sorption process may also encompass a redox-reaction between HS^- and structural Fe^{3+} in bentonite, resulting in the precipitation of HS^- as elemental sulfur (S(0)), as proposed in literature (Pedersen et al., 2017; Hadi et al., 2023) (also see discussion in Section 2.4.2 in Chapter 2).

Moreover, the sorption behaviour in response to the pH and ionic strength variation could indicate the potential involvement of the surface complex reactions with the OH functional groups, as observed in several other anion sorption studies in the literature (see discussion in Section 5.3.1). Altogether, it can be hypothesized that HS^- likely sorbed onto bentonite through forming S(0), FeS, and surface complexes. However, unravelling the intricate interplay of these

mechanisms and quantification of their respective contribution to the overall sorption/retardation process was challenging from experimentation and surface analysis. This underscores the need to develop a mechanistic sorption model to better understand the underlying sorption mechanisms of HS^- onto bentonite.

5.5 Summary

The study explored HS^- sorption onto bentonite sensitivities to three key geochemical factors relevant to DGRs, i.e., temperature, pH, and ionic strength, including the interaction effects of the variables through laboratory batch experiments and statistical analysis. The experimental results indicated that at all pH and ionic strength conditions investigated, the sorption increased with increasing temperature from 10°C to 40°C. However, sorption decreased with increasing pH (9-11) with a relatively sharper drop at higher ionic strength conditions (i.e., at 0.1 M and 1 M background NaCl). Moreover, sorption decreased with increasing ionic strength from 0.01 M to 0.1 M, but very little to no effect was observed when increased from 0.1 M to 1M. The 3-way-ANOVA tests revealed that the individual and 2-way interaction effects were statistically significant and, hence, need to be considered while explaining the sorption mechanisms. Overall, the results suggest that HS^- sorption onto bentonite might be complex, and more than one concurrent process might have been involved. The desorption test results indicated that HS^- was irreversibly sorbed on bentonite under the applied test conditions, which further supports that the sorption was a chemisorption process. The FESEM/EDS analysis suggests that HS^- sorption on bentonite might have been governed by the chemical interactions with the Fe present in bentonite and subsequent precipitation of FeS minerals. The study results led to a hypothesis of the overall sorption mechanism of HS^- onto bentonite, which helped develop a thermodynamic-based sorption model of HS^- in the following chapter, Chapter 6.

CHAPTER 6
DEVELOPMENT OF THERMODYNAMIC SORPTION MODEL USING PHREEQC

6 Chapter Overview

This chapter is organized into six sections. Firstly, Section 6.1 presents the study objective. Secondly, Section 6.2 provides an overview of the model hypothesis. Later, Section 6.3 details the model development procedures, while Section 6.4 discusses the model results. Next, Section 6.5 discusses the implication of the model findings in the context of the DGR. Finally, Section 6.6 concludes the chapter.

6.1 Study Objective

The preceding chapter shed light on the potential sorption mechanisms of HS^- onto bentonite, laying the groundwork for the development of a mechanistic sorption model to validate the hypothesized processes. Consequently, the primary objective of this study , was to develop a robust thermodynamic sorption model (TSM), that can describe the experimental results by simulating the possible reactions driving HS^- sorption onto bentonite surface. Additionally, the TSM aimed to facilitate predictions of the sorption process across a broader range of geochemical conditions. The findings from this study provide a solid foundation for future investigations within this research domain.

6.2 Model Hypothesis

Based on the literature review and experimental observations, the model hypothesized three key processes to be involved in the overall HS^- sorption onto bentonite. The processes include:

1) **Surface redox reactions**: reduction of structural Fe^{3+} to Fe^{2+} and corresponding oxidation of HS^- to elemental sulfur, S(0).
2) **Surface precipitation**: reaction of HS^- with Fe^{2+} released in the solution (i.e., due to dissolution of iron minerals) and subsequent precipitation as FeS (likely, as mackinawite).
3) **Surface complexation reactions**: formation of inner and outer-sphere complexes with surface OH^- groups at the edge sites of montmorillonite.

To enhance clarity and comprehension regarding the functioning of each process, Figure 6.1 illustrates the processes in a bentonite-water system.

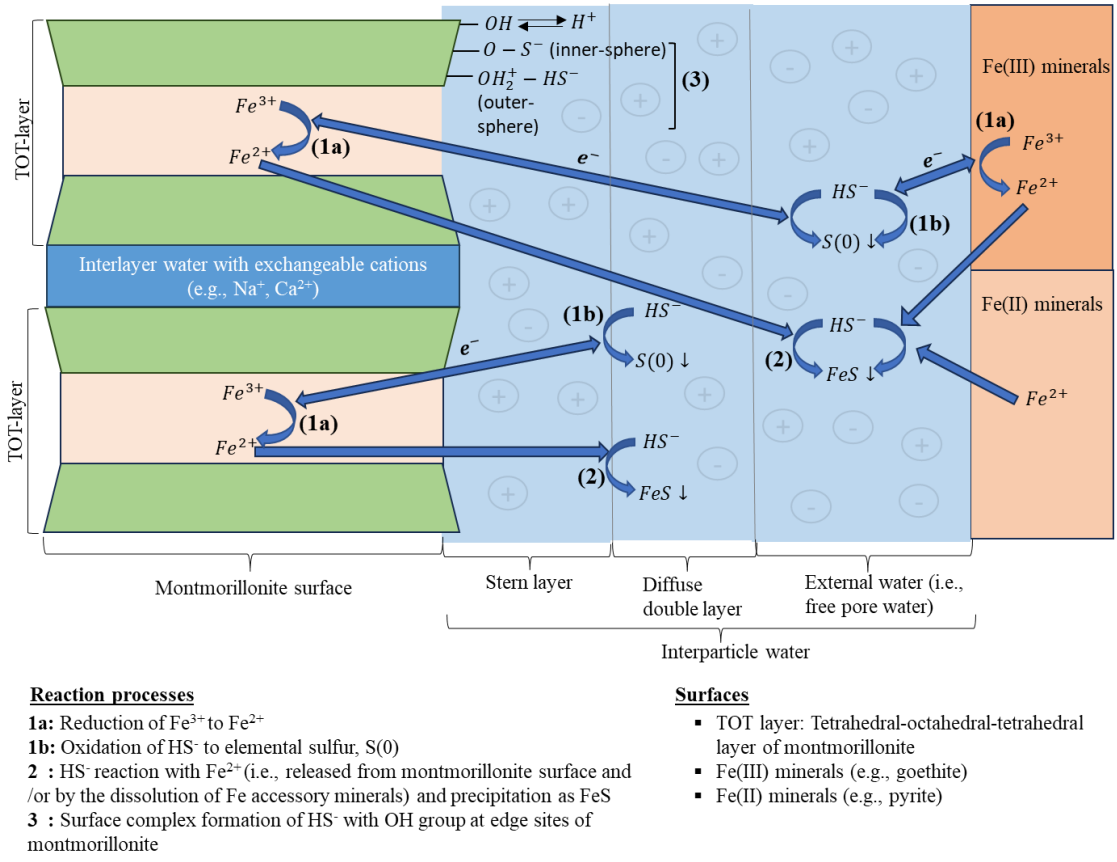

Figure 6.1 Schematic diagram of the HS^- sorption processes predicted in a bentonite-water system. The concept of the bentonite-water system was adapted from (Wersin et al., 2004; Rautioaho et al., 2009; Wigger and Van Loon, 2017).

6.3 Model Development

The sorption model was developed using PHREEQC Interactive (version 3.4.0.12927). PHREEQC, which stands for PH REdox EQuilibrium is written in C, and is a widely used geochemical program for simulating chemical reactions (including sorption) and transport processes. Once the possible sorption processes are determined from experimentation, PHREEQC can model the processes based on the thermodynamic equilibrium constants (*log K* and ΔH values) of the various sorption reactions and, thus, can help predict the sorption mechanisms over various geochemical conditions. To model the chemical reactions, PHREEQC uses a thermo-dynamic database (TDB), as a source of reference values to perform all the necessary calculations (Payne et al., 2013; P. Wang, Anderko, & Turner, 2001b). Some of the

database files included with the program are wateq4f.dat, llnl.dat, minteq.dat, minteq.v4.dat, and sit.dat. In this study, a diffuse-layer surface complexation model (SCM) with electrostatic forces was included to simulate the surface complex reactions (i.e., process 3, Figure 6.1) along with the surface redox reactions (process 1(a) and 1(b)) and surface precipitation reactions (process 2). The theory of the surface complexation model is presented in Section C.1 Theory of surface complexation model (SCM) in APPENDIX C.

Figure 6.2 represents a framework of the model delineating the model inputs, such as solution and surface data as well as the possible sorption reactions (as listed in the previous section). Based on the model outputs, the sorption capacity (moles HS^- per g bentonite) was determined by summing the simulated amounts of elemental sulfur, mackinawite, inner- and outer-sphere complexes formed. Later, the model-derived sorption capacity results were plotted against various conditions (e.g., pH, ionic strength, temperature) and the unknown parameters of the model were calibrated and validated by comparing them against the batch experimental results (as presented in Section 5.3.1 in Chapter 5) under the defined conditions. The following sections further detail the model inputs and model development processes.

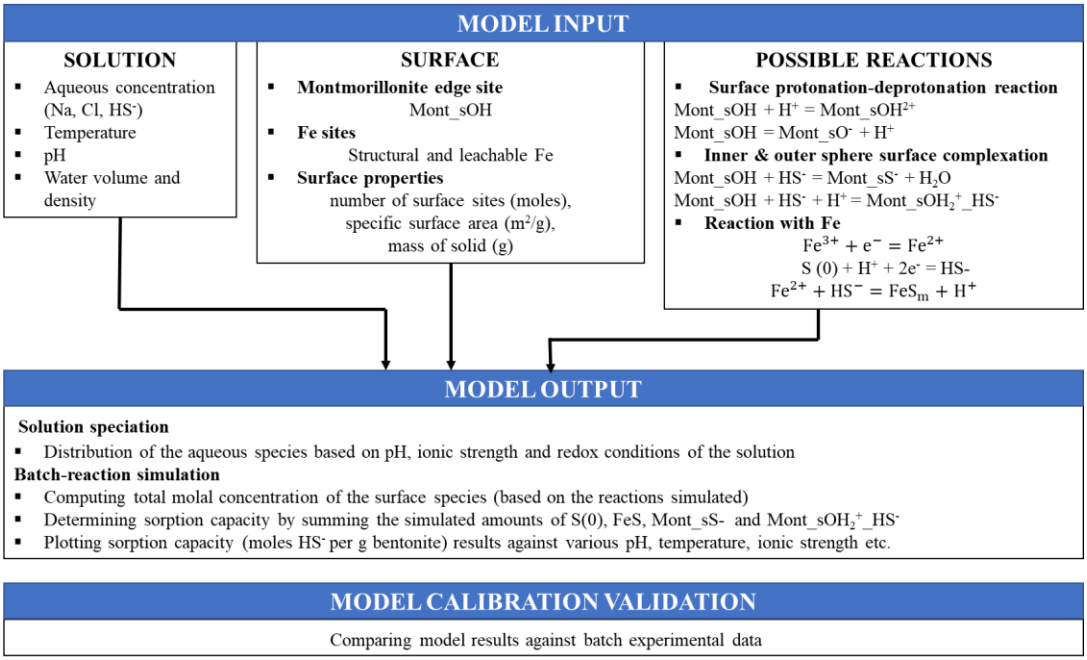

Figure 6.2 Framework of the thermodynamic sorption model.

6.3.1 Model Inputs

Na-montmorillonite was used as the reference surface for the surface complexation model development, considering that the adsorption properties of MX-80 bentonite would be very similar to that of montmorillonite (since MX-80 bentonite contains ≈ 85-90% montmorillonite (Dixon et al., 2018)). Moreover, montmorillonite is a simple and well-defined mineral that permits modeling based on systematic datasets under varied conditions (Tachi et al., 2014). The surface properties used in the model are listed in Table 6.1. As indicated in the table, two surface sites were considered in the model (i.e., Fe-site and montmorillonite edge site). The surface redox reactions (i.e., process 1, as listed in Section 6.2) and surface precipitation reactions (process 3) were assumed to take place on the surface i.e., on the total Fe-sites (the structural iron) and montmorillonite edge sites ($\equiv SOH$), respectively. On the other hand, the surface precipitation reaction (process 2) was considered to occur in the solution phase (i.e., the reaction of HS^- with the leachable iron) and subsequent precipitation as FeS (also see an illustration in Figure 6.1).

Table 6.1 Surface data used in the model.

Surface parameters		Values	References
Fe- site	Total Fe[a] (moles/g)	4.48×10^{-4} (i.e., 2.5 wt% of bentonite)	(Torstenfelt et al., 1983; Karnland et al., 2006; Dixon, 2019)
	Leachable iron[b] (moles/g)	1.97×10^{-5} (i.e., 0.11 wt% of bentonite)	
Montmorillonite edge site ($\equiv SOH$)	Site density (moles/g)	$2.03 * 10^{-4}$	(Gu et al., 2010)
	Specific surface area (m^2/g)	46	

Notes: (a) Total Fe indicates the structural iron (i.e., Fe^{3+} ions located in the octahedral layer of montmorillonite or structural component of other accessory Fe minerals (e.g., goethite, hematite. magnetite)
(b) Leachable iron indicates the available "free" iron (i.e., Fe^{2+} released in the solution from the montmorillonite surface or by the dissolution of the accessory Fe minerals (e.g., goethite, hematite. magnetite) to react with HS^- in the solution and precipitate as FeS (mackinawite).

The solution data in the model (such as temperature, pH, ionic strength, and initial concentration of HS^-) were used as per the conditions applied in the batch experiments (see Table 5.1 in Chapter 5). As mentioned in Chapter 5, the "ionic strength" term used in this chapter also corresponds to the background NaCl solution concentration. To simulate the liquid-to-solid mass ratio (i.e., 1000) applied in the batch experiment, the solution volume and mass of the solid used

in the models were 1 L and 1 g, respectively. The reactions and respective thermodynamic constants used in the model are listed in Table 6.2. As indicated in the table, the thermodynamic constants (i.e., log K and ΔH values) for the Fe and montmorillonite surface protonation-deprotonation reactions were used from existing databases and literature; however, the constants for surface complexation reactions (i.e., ***log K$_I$, log K$_O$***, **Δ*H$_I$*** and **Δ*H$_O$***) needed to be calibrated for the study context.

Table 6.2 Reactions included in the model

Reactions			log K (25°C)	ΔH (KJ/mole)	Sources/ Remarks
Surface redox reactions		$Fe^{3+} + e^- \rightarrow Fe^{2+}$	-13.02	-40.5	Thermodynamic database files included with the PHREEQC program: phreeqc.dat, wateq4f.dat, minteq.v4.dat, thermochyme.dat
		$S + H^+ + 2e^- \rightarrow HS^-$	-15.026	39.75	thermochyme.dat
Surface precipitation		$Fe^{2+} + HS^- \rightarrow FeS + H^+$	4.6	45	phreeqc.dat, wateq4f.dat, minteq.v4.dat, thermochyme.dat
SCM	Protonation-deprotonation	$\equiv SOH + H^+ \rightarrow \equiv SOH_2^+$	4.5	-14	(Bradbury and Baeynes, 2005; Gu et al., 2010; Morel et al., 2015)
		$\equiv SOH \rightarrow \equiv SO^- + H^+$	-7.9	-17	
	Surface complexation reactions	$\equiv SOH + HS^- \rightarrow \equiv S{-}S^- + H_2O$ (inner-sphere)	***log K$_I$***	**Δ*H$_I$***	By fitting to experimental data at 25°C and 40°C
		$\equiv SOH + HS^- + H^+ \rightarrow \equiv SOH_2^+ - HS^-$ (outer-sphere)	***log K$_O$***	**Δ*H$_O$***	

Notes: (i) ***log K$_I$*** and ***log K$_O$*** indicate the inner and outer-sphere equilibrium constants, respectively.
(ii) **Δ*H$_I$*** and **Δ*H$_O$*** indicate the inner and outer-sphere enthalpy values, respectively.
(iii) ***log K$_I$, log K$_O$***, **Δ*H$_I$*** and **Δ*H$_O$*** are the calibration parameters.

Based on the input data, the model was developed in 3 stages as follows:

1. Model verification (step 1)
2. Calibration (steps 2-4)
3. Validation (step 5)

6.3.2 Model Verification

Step 1: The main challenge of the model development was finding the optimal range of $logK_I$ and $logK_0$ values to initiate the calibration process. It is important to note that the *logK* value depends on temperature but not on the solution's pH and ionic strength. As such, to verify the initial model, several trial simulations were performed at the studied pH range (i.e., 9-11), but at a fixed temperature of 25°C (i.e. the reference temperature in PHREEQC) and at a fixed ionic strength (i.e., lowest ionic strength, 0.01 M). Based on the trials, an approximate range of $logK_I$ and $logK_0$ values was selected at which the model could predict the sorption trend with the pH as observed in the experiments (i.e., decreasing sorption with increasing pH).

6.3.3 (Model Calibration and Validation

Step 2: From the optimized range of values (as determined from **Step 1**), the $logK_I$ and $logK_O$ *values* were calibrated by fitting the model-derived sorption capacity data to the experimental data at all pH (i.e., 9-11) and ionic strength conditions (i.e., 0.01M, 0.1M and 1 M) studied at 25°C (i.e., the experimental results presented in Section 5.3 in Chapter 5). The best-fit was determined by graphical observation as well as by minimizing the root mean squared error (RMSE) between experimental and model results.

Step 3: Further calibration was performed with various Fe fractions to check the sensitivity of the available Fe sites on the log K values (the results are presented in Table C.5 in APPENDIX C and discussed in the following section). The log K(25°C) values and the amount of Fe, at which the model results were closest to the experiment result at 25°C (i.e., minimum error) and could successfully predict both the pH and ionic strength trends, were used for subsequent simulations (i.e., for calibrating $\Delta \boldsymbol{H}$ values and validation). At the end of this step, the log K values ($logK_I$ and $logK_O$) were established. It is important to note that up to step 3, no ΔH value was required.

Step 4: PHREEQC uses the standard enthalpy (ΔH) in the Van't Hoff equation ($\log\frac{K(T_2)}{K(T_1)} = \frac{\Delta \boldsymbol{H}}{2.303R}(\frac{1}{T_1} - \frac{1}{T_2})$) or an analytical expression ($logK = A_1 + A_2T + \frac{A_3}{T} + A_4 logT + \frac{A_5}{T^2} + A_6T^2$, where temperature T is in Kelvin and A_1 to A_6 are co-efficients of the equation) to simulate the reactions at a temperature other than 25°C. Using the calibrated log K (25°C) values (from step

3) in the Van't Hoff equation, the model was simulated at 40°C and the ΔH_I and ΔH_O values were calibrated by fitting the model data to the experimental data at 40°C.

Step 5: Finally, using the calibrated *log K* and ΔH values at 25 and 40°C (from steps 3 and 4), the model was simulated at 10°C and compared against the experimental data (at 10 °C) for validation.

As the calibration and validation were performed by comparing the model results with the experimental results, these modelling steps are further detailed in the following section. A schematic diagram outlining the verification, calibration and validation process is presented in Figure 6.3.

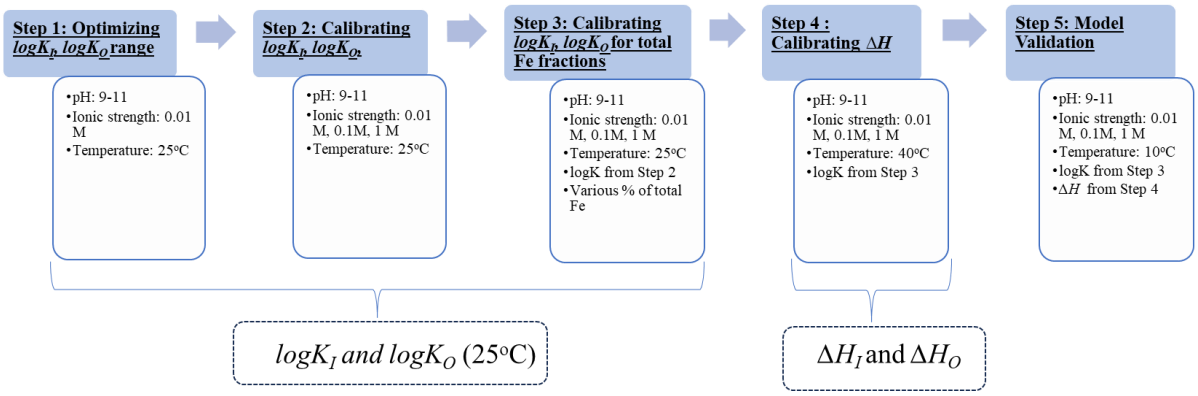

Figure 6.3 Schematic diagram of model verification, calibration and validation process

6.4 Model Results

Figure 6.4 presents the thermodynamic sorption model results as a function of pH and ionic strength at 25°C. This figure suggests that the simulated sorption capacity values agreed reasonably well with the experiment results across geochemical conditions (i.e., with RSME ranging between 3.3-6.18 x10^{-06}, Table C.5 in APPENDIX C). This good agreement implies that the model captured the fundamental mechanisms governing HS^- sorption onto bentonite as a function of pH and ionic strength. The model simulation suggests that reaction with Fe (i.e., process 1 and 2: S(0) and FeS formation) contributed most to HS^- sorption onto bentonite, i.e., 63-87% (at 0.01 M); 69-96% (at 0.1 M) and 67-99% (at 1M) over the pH range considered. Next highest contribution came from outer-sphere complex reactions at lower pH levels (i.e., 9-9.5) and lower ionic strength conditions (i.e., 0.01M), but were nearly negligible at higher pH (i.e.,

10-11) and higher ionic strength conditions (i.e., > 0.1 M). In all cases inner-sphere complex reactions were negligible.

Figure 6.4 also shows that the model predicted S(0) formation (i.e., resulting from Fe^{3+} reduction by HS^-) increasing with increasing pH. This prediction is consistent with the experimental results of Hadi et al. (2023), who observed a decrease in Fe^{3+} reduction by sulfide when the pH was decreased from 12 to 8. Moreover, Pederson et al., (2017) observed a drop of sulfide immobilization as S(0) due to a decline in pH from 7 to 2. However, no significant influence of ionic strength conditions on S(0) formation was predicted by the model Figure 6.4 (b) and (c).

Moreover, the model results show that FeS (likely mackinawite) precipitation was relatively insensitive to the pH and ionic strength conditions considered in the study (i.e., FeS precipitation only slightly increased with increasing pH and ionic strength). The experiments conducted by Nielsen et al. (2008) observed that at pH above 8, almost all (i.e., >80%) of the Fe^{2+} added in the sulfide solution precipitated as mackinawite, while only 40% precipitated as mackinawite at a pH below 7. This observation supports the model results, i.e., at the pH levels studied (9-11), most of the available Fe^{2+} (i.e., the leachable might have reacted with HS^- to form FeS across all conditions. Bolney et al. (2021) reported that increased NaCl may lead to increased Fe^{2+} release into solution, which can be further precipitated as FeS if there is excess sulfide. However, due to the low HS^- concentration used in the study, the additional FeS might not have been able to form, which could explain the limited sensitivity to ionic strength observed in this study.

On the other hand, Figure 6.4 shows that the model predicted the surface complexations were highly sensitive to pH and ionic strength. Both inner- and outer-sphere complexes were predicted to decrease with increasing pH, while outer-sphere complexes decreased and inner-sphere complexes increased with increasing ionic strength. These predictions are highly consistent with the literature (see detailed discussion in Section 5.3.1 in Chapter 5). Moreover, the simulated total sorption results complied with experimental results when the outer-sphere complexation was dominant over the inner-sphere complexation. A suite of exploratory simulations considering either: (i) both complexations significant or (ii) only inner-sphere complexations poorly predicted experimental trends. That is, these exploratory simulations predicted increasing sorption with increasing ionic strength, which is opposite to the trend observed in the experiments. Therefore, only the outer-sphere log K (i.e., $\boldsymbol{log\ K_O}$) was calibrated against

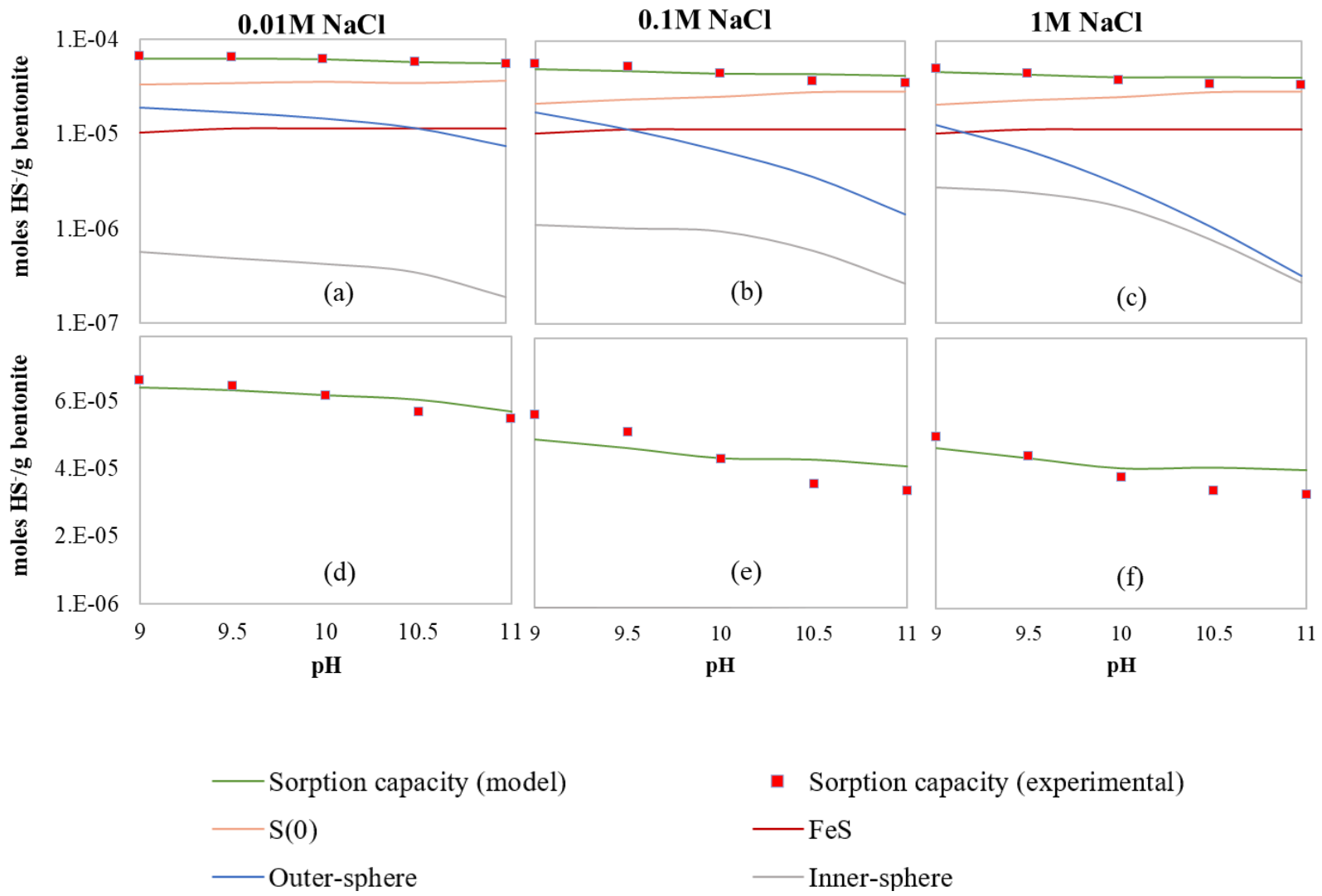

Figure 6.4 Model results (a-f) on HS^- sorption onto bentonite as a function of pH and ionic strength at 25°C. Figures in the second row (d-f) represent the higher resolution of the model fitting to the experimental data.

experimental results. The inner-sphere log K (i.e., ***log K_I***) was kept fixed at an arbitrary upper bound value (i.e., 5.2±0.5) at which its effect was found negligible (at least an order of magnitude lower than other reactions). While this modeling approach does not provide a valuable estimate of the inner-sphere complexation reaction parameters, it does identify that outer-sphere complexations were much more important than inner-sphere complexations; therefore, inner-sphere complexations can be safely neglected when considering HS^- sorption onto bentonite over the geochemical ranges investigated. Furthermore, as depicted in Figure 6.4, the outer-sphere complexation exhibits increasing sensitivity to pH variation at higher ionic strengths. This heightened sensitivity likely stems from the increased propensity of OH^- ions to interact with Na^+ cations rather than forming bonds with HS^-. Consequently, the sorption contribution from outer-sphere complexes decreases at higher ionic strengths. This finding can explain the minimal HS^- sorption capacity changes observed in experiments when the ionic strength was increased from 0.1 M to 1 M (also see discussion in Section 5.3.1 in Chapter 5). In addition, the model findings validate the two-way interaction effect of pH and ionic strength as revealed from the ANOVA analysis presented in Section 5.3.2.

In the model, the outer-sphere log K was found sensitive to the number of available Fe-sites considered. Figure 6.5 presents the best fit outer-sphere log K(25°C) values (at 0.01 M ionic strength) which were observed at various fractions of the total Fe. However, the model successfully predicted the pH and ionic strength effects trends when only 10-20% of the total Fe was considered reactive to HS^- (see Table C.5 in APPENDIX C). This finding agrees with Hadi et al., (2023), who observed that only 19% of the total Fe in Wyoming bentonite was reducible by HS^-. As such, for all subsequent simulations (i.e., for 40° and 10°C), 20% of total Fe was used as available Fe sites for the surface redox reactions and the corresponding outer-sphere *log K_O* value (i.e., 16.7±0.3) was used to simulate outer-sphere complex reactions.

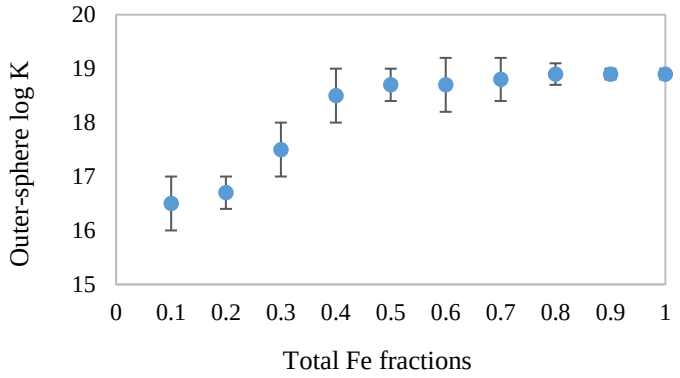

Figure 6.5 Outer-sphere log K(25°C) values at which the best fit to the experimental data (at 0.01 M ionic strength) was observed at various total Fe fractions.

The model simulation results at 40°C (Figure 6.6) show that the model also successfully predicted the temperature effects on HS^- sorption onto bentonite with a good fit to the experimental data (RMSE 3.02-7.10 $x10^{-06}$). The positive enthalpy of the outer-sphere complex reaction, $\Delta \boldsymbol{H_O}$ (i.e., 80 KJ/mole; calibrated by the experimental data at 40°C), indicates these reactions were endothermic and, thus, increased with increasing temperature. Additionally, the model simulated a slight increase in S(0) and FeS formation with increasing temperature based on the established ΔH values used (Table 6.2). Considering the negligible effects of the inner-sphere complex, $\Delta \boldsymbol{H_I}$ was kept constant at an arbitrary value (i.e., +40KJ/mole).

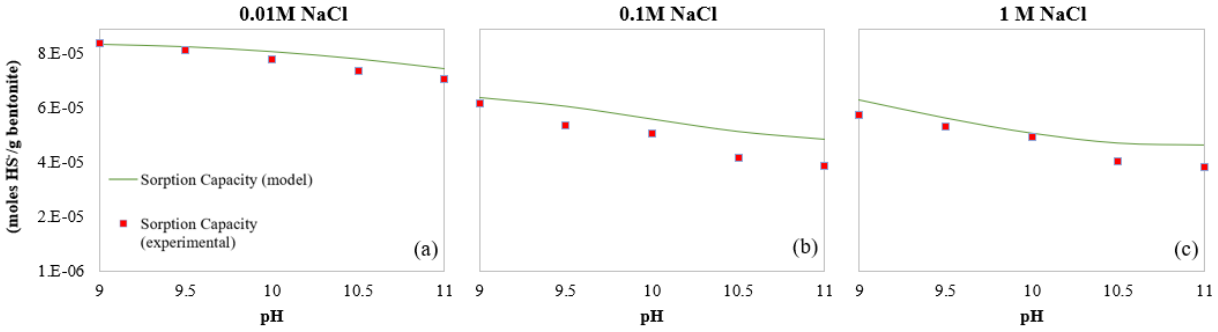

Figure 6.6 Experimental and model results (a-c) of HS^- sorption onto bentonite as a function of pH and ionic strength at 40°C.

Figure 6.7 shows the fit between the simulated and experimental sorption results at 10°C. This excellent agreement validates the model, as all unknown parameters (the log K and ΔH values of the surface complexation reactions) were calibrated at 25 and 40°C. The model simulation results at 40°C and 10°C are presented in detail in Figure C.6 and Figure C.7 in APPENDIX C.

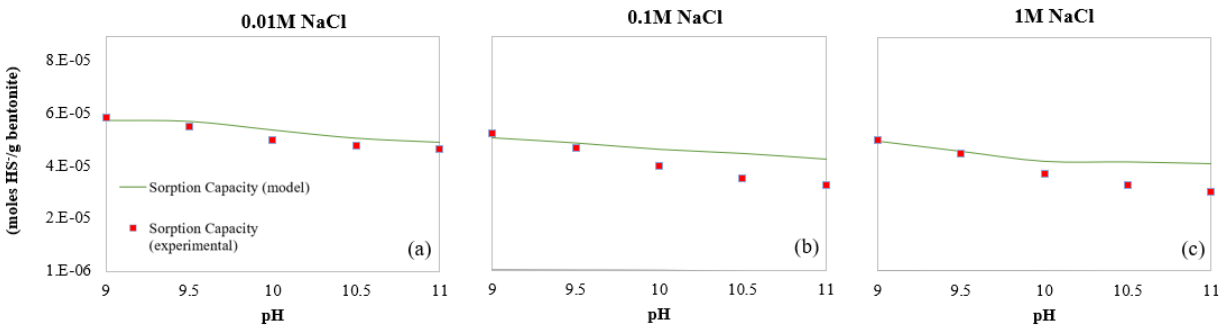

Figure 6.7 Experimental and model results (a-c) of HS^- sorption onto bentonite as a function of pH and ionic strength at 10°C

Altogether, it can be said that by integrating the reactions listed in Table 6.2, the model effectively characterized the HS^- sorption phenomenon under the effects of pH, ionic strength and temperature, exhibiting a satisfactory agreement with experimental data. Additionally, the model's predictions for each process were consistent with findings from previous studies. However, since the model relied on literature values for the surface data (as listed in Table 6.2), the model predicted sorption capacity results were slightly higher than those observed in experiments. Further model improvement can be done by including the surface data specifically measured on the bentonite sample used in the experiments. Nevertheless, the model (i.e., calibrated and validated by experimental sorption results) can be used as a framework model to predict and better understand HS^- sorption onto bentonite across a broad spectrum of geochemical conditions expected in a DGR.

6.5 DGR Implications

This study yields valuable insights into fundamental aspects of HS^- sorption onto bentonite and, sheds light on how a key DGR engineered barrier component may respond to evolving geochemical conditions over its operational lifespan. The temperature range (10-40°C) examined corresponds to the long-term condition of the repository (i.e. when the temperature range returns to ambient level) and the bentonite buffer will be completely saturated (King et al., 2017; Hall et al., 2021). After the peak temperature is reached, sorption is expected to decrease with decreasing temperature, particularly favoring low pH and low ionic strength conditions.

The pH levels studied could reflect a scenario where the DGR pH may approach 9 or higher (possibly by the dissolution of carbonaceous minerals from bentonite buffer or host rock) and HS^- may become the predominant sulfide species. However, the reference pH levels for

crystalline (CR-10) and sedimentary (SR-270-PW) host rocks by NWMO are 7.1 and 5.88, respectively (Hall et al. 2020). As such, the base model was extrapolated up to pH 5 at 0.1 M and 1 M ionic strengths to obtain insight into HS^- sorption onto bentonite at these pH conditions. The extrapolation results in Figure 6.8 suggest that adsorption through surface complexation reactions may contribute most to the overall sorption at low pH values (i.e., 5-8). Conversely, reducing Fe and the corresponding oxidation of HS^- to S(0) would likely be diminished (i.e., as discussed in the previous section). Additionally, the formation of FeS (i.e., likely as mackinawite) is expected to decrease significantly if the repository pH falls below 7, while HS^- may partly convert to H_2S (gas). However, it should be emphasized that the model's predictions for the lower pH range (5-7), particularly concerning the possibility of H_2S gas formation, have not been validated through corresponding experiments. Therefore, the model is more appropriate for describing the scenarios above pH 7.

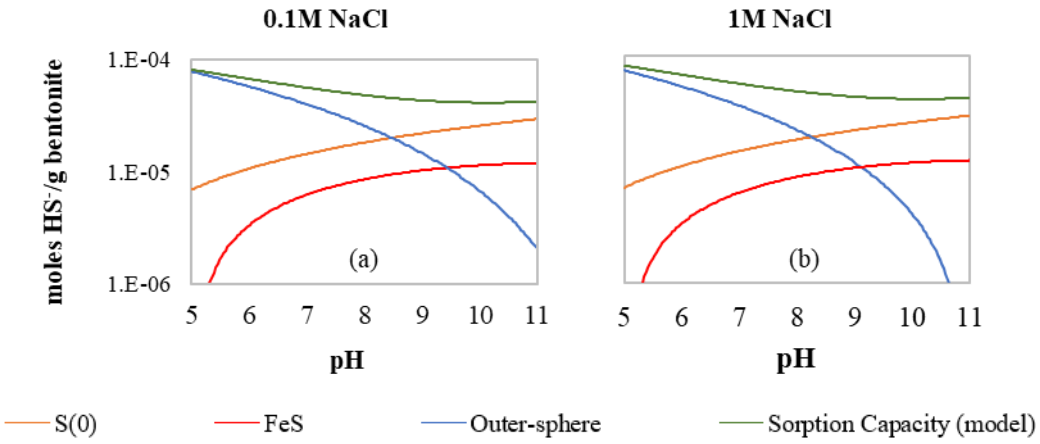

Figure 6.8 Extension of base model data down to pH 5 (temperature: 25°C).

Although this study used dispersed bentonite at a high liquid to solid ratio, which does not mimic the compacted bentonite planned for use in the DGR, the sorption results still provide valuable insight into the relevant fundamental mechanisms. Moreover, the total sorption results provide valuable measurements of the maximum amount achievable on bentonite with limited HS^- concentrations (i.e., 3 mg L^{-1}). This information can be useful in scenarios with lower-density bentonite, e.g., bentonite-based gap-fill materials or areas with bentonite erosion.

It is important to note that clay compaction and the consequent “anion exclusion” effect, i.e., the exclusion of anions from the diffuse double layer (Wigger and Van Loon, 2017), would limit the overall interaction between HS^- and bentonite. The sorption processes illustrated in Figure 6.1

may provide insight into how the compaction can impact each sorption process. Since adsorption by surface complexations occurs in the stern layer (as indicated in Figure 6.1), compaction would likely have a more significant reduction on the surface complexation reactions – but a lesser reduction on the surface redox and precipitation reactions because these reactions may occur in the pore water. As such, the reactions with Fe will likely be the principal HS^- sorption mechanism onto compacted bentonite. However, the possibility of adsorption by outer-sphere complexes should not be ruled out completely, particularly at neutral to slightly acidic pH range expected in Canadian DGR.

The model developed in the study (i.e., calibrated and validated by experimental data) provides valuable information on the underlying sorption mechanisms of HS^- onto bentonite, and offers a foundation for deeper investigations. Additionally, this newly developed and validated sorption model can be incorporated into existing transport models to provide valuable insights into the reactive transport of HS- under DGR conditions in Canada and other repositories worldwide.

6.6 Summary

A thermodynamic sorption model was developed considering 3 key processes contributing to HS^- retention on bentonite: (i) oxidative sorption as S(0), (ii) surface precipitation as FeS, (iii) inner and/or outer-sphere surface complexation formation at the edge site of montmorillonite. With a combination of these processes, the model could successfully describe the sorption phenomenon as a function of pH, temperature, and ionic strength with reasonably good agreement with experimental data. Furthermore, the model prediction for each process aligned with the previous studies. The model's findings indicated that S(0) and FeS formation may contribute 63-99% to the total sorption at the chemical conditions tested. In addition, outer-sphere complexations may also contribute at low pH (9-9.5) and low ionic strength but become less effective or negligible at higher pH (i.e., 10-11) and higher ionic strengths. The model, thus, provides vital information on the underlying sorption mechanisms of HS^- onto bentonite and can be used as a base/framework model for further investigation of the process such as in a compacted bentonite system by including bentonite pore water chemistry. Eventually, this newly validated sorption model can be used in a HS^- reactive transport model to support the broader effort towards establishing the long-term DGR performance assessment.

CHAPTER 7

CONCLUSIONS AND FUTURE WORK

7 Chapter Overview

This chapter presents the contribution and critical findings of the research conducted in Chapter 3 to 6 (Section 7.1). Section 7.2 discusses the study's limitations and potential avenues for future works.

7.1 Research Summary and Contributions

Bentonite clay is widely utilized as an engineered barrier in the design of DGRs for the purpose of long-term management of radioactive wastes. In Canadian DGR, the engineered barrier system (EBS) is planned to include copper-coated used fuel containers (UFCs) surrounded by a highly compacted bentonite buffer and backfill. However, microbiologically influenced corrosion becomes a possible mode of degradation for UFC under anaerobic conditions, where sulfate may be reduced to bisulfide (HS^-) by sulfate-reducing bacteria and then transported to the UFC surface, leading to copper corrosion. The overall corrosion process is expected to be controlled by HS^- flux to the UFC surface; therefore, understanding the HS^- sorption mechanisms onto bentonite is critical to aid in the safety assessment of the DGR.

Sorption is a critical process related to the prevention or retardation of corrosive agents migrating through compacted bentonite buffer in a DGR. Although the corrosive effects of HS^- on UFCs have drawn significant attention over recent years, its sorption behaviour onto bentonite in the hydrogeochemical context of a DGR has not yet been thoroughly investigated. For this purpose, it is essential to study the sorption of HS^- onto bentonite to gather reliable values of sorption parameters (e.g., sorption capacity) for long-term prediction of the EBS performance. In addition, it is imperative to understand how the geochemical evolution of the DGR may affect the bentonite sorption characteristics. Therefore, the objective of this research is to evaluate the sorption capacity of bentonite to retard the transport of HS^- under varying critical geochemical conditions through laboratory experiments and numerical modelling.

Although compacted bentonite is planned to be used in the actual repository, the study used dispersed bentonite slurry to better control for experimental variables to study the fundamental sorption dynamics. As part of the research, a thorough literature review was conducted to understand the overall sorption phenomenon in bentonite and identify the key factors influencing its sorption capacity. In light of the literature review, six factors were primarily selected for this study to explore HS^- sorption onto bentonite. The selected factors included: (i) contact time (ii) temperature (iii) initial HS^- concentration (iv) liquid to solid mass ratio (L:S) (v) pH and (vi) ionic strength of background solution. Temperature, pH, and ionic strength were chosen because they align with the crucial geochemical conditions of the DGR. The selection of other factors aimed to establish the suitable range for conducting batch experiments in a laboratory setting and to better understand the sorption mechanism of HS^-.

Subsequently, a robust methodology was devised to ensure the reliability of the experimental procedure, which involved conducting preliminary experiments to determine the appropriate range of contact time, liquid to solid ratio (L:S), and initial HS^- concentration for laboratory batch experiments. Drawing insights from the literature review and preliminary experiments, six sets of batch experiments, including desorption tests, were designed and executed to explore the fundamentals of HS^- sorption behaviour and the possible sorption mechanisms under the effects of the selected key factors. Additionally, surface analyses, such as field emission scanning electron microscopy and energy dispersive spectroscopy (FESEM/EDS), were carried out to gain further understanding of the interactions between HS^- and bentonite. Lastly, a thermodynamic sorption model was developed, calibrated, and validated using experimental results to comprehend the processes governing HS^- sorption onto bentonite, including the individual contributions of each process to the overall sorption.

The major research contribution is its pioneering effort to systematically explore the sorption dynamics of HS^- onto bentonite, comprehensively covering kinetics, isotherms, and thermodynamic characteristics. Through the lens of experiments and mechanistic sorption modelling, the study provided a micro-level insight into the sorption mechanism under the effects of three critical geochemical factors (i.e., temperature, pH, and ionic strength) of the DGR. The research findings will facilitate decision-makers to accurately predict the reactive transport of HS^- under real DGR conditions in Canada and worldwide.

In addition, other notable contributions are as follows:

- Chapter 3 detailed the methodology development work, including the QA/QC approaches rigorously followed to bolster confidence in the experimental process. While the study followed traditional batch experiment steps, improvements were made at each stage, aiming to pinpoint the most effective approach for evaluating the capacity of bentonite to sorb HS^- through laboratory batch experiments, achieving creditable outcomes from the experiments.

  The initial experiments underscored that the extent of experimental loss (i.e. other than sorption onto bentonite) of HS^- increases with prolonged shaking time and higher temperatures, and the material of the centrifuge tube significantly influences this process. Consequently, based on these findings, the choice of glass centrifuge tubes proved optimal instead of plastic tubes for conducting batch experiments, effectively minimizing HS^- loss resulting from the experimental procedures.

  Moreover, from the initial experimental results, it was established that a minimum (i) L:S ratio of 100 and (ii) initial HS^- concentration of 1 mg/L are necessary to maintain detectable HS^- in the aqueous phase after sorption. The results also indicated that a minimum of 24 hours of shaking is essential to ensure the sorption equilibrium. These insights from the study were instrumental in designing the batch experiments carried out in the subsequent chapters.

- Chapter 4 revealed the fundamental aspects of the HS^- sorption phenomenon onto bentonite as a function of four critical parameters, such as contact time, temperature, liquid to solid ratio (L:S), and initial HS^- concentration. The findings suggest that the sorption of HS^- onto bentonite increased with longer contact times and occurred more rapidly at higher temperatures, reaching equilibrium after 16 hours (at 40°C), 24 hours (at 22 and 30°C), and 96 hours (at 10°C). Furthermore, the sorption capacity increased by approximately 3% with rising temperature from 10 to 40°C. Among the kinetic models examined, the pseudo-second-order model exhibited the best agreement with the experimental results, suggesting that the sorption rate may have been limited by chemical processes.

Moreover, the results indicated that increasing L:S facilitated better interaction of HS^- with bentonite surface, resulting in higher HS^- sorption on per unit mass of bentonite. The Freundlich isotherm constant (n > 1) indicated that the sorption process was favourable, and bentonite displayed a high affinity for HS^-. Under the studied experimental conditions, the Langmuir and Freundlich isotherm models adequately fit the data, as evidenced by high R^2 values (> 0.9). However, high χ^2 values suggested potential limitations of these models in describing HS^- sorption onto bentonite, particularly at high liquid to solid ratios. Thermodynamic analysis results indicated that the sorption process was endothermic and spontaneous.

Utilizing the maximum sorption capacity values derived from the experimental results (ranging from 580 to 2564 mg HS^-/kg bentonite, equivalent to 0.018-0.078 moles HS-/kg bentonite), initial calculations can be made to quantify the impact of HS^- sorption on reducing Cu corrosion in a DGR. Based on this preliminary estimation, the maximum potential reduction in Cu corrosion is projected to be in the range of 0.25-1.10 µm m^{-2} per 1 kg of bentonite, considering an HS^- flux ranging from 1 to 6 mg L^{-1}.

- Chapter 5 delved into the sensitivity of HS^- sorption onto bentonite concerning three crucial geochemical factors pertinent to DGR: temperature, pH, and ionic strength. This exploration encompassed the interaction effects of these variables through laboratory batch experiments and statistical analysis. The experimental outcomes revealed that, across all pH and ionic strength conditions examined, sorption increased as temperature rose from 10°C to 40°C. However, sorption declined with higher pH levels (9-11), showing a more pronounced decrease at elevated ionic strength conditions (i.e., at 0.1 M and 1 M background NaCl). Additionally, sorption decreased with increasing ionic strength from 0.01 M to 0.1 M, but minimal to no effect was observed when ionic strength increased from 0.1 M to 1M. In general, the findings of the experiments indicated that HS^-sorption onto bentonite was more favourable under conditions of elevated temperatures, lower pH levels, and reduced ionic strengths. Under the investigated experimental parameters, the maximum estimated sorption capacity

(corresponding to 3 mgL^{-1} initial HS^- concentration) was determined to be 8.52×10^{-5} moles HS^-/g bentonite, observed at 40°C, pH 9, and an ionic strength of 0.01 M.

The three-way ANOVA tests demonstrated that individual and two-way interaction effects of the variables (i.e., temperature, pH and ionic strength) were statistically significant, emphasizing the need to consider these factors in explaining the sorption mechanism. Overall, the results suggest that HS^- sorption onto bentonite may involve multiple concurrent processes, making it a complex phenomenon. Desorption tests indicated that HS^- was irreversibly sorbed on bentonite under all the applied test conditions, supporting the notion that chemical reactions, such as precipitation and/or chemical adsorption, like surface complexation, might be the primary drivers of the sorption process.

The surface analysis results (via FESEM/EDS) suggested that HS^- sorption on bentonite might be governed by chemical interactions with the iron (Fe) present in bentonite, leading to the subsequent precipitation of FeS minerals. It is also plausible that the sorption process involves a redox reaction between HS^- and structural Fe^{3+} in bentonite, resulting in the precipitation of HS^- as elemental sulfur (S(0)), as proposed in the literature. Furthermore, the observed sorption behaviour in response to pH and ionic strength variations could suggest the potential involvement of surface complex reactions with the hydroxyl (OH) functional groups, as seen in various other anion sorption studies in the literature. These findings, thus, contributed to formulating a hypothesis regarding the overall sorption mechanism of HS^- onto bentonite, paving the way for developing a thermodynamic-based sorption model in the subsequent chapter.

- In Chapter 6, a thermodynamic sorption model was developed, taking into account three key processes contributing to HS^- retention on bentonite: (i) oxidative sorption as elemental sulfur, S(0), (ii) surface precipitation as FeS, and (iii) formation of inner and/or outer-sphere surface complexes at the edge site of montmorillonite. By incorporating these processes, the model could effectively explain the sorption phenomenon in relation to pH, temperature, and ionic strength, displaying reasonably good agreement with the experimental data. Furthermore, the model predictions for each process were consistent with previous studies.

The model's outcomes suggested that the formation of S(0) and FeS could contribute significantly under the tested chemical conditions, accounting for 63-99% of the total sorption. Additionally, outer-sphere complexations might play a role, particularly at low pH levels (9-9.5) and low ionic strengths, but their effectiveness diminished or became negligible at higher pH (10-11) and higher ionic strengths (0.1M-1M).

The model developed in this study, calibrated and validated using experimental data, provides valuable insights into the underlying sorption mechanisms of HS^- onto bentonite. The outcomes are directly applicable in scenarios involving lower-density bentonites, such as with gap-fill materials or areas susceptible to bentonite erosion. It is essential to acknowledge that clay compaction and the resultant "anion exclusion" effect could restrict the overall interaction between HS^- and bentonite. Given that surface complexation reactions occur in the stern layer, compaction is likely to significantly reduce these reactions, but have a lesser effect on surface redox and precipitation reactions, as they may take place in the pore water. Consequently, reactions with Fe are likely to be the principal HS^- sorption mechanism onto compacted bentonite. However, the possibility of adsorption by outer-sphere complexes should not be entirely dismissed, especially within the neutral to acidic pH range expected in the Canadian DGR.

7.2 Limitations and Future Work

While the study offers valuable insights into sorption behaviour of HS^- onto bentonite, it is essential to acknowledge certain limitations that require attention. Nevertheless, these identified points not only highlight areas for improvement but also pave the way for future research endeavours.

1. The sorption capacity values obtained from batch experiments (i.e., using dispersed bentonite) may overestimate the real performance in a DGR setting. This discrepancy arises from using dispersed rather than compacted bentonite, which results in reduced accessible surface area and available sorption sites in compacted clay, attributed to the presence of small and blocked pores. To address this, the impact of bentonite compaction on the sorption behaviour of HS^- can be investigated in future through either (i) flow-through column experiments utilizing columns packed with compacted bentonite or a

sand-bentonite mixture or (ii) sorption experiments employing a specially designed cell (e.g., stainless steel cell with a compacted bentonite puck). Comparing the compacted method and batch method results would help determine the extent to which compaction reduces HS^- sorption.

2. The study used NaCl as the background solution, considering that Na^+ and Cl^- are the predominant ions in Canadian groundwater and bentonite porewater. In future, synthetic water simulating the Canadian groundwater can be used in the experiments to investigate the effects of other co-existing ions on HS^- sorption onto bentonite. In addition, possibility of "trisulfates" formation can be investigated in future.

3. The surface analysis technique employed in this study, i.e., EDS analysis, serves as a semi-quantitative tool for elemental analysis. It offers percentage data of surface elements but lacks the ability to identify chemical compounds and their diverse forms. Notably, quantifying sorption processes from EDS mapping proved challenging due to the heterogeneous nature of the bentonite surface, low initial concentration of HS^-, and the interference from high background sulfur (S). Looking ahead, the study could benefit from applying more advanced analytical techniques capable of providing a deeper understanding and quantification of the HS^- sorption in the solid phase. These techniques could facilitate a comprehensive mass balance, offering insights beyond surface elemental percentages.

4. The statistical analysis presented in Chapter 5 validates the individual and interaction effects of the studied geochemical conditions on the HS^- sorption onto bentonite. However, to what extent they would affect the sorption capacity requires further investigation to better understand the interplay of the geochemical variables on the sorption mechanisms.

5. The thermodynamic sorption model presented in Chapter 6 was based on surface data obtained from existing literature. Improvement to the model could be achieved by incorporating surface data directly measured from the bentonite sample utilized in the experiments. Additionally, refining the model could incorporate dissolution-precipitation reactions of iron minerals to provide a more accurate prediction of the available iron sites.

6. While the model simulation within the investigated pH range (9-11) has been validated against experimental data, it is important to note that the model's predictions in the lower pH range (5-8) lack corresponding experimental validation. As such, additional research is required to comprehend the scenarios at low pH conditions, especially when there is a potential for H_2S gas formation.

7. The study aimed at providing a comprehensive insight into the sorption phenomenon of HS^- onto bentonite. It is important to note that quantifying or predicting the transport of HS^- flux to the UFC surface was not within the scope of this research. However, as a next step in the immediate future, the thermodynamic sorption model developed in Chapter 6 can be applied to develop an integrated sorption and diffusion (ISD) model to simulate the diffusive-sorptive transport of HS^- in a compacted bentonite system. The ISD model approach, first conceptualized by (Ochs et al., 2001) and modified by (Tachi & Yotsuji, 2014), is based on the consistent integration of three sub-models: (i) a clay–water interaction/porewater model, (ii) a thermodynamic sorption model and (iii) a mechanistic diffusion model based on the electrical double layer theory. As such, the ISD model allows simultaneous calculation of sorption parameters, effective and apparent diffusivities (D_e and D_a), which are key parameters in Fick's second law describing solute transport governed by diffusion and sorption processes in compacted media. Alternatively, a reactive transport model of HS^- through a bentonite buffer in the repository can be developed by coupling the thermodynamic sorption model with a transport model using COMSOL Multiphysics (i.e., a commercial finite element software package), thereby expanding the scope of the study to encompass both sorption and diffusion aspects.

Since microbiologically influenced corrosion of UFCs in the presence of HS^- is a concern that may impact the long-term performance of the DGR, the findings from this study will eventually support the broader effort for developing a safety assessment model of the DGR system. Above all, the detailed experimental methodology and model development procedures documented in this study may serve as a research framework/ baseline study for future DGR investigations and other environmental-related research.

References

Ahlatci, F., Yilmaz, E., & Celep, O. (2016). Sulphide precipitation of gold and silver from thiosulphate. *15th International Mineral Processing Symposium, Istanbul-Turkey, October 19-21, 2016, October*.

Al-Ani, T., & Sarapää, O. (2008). Clay and Clay Mineralogy. *Industrial and Engineering Chemistry Research*, *31*(8), 1937–1946.

Alshameri, A., He, H., Xin, C., Zhu, J., Xinghu, W., Zhu, R., & Wang, H. (2019). Hydrometallurgy Understanding the role of natural clay minerals as effective adsorbents and alternative source of rare earth elements: Adsorption operative parameters. *Hydrometallurgy*, *185*(September 2018), 149–161. https://doi.org/10.1016/j.hydromet.2019.02.016

A.O, D. (2012). Langmuir, Freundlich, Temkin and Dubinin–Radushkevich Isotherms Studies of Equilibrium Sorption of Zn^{2+} Unto Phosphoric Acid Modified Rice Husk. *IOSR Journal of Applied Chemistry*, *3*(1), 38–45. https://doi.org/10.9790/5736-0313845

APHA. (2017). Standard Methods for the Examination of Water and Wastewater (23rd ed.). American Public Health Association, American Water Works Association and Water Environmental Federation.

Appelo, C. A. J., Loon, L. R. Van, & Wersin, P. (2010). Multicomponent diffusion of a suite of tracers (HTO , Cl , Br , I , Na , Sr , Cs) in a single sample of Opalinus Clay. *74*, 1201–1219. https://doi.org/10.1016/j.gca.2009.11.013

Ayawei, N., Ebelegi, A. N., & Wankasi, D. (2017). Modelling and interpretation of adsorption isotherms. *Journal of Chemistry*, *2017*(1), 3039817.

Azizian, S. (2004). Kinetic models of sorption: a theoretical analysis. *Journal of colloid and Interface Science*, *276*(1), 47-52.

Baeyens, B., & Bradbury, M. H. (1997). A mechanistic description of Ni and Zn sorption on Na-montmorillonite Part I: Titration and sorption measurements. *Journal of Contaminant Hydrology*, *27*(3-4), 199-222.

Baumgartner, P., Bilinsky, D. M., Ates, Y., Read, R. S., Crosthwaite, J. L., & Dixon, D. A. (1996). Engineering for a Disposal Facility Using the In-Room Emplacement Method *(AECL-11595)*.

Behazin, M., Pedersen, K., & Li, L. (2021). State of science review of sulfide production in deep Geological repositories for used Nuclear fuel, *NWMO-TR-2021-18* (Issue November).

Bell, S. (2004). Measurement good practice guide No. 11. *National Physical Laboratory*, *2*, 1–41. https://doi.org/10.1111/j.1468-3148.2007.00360.

Bengtsson, A., & Pedersen, K. (2016). Microbial sulphate-reducing activity over load pressure and density in water saturated Boom Clay. *Applied Clay Science*, *132–133*, 542–551. https://doi.org/10.1016/j.clay.2016.08.02

Bengtsson, A., & Pedersen, K. (2017). Microbial sulphide-producing activity in water saturated Wyoming MX-80, Asha and Calcigel bentonites at wet densities from 1500 to 2000 kg m^{-3}. *Applied Clay Science*, *137*, 203–212. https://doi.org/10.1016/j.clay.2016.12.024

Benning, L. G., Wilkin, R. T., & Barnes, H. L. (2000). Reaction pathways in the Fe-S system below 100°C. *Chemical Geology*, *167*(1–2), 25–51. https://doi.org/10.1016/S0009-2541(99)00198-9

Bolney, R., Grosch, M., Winkler, M., van Slageren, J., Weigand, W., & Robl, C. (2021). Mackinawite formation from elemental iron and sulfur. *RSC Advances*, *11*(51), 32464–32475. https://doi.org/10.1039/d1ra03705f

Boparai, H. K., Joseph, M., & Carroll, D. M. O. (2011). Kinetics and thermodynamics of cadmium ion removal by adsorption onto nano zerovalent iron particles. *Journal of Hazardous Materials*, *186*(1), 458–465. https://doi.org/10.1016/j.jhazmat.2010.11.029

Bradbury, M. H., & Baeyens, B. (2003). Porewater chemistry in compacted re-saturated MX-80 bentonite. *61*, 329–338.

Bradbury, M. H., Berner, U., Curti, E., Hummel, W., & Kosakowski, G.Thoenen, T. (2014). The long-Term geochemical evolution of the nearfield of the HLW repository.

Bradbury, Mi. H., & Baeynes, B. (2005). Modelling the sorption of Mn (II), Co (II), Ni (II), Zn (II), Cd (II), Eu (III), Am (III), Sn (IV), Th (IV), Np (V) and U (VI) on montmorillonite : Linear free energy relationships and estimates of surface binding constants for some. *Geochimica et Cosmochimica Acta*, *69*(4), 875–892. https://doi.org/10.1016/j.gca.2004.07.020

Briggs, S., McKelvie, J., Sleep, B., & Krol, M. (2017). Multi-dimensional transport modelling of corrosive agents through a bentonite buffer in a Canadian deep geological repository. *Science of the Total Environment*, *599–600*, 348–354. https://doi.org/10.1016/j.scitotenv.2017.04.242

Butler, I.B., Schoonen, M.A.A., and Rickard, D.T. (1994). Removal of dissolved oxygen from water: A comparison of four common techniques. Talanta, 41(2): 211–215. doi:10.1016/0039-9140(94)80110-X.

Bujdák, J. (2020). Applied Clay Science Adsorption kinetics models in clay systems . The critical analysis of pseudo- second order mechanism. *Applied Clay Science*, *191*(April), 105630. https://doi.org/10.1016/j.clay.2020.105630

Can, M. (2015). *Studies of the Kinetics for Rhodium Adsorption onto Gallic Acid Derived Polymer: the Application of Nonlinear Regression Analysis*. *127*(4), 1308–1310. https://doi.org/10.12693/APhysPolA.127.1308

Chai, J. C., & Prongmanee, N. (2020). Barrier properties of a geosynthetic clay liner using polymerized sodium bentonite. *Geotextiles and Geomembranes*, *48*(3), 392–399.

Chen, J., Behazin, M., Binns, J., Birch, K., Blyth, A., Briggs, S., Cheema, G., Crowe, R., Doyle, D., Garisto, F., Giallonardo, J., Gobien, M., Guo, R., Hirschorn, S., Hobbs, M., Ion, M.,

Jacyk, J., Keech, P., Kremer, E., … Zhao, B. (2019). *Technical Program for Long-Term Management of Canada ' s Used Nuclear Fuel – Annual Report 2018* (Issue December).

Chen, J., Behazin, M., Binns, J., Birch, K., Boyle, C., Crowe, R., Doyle, D., Garisto, F., Giallonardo, J., Gobien, M., Hobbs, M., Hunt, N., Ion, M., Jensen, M., Keech, P., Kremer, E., Lawrence, C., Leung, H., Liyanage, T., … Zhang, X. (2018). *Technical Program for Long-Term Management of Canada's Used Nuclear Fuel – Annual Report 2017* (Issue December).

Chen, J., Qin, Z., Wu, L., Noël, J. J., & Shoesmith, D. W. (2014). The influence of sulphide transport on the growth and properties of copper sulphide films on copper. *Corrosion Science*, *87*, 233–238. https://doi.org/10.1016/j.corsci.2014.06.027

Chen, W. C., & Huang, W. H. (2013). Effect of groundwater chemistry on the swelling behavior of a Ca-bentonite for deep geological repository. *Physics and Chemistry of the Earth*, *65*, 42–49. https://doi.org/10.1016/j.pce.2013.05.012

Chowdhury, F., Rashwan, T. L., Mondal, P., Behazin, M., Keech, P. G., Sharma, J. S., & Krol, M. (2024). Effect of compaction on bisulfide diffusive transport through MX-80 bentonite. *Journal of Contaminant Hydrology*, *104341*.

Clark, M. M. (2009). Transport modeling for environmental engineers and scientists.

Cloet, V., Pekala, M., Smith, P., Wersin, P., & Diomidis, N. (2017). An evaluation of sulphide fluxes in the near field of a HLW repository April (Issue April).

Crini, G., Peindy, H. N., Gimbert, F., & Robert, C. (2007). Removal of C.I. Basic Green 4 (Malachite Green) from aqueous solutions by adsorption using cyclodextrin-based adsorbent: Kinetic and equilibrium studies. *Separation and Purification Technology*, *53*(1), 97–110. https://doi.org/10.1016/j.seppur.2006.06.018

Dada, A. O., Adekola, Folahan. A., Odebunmi, Ezekiel. O., Inyinbor1, Adejumoke. A., Akinyemi, B. A., & Ilesanmi, D. A. (2019). Kinetics and Thermodynamics of Adsorption of Rhodamine B onto Bentonite Supported Nanoscale Zerovalent Iron Nanocomposite. *Journal of Physics: Conference Series*, *Vi*. https://doi.org/10.1088/1742-6596/1299/1/012106

Dawodu, F. A., Akpomie, K., & Abuh, M. (2012). Equilibrium Isotherm Studies on the Batch Sorption of Copper (II) ions from Aqueous Solution unto Nsu Clay. December.

Derakhshani, E., Naghizadeh, A., & Khodadadi, M. (2016). Application of Different Isotherm Models for Humic Acid Adsorption on to Bentonite and Montmorillonite Nanoparticles. *Health Scope*, *6*(2). https://doi.org/10.5812/jhealthscope.40416

Diffusive Transport Modelling of Engineered Barrier System in a Deep Corrosion Agents through the Engineered Barrier System in a Deep Corrosion Agents through the Geological Repository for Used Nuclear Fuel (2018).

Dixon, D. A. (2019). Review of the T-H-M-C Properties of MX-80 Bentonite, *NWMO-TR-2019-07* (Issue June).

Dixon, D., Man, A., Rimal, S., Stone, J., & Siemens, G. (2018). Bentonite Seal Properties in Saline Water, *NWMO TR-2018-20* (Issue December).

Edet, U. A., & Ifelebuegu, A. O. (2020). Kinetics, isotherms, and thermodynamic modeling of the adsorption of phosphates from model wastewater using recycled brick waste. *Processes*, *8*(6). https://doi.org/10.3390/PR8060665

Alvarenga, E., Hayrapetyan, S., Skipperud, L., Hayrapetyan, L., Linjordet, M., & Salbu, B. (2016). Sorption properties of a bentonite based material for removal of uranium from alum shale leachate. *ournal of Chemistry and Chemical Engineering*, *10*(4), 170–179. https://doi.org/10.17265/1934-7375/2016.04.004

Falahian, Z., Torki, F., & Faghihian, H. (2018). *Synthesis and Application of Polypyrrole / Fe 3 O 4 Nanosize Magnetic Adsorbent for Efficient Separation of Hg 2 + from Aqueous Solution*. *4*. https://doi.org/10.1002/gch2.201700078

Fern, R., Ruiz, A. I., Ortega, A., Cuevas, J., & Gonz, D. E. (2020). Bentonite / CEM-II cement mortar interface experiments: A proxy to in situ deep geological repository engineered barrier system surface reactivity. *Applied Geochemistry*

Fetter, C. W. (2018). *Applied Hydrogeology*. Waveland Press.

Fukushi, K., & Sverjensky, D. A. (2007). *A surface complexation model for sulfate and selenate on iron oxides consistent with spectroscopic and theoretical molecular evidence*. *71*, 1–24. https://doi.org/10.1016/j.gca.2006.08.048

Galambos, M., Krajnak, A., Rosskopfova, O., Viglasova, E., Adamcova, R., & Rajec, P. (2013). *Adsorption equilibrium and kinetic studies of strontium on Mg-bentonite , Fe-bentonite and illite / smectite*. 1031–1040. https://doi.org/10.1007/s10967-013-2511-1

Glaus, M. A., Frick, S., & Loon, L. R. Van. (2017). *Diffusion of selected cations and anions in compacted montmorillonite and bentonite November*.

Gleason, M. H., Daniel, D. E., & Eykholt, G. R. (1997). Calcium and Sodium Bentonite for Hydraulic Containment Applications. *Journal of Geotechnical and Geoenvironmental Engineering*, *123*(5), 438–445. https://doi.org/10.1061/(asce)1090-0241(1997)123:5(438)

Goldberg, S. (2014). Application of surface complexation models to anion adsorption by natural materials. *Environmental Toxicology and Chemistry*, *33*(10), 2172–2180. https://doi.org/10.1002/etc.2566

Gomdje, V. H., Kombo, S. P. M., & Loura, B. (2015). Adsorption of tartaric acid onto bentonite. A kinetic study. *Research & Reviews: Journal of Pharmaceutics and Nanotechnology*, *3*(3), 37–47.

González-lópez, M. E., Laureano-anzaldo, C. M., Pérez-, A. A., Arellano, M., Robledo-ortíz, J. R., Laureano-anzaldo, C. M., & Pérez-, A. A. (2022). A Critical Overview of Adsorption Models Linearization : Methodological and Statistical Inconsistencies. *Separation & Purification Reviews*, *51*(3), 358–372. https://doi.org/10.1080/15422119.2021.1951757

González-Santamaría, D. E., Fernández, R., Ruiz, A. I., Ortega, A., & Cuevas, J. (2020). Applied Clay Science High-pH / low pH ordinary Portland cement mortars impacts on compacted bentonite surfaces : Application to clay barriers performance. *Applied Clay Science*, *193*(January), 105672. https://doi.org/10.1016/j.clay.2020.105672

Glocheux, Y. (2014). Investigations on iron and aluminium oxides and oxyhydroxides based sorbents for the removal of arsenic from groundwater (Doctoral dissertation, Queen's University Belfast).

Gu, X., Evans, L. J., & Barabash, S. J. (2010). Modeling the adsorption of Cd (II), Cu (II), Ni (II), Pb (II) and Zn (II) onto montmorillonite. *Geochimica et Cosmochimica Acta*, *74*(20), 5718–5728. https://doi.org/10.1016/j.gca.2010.07.016

Güngör, N., & Dilmac, S. (1996). Difference in the influence of Na and Ca ions on the zeta potentials of anatolian bentonitic clays. *Journal of Inclusion Phenomena and Molecular Recognition in Chemistry*, *26*(1–3), 93–101. https://doi.org/10.1007/bf01029933

Gupt, C. B., Yamsani, S. K., Prakash, A., Medhi, C. R., & Sreedeep, S. (2019). Appropriate Liquid-to-Solid Ratio for Sorption Studies of Bentonite. *Journal of Environmental Engineering (United States)*, *145*(2), 1–9. https://doi.org/10.1061/(ASCE)EE.1943-7870.0001488

Hadi, J., Greneche, J. M., Wersin, P., Koho, P., & Pastina, B. (2023). Determination of Sulfide Consumption by Fe-bearing Components of Bentonites. *Clays and Clay Minerals*. https://doi.org/10.1007/s42860-023-00254-4

Hall, D. S., Behazin, M., Jeffrey Binns, W., & Keech, P. G. (2020). An evaluation of corrosion processes affecting copper-coated nuclear waste containers in a deep geological repository. *Progress in Materials Science*, 100766. https://doi.org/10.1016/j.pmatsci.2020.100766

Hall, D. S., Behazin, M., Jeffrey Binns, W., & Keech, P. G. (2021). An evaluation of corrosion processes affecting copper-coated nuclear waste containers in a deep geological repository. *Progress in Materials Science*, *118*(April 2020), 100766. https://doi.org/10.1016/j.pmatsci.2020.100766

Hansel, C. M., Lentini, C. J., Tang, Y., Johnston, D. T., Wankel, S. D., & Jardine, P. M. (2015). *Dominance of sulfur-fueled iron oxide reduction in low-sulfate freshwater sediments*. 2400–2412. https://doi.org/10.1038/ismej.2015.50

Hayes, K. I. M. F., Papelis, C., & Leckie, J. O. (1988). Modeling Ionic Strength Effects on Anion Adsorption at Hydrous Oxide / Solution Interfaces.

He, H., Chai, K., Wu, T., Qiu, Z., Wang, S., & Hong, J. (2022). Adsorption of Rhodamine B from Simulated wastewater onto Kaolin-Bentonite composites. *Materials*, *15*(12), 1–15. https://doi.org/10.3390/ma15124058

He, L. M., Zelazny, L. W., Baligar, V. C., Ritchey, K. D., & Martens, D. C. (1997). Ionic Strength Effects on Sulfate and Phosphate Adsorption on -Alumina.

Ho, Y. S., & Mckay, G. (1998). A comparison of chemisorption kinetic models applied to pollutant removal on various sorbents. *76*(November).

Ho, Y. S., & Mckay, G. (1999). Pseudo-second order model for sorption processes. *Process Biochemistry*, *34*, 451–465.

House, M. W., & Weiss, W. J. (2014). Review of microbially induced corrosion and comments on needs related to testing procedures. *Proceedings of the 4th International Conference on the Durability of Concrete Structures, ICDCS 2014, July 2014*, 94–103. https://doi.org/10.5703/1288284315388

Hu, J., Xu, D., Chen, L., & Wang, X. (2009). Characterization of MX-80 bentonite and its sorption of radionickel in the presence of humic and fulvic acids. *Journal of Radioanalytical and Nuclear Chemistry*, *279*(3), 701–708. https://doi.org/10.1007/s10967-007-7252-6

Idiart, A., & Pękala, M. (2020). Models for Diffusion in Compacted Bentonite. *NWMO TR-15-06* (Issue April 2016).

Ikpe, A., & Okovido, J. (2018). Geotechnical Evaluation of Bentonite Clay for Municipal Solid Waste Landfill Geotechnical Evaluation of Bentonite Clay for Municipal Solid Waste Landfill Lining Membrane. *Environmental Engineering Science, September*, 337–351.

Jaafer, S. (2014). Kinetic study for adsorption of para nitroaniline (PNA) on Bentonite clay surface. January 2008.

Kadoshnikov, V. M., Zlobenko, B. P., & Bugera, S. P. (n.d.). Study of uranium sorption by bentonite.

Kajjumba, G. W., Emik, S., Öngen, A., Özcan, H. K., & Serdar Aydın. (2018). Modelling of Adsorption Kinetic Processes—Errors, Theory and Application (Issue November). https://doi.org/10.5772/intechopen.80495

Kaplan, D. I. (1999). Understanding Variation in Partition Coefficient , K_d Values . *Volume 1*. *USEPA*

Karakaya, M. Ç., Karakaya, N., & Bakir, S. (2011). Some properties and potential applications of the Na- and Ca-bentonites of ordu (N.E. Turkey). *Applied Clay Science*, *54*(2), 159–165. https://doi.org/10.1016/j.clay.2011.08.003

Karnland, O. (2010). Chemical and mineralogical characterization of the bentonite procedure in a KBS-3 repository. *SKB Technical Report TR-10-60*, *10–60*, 25.

Karnland, O., Olsson, S., Dueck, A., Birgersson, M., Nilsson, U., & Hernan-håkansson, T. (2009). TR-09-29 Long term test of buffer material. November.

Karnland, O., Olsson, S., & Nilsson, U. (2006). Mineralogy and sealing properties of various bentonites and smectite-rich clay materials, TR-06-30, Svensk Kärnbränslehantering AB *Swedish Nuclear Fuel and Waste Management Co*.

Kaufhold, S., & Dohrmann, R. (2016). Distinguishing between more and less suitable bentonites for storage of high-level radioactive waste. *Clay Minerals*, *51*(2), 289–302. https://doi.org/10.1180/claymin.2016.051.2.14

Kazerouni, A. M. (2009). Design and Analysis of Gauge R & R Studies : Making Decisions Based on ANOVA Method. 31–35.

Khalili, F. I., Salameh, N. A. H., & Shaybe, M. M. (2013). Sorption of uranium (VI) and thorium (IV) by Jordanian bentonite. *Journal of Chemistry*, *2013*(1), 586136.

Khalili, F. I., Sultan, M., Robl, C., & Al-ghouti, M. A. (2015). Insights into the remediation characterization of modified bentonite in minimizing organosulphur compounds from diesel fuel. *Journal of Industrial and Engineering Chemistry 28*, 282–293.

King, F., Hall, D. S., & Keech, P. G. (2017). Nature of the near-field environment in a deep geological repository and the implications for the corrosion behaviour of the container. *Corrosion Engineering Science and Technology*, *52*, 25–30. https://doi.org/10.1080/1478422X.2017.1330736

Kocer, N. N., Uslu, G., & Cuci, Y. (2008). The Adsorption of Zn(II) Ions onto Chitin: Determination of Equilibrium, Kinetic and Thermodynamic Parameters. *June 2015*. https://doi.org/10.1260/026361708787548774

Koch, D. (2007). European bentonites as alternatives to MX-80. *Science & Technology Series*, *334*, 23-30.

Krechmer, K. (2016). Relational measurements and uncertainty. Measurement: *Journal of the International Measurement Confederation*, *93*, 36–40. https://doi.org/10.1016/j.measurement.2016.06.058

Lanson, B., Muller, F., Bauer, A., & Jullien, M. (2005). Experimental study of smectite interaction with metal Fe at low temperature: Smectite destabilization. *January*. https://doi.org/10.1346/CCMN.2005.0530606

Lee, J. O., Cho, W. J., Kang, C. H., & Chun, K. S. (2001). Swelling and Hydraulic Properties of Ca-Bentonite for the Buffer of a Waste Repository. *Technologies for the Management of Radioactive Waste from Nuclear Power Plants and Back End Nuclear Fuel Cycle Activities*, *3523*(6 2), 1–10.

Lemire, R. J., Palmer, D. A., Taylor, P., & Schlenz, H. (2020). Chemical thermodynamics of iron-Part 2. In *Chemical thermodynamics* (Vol. 13b). Nuclear Energy Agency of the OECD (NEA), Paris, France.

Lewis, A. E. (2010). Review of metal sulphide precipitation. *Hydrometallurgy*, *104*(2), 222–234. https://doi.org/10.1016/j.hydromet.2010.06.010

Li, Q., Yue, Q., Su, Y., Gao, B., & Fu, L. (2007). Cationic polyelectrolyte / bentonite prepared by ultrasonic technique and its use as adsorbent for Reactive Blue K-GL dye. 147, 370–380. https://doi.org/10.1016/j.jhazmat.2007.01.024

Limousin, G. (2007). Sorption isotherms: A review on physical bases , modeling and measurement. *22*, 249–275. https://doi.org/10.1016/j.apgeochem.2006.09.010

Liu, Z. rong, & Zhou, S. qi. (2010). Adsorption of copper and nickel on Na-bentonite. *Process Safety and Environmental Protection*, *88*(1), 62–66. https://doi.org/10.1016/j.psep.2009.09.001

Loon, L. R. Van, Glaus, M. A., & Mu, W. (2007). Anion exclusion effects in compacted bentonites : Towards a better understanding of anion diffusion. *22*, 2536–2552. https://doi.org/10.1016/j.apgeochem.2007.07.008

Loon, L. R. Van, Soler, J. M., & Bradbury, M. H. (2003). Diffusion of HTO , 36 Cl À and 125 I À in Opalinus Clay samples from Mont Terri Effect of confining pressure. *61*, 73–83.

López, J., Loida, L., Montes, E. R., Martinez, S., & Arturo, V. (2019). Linear and nonlinear kinetic and isotherm adsorption models for arsenic removal by manganese ferrite nanoparticles. *SN Applied Sciences*, *1*(8), 1–19. https://doi.org/10.1007/s42452-019-0977-3

Maanoja, S., Lakaniemi, A. M., Lehtinen, L., Salminen, L., Auvinen, H., Kokko, M., Palmroth, M., Muuri, E., & Rintala, J. (2020). Compacted bentonite as a source of substrates for sulfate-reducing microorganisms in a simulated excavation-damaged zone of a spent nuclear fuel repository. *Applied Clay Science*, *196*(April), 105746. https://doi.org/10.1016/j.clay.2020.105746

Marić, I., Štefanić, G., Gotić, M., & Jurkin, T. (2019). The impact of dextran sulfate on the radiolytic synthesis of magnetic iron oxide nanoparticles. *Journal of Molecular Structure*, *1183*, 126–136. https://doi.org/10.1016/j.molstruc.2019.01.075

Martino, T., Partovi-Nia, R., Chen, J., Qin, Z., & Shoesmith, D. W. (2014). Mechanisms of Film Growth on Copper in Aqueous Solutions Containing Sulphide and Chloride under Voltammetric Conditions. *Electrochimica Acta*, *127*, 439–447. https://doi.org/10.1016/j.electacta.2014.02.050

McBridge, M. B. (1997). A critique of diffuse double layer models applied to colloid and surface chemistry. *Clays and Clay Minerals*, *45*(4), 598–608.

Miettinen, H., Bomberg, M., Bes, R., Tiljander, M., & Vikman, M. (2022). Transformation of inherent microorganisms in Wyoming-type bentonite and their effects on structural iron. *Applied Clay Science*, *221*(September 2021). https://doi.org/10.1016/j.clay.2022.106465

Miraoui, A., & Amine, M. (2015). Thorium (Iv) Sorption Onto Sodium Bentonite and Magnetic Bentonite. *Iv*, 512–521. https://doi.org/10.17628/ECB.2015.4.512

Morel, J.-P., Marmier, N., Hurel, C., & Morel-Desrosiers, N. (2015). Thermodynamics of selenium sorption on alumina and montmorillonite. *Cogent Chemistry*, *1*(1), 1070943. https://doi.org/10.1080/23312009.2015.1070943

Moussout, H., Ahlafi, H., Aazza, M., & Maghat, H. (2018). ScienceDirect Critical of linear and nonlinear equations of pseudo-first order and pseudo-second order kinetic models. *Karbala International Journal of Modern Science*, *4*(2), 244–254. https://doi.org/10.1016/j.kijoms.2018.04.001

Mukherjee, S., & Ghosh, B. (2013). The science of clays: Applications in industry, engineering and environment. In *The Science of Clays: Applications in Industry, Engineering and Environment* (Vol. 9789400766). https://doi.org/10.1007/978-94-007-6683-9

Muurinen, A., & Carlsson, T. (2010). Experiences of pH and Eh measurements in compacted MX-80 bentonite. *Applied Clay Science*, *47*(1-2), 23-27.

Musso, T. B., Parolo, M. E., & Pettinari, G. (2019). *pH , Ionic Strength , and Ion Competition Effect on Cu (II) and Ni (II) Sorption by a Na-bentonite Used as Liner Material*. *January*. https://doi.org/10.15244/pjoes/84922

Neto, E. S. C., Aguiar, A. B. S., & Rodriguez, R. P. (2018). Acid mine drainage treatment and sulfate-reducing process. *Brazilian Journal of Chemical Engineering*, *35*(02), 543–552.

Nguyen, H., You, S., & Hosseini-bandegharaei, A. (2017). Mistakes and inconsistencies regarding adsorption of contaminants from aqueous solutions : A critical review. *Water Research*, *120*, 88–116. https://doi.org/10.1016/j.watres.2017.04.014

Nguyen-Thanh, D., Block, K., & Bandosz, T. J. (2005). Adsorption of hydrogen sulfide on montmorillonites modified with iron. *Chemosphere*, *59*(3), 343–353. https://doi.org/10.1016/j.chemosphere.2004.10.022

Nielsen, A. H., Hvitved-Jacobsen, T., & Vollertsen, J. (2008). Effects of pH and Iron Concentrations on Sulfide Precipitation in Wastewater Collection Systems. *Water Environment Research*, *80*(4), 380–384. https://doi.org/10.2175/106143007x221328

Noronha, J. (2016). Deep Geological Repository Conceptual Design Report Crystalline / Sedimentary Rock Environment. *NWMO* (Issue May).

Ochs, M., Lothenbach, B., Wanner, H., Sato, H., & Yui, M. (2001). *An integrated sorption – diffusion model for the calculation of consistent distribution and diffusion coefficients in compacted bentonite*. 283–296.

Oscarson, D. W., Hume, H. B., & King, F. (1994). Sorption of cesium on compacted bentonite. *Clays and Clay Minerals*, *42*(6), 731–736. https://doi.org/10.1346/CCMN.1994.0420609

Otunola, B. O., & Ololade, O. O. (2020). Environmental Technology & Innovation A review on the application of clay minerals as heavy metal adsorbents for remediation purposes. *Environmental Technology & Innovation*, *18*, 100692. https://doi.org/10.1016/j.eti.2020.100692

Pająk, M., Dzieniszewska, A., Kyzioł-komosińska, J., Pająk, M., Dzieniszewska, A., & Kyzioł-komosińska, J. (2019). Sorption of Acid Black 1 dye onto bentonite – equilibrium and kinetic studies. *Journal of Environmental Science and Health, Part A*, *0*(0), 1–10. https://doi.org/10.1080/10934529.2019.1631654

Papry, S. A., Rashwan, T. L., Mondal, P. K., Behazin, M., Keech, P. G., & Krol, M. M. (2023). Investigating bisulfide sorption onto bentonite through laboratory batch experiments. *Applied Geochemistry*, *152*(October 2022), 105626. https://doi.org/10.1016/j.apgeochem.2023.105626

Pedersen, K., Bengtsson, A., Blom, A., Johansson, L., & Taborowski, T. (2017). Mobility and reactivity of sulphide in bentonite clays – Implications for engineered bentonite barriers in geological repositories for radioactive wastes. *Applied Clay Science*, *146*(February), 495–502. https://doi.org/10.1016/j.clay.2017.07.003

Raihan Taha, M., Ahmad, K., Abdul Aziz, A., & Chik, Z. (2004). Geoenvironmental aspects of tropical residual soils. *Tropical Residual Soils Engineering*, 213–229. https://doi.org/10.1201/9780203024621.ch12

Randall, M. (2012). Review of radionuclide Sorption on bentonite and forsmark Bedrock material. *Newsite.Mkg.Se*, 36 pp.

Rani, S., & Mahajan, R. K. (2016). Equilibrium , kinetics and thermodynamic parameters for adsorptive removal of dye Basic Blue 9 by ground nut shells and Eichhornia. *Arabian Journal of Chemistry*, *9*, S1464–S1477. https://doi.org/10.1016/j.arabjc.2012.03.013

Rashwan, T. L., Asad, M. A., Molnar, I. L., Behazin, M., Keech, P. G., & Krol, M. M. (2022). Exploring the governing transport mechanisms of corrosive agents in a Canadian deep geological repository. *Science of The Total Environment*, 828, 153944

Revellame, E. D., Lord, D., Sharp, W., Hernandez, R., & Zappi, M. E. (2020). Adsorption kinetic modeling using pseudo- fi rst order and pseudo-second order rate laws : A review. *Cleaner Engineering and Technology*, *1*(December), 100032. https://doi.org/10.1016/j.clet.2020.100032

Rickard, D., & Luther, G. W. (2007). Chemistry of iron sulfides. In *Chemical Reviews* (Vol. 107, Issue 2, pp. 514–562). https://doi.org/10.1021/cr0503658

Rautioaho, E., & Korkiala-Tanttu, L. (2009). Bentomap: Survey of bentonite and tunnel backfill knowledge. *VTT Technical Research Centre of Finland*

Saeed, M. M., & Ahmed, M. (2006). Effect of temperature on kinetics and adsorption profile of endothermic chemisorption process: -Tm(III)-PAN loaded PUF system. *Separation Science and Technology*, *41*(4), 705–722. https://doi.org/10.1080/01496390500527993

Sahoo, T. R., & Prelot, B. (2020). Adsorption processes for the removal of contaminants from wastewater: the perspective role of nanomaterials and nanotechnology. *Nanomaterials for the Detection and Removal of Wastewater Pollutants*, 161–222. https://doi.org/10.1016/B978-0-12-818489-9.00007-4

Sellin, P., & Leupin, O. X. (2014a). The use of clay as an engineered barrier in radioactive-waste management - A review. *Clays and Clay Minerals*, *61*(6), 477–498. https://doi.org/10.1346/CCMN.2013.0610601

Sena, C., Salas, J., & Arcos, D. (2010). Thermo-hydro-geochemical modelling of the bentonite buffer - LOT A2 experiment. *Sbb Tr-10-65*, *TR-10-65*, 57.

Senthilkumaar, S., Kalaamani, P., & Subburaam, C. V. (2006). Liquid phase adsorption of Crystal violet onto activated carbons derived from male flowers of coconut tree. *Journal of Hazardous Materials*, *136*(3), 800–808. https://doi.org/10.1016/j.jhazmat.2006.01.045

Shahmohammadi-Kalalagh, S., Babazadeh, H., & Nazemi, A. (2015). *Comparison of linear and nonlinear forms of isotherm models for Zn(II) and Cu(II) sorption on a kaolinite*. https://doi.org/10.1007/s12517-013-1114-z

Simonin, J. (2016). On the comparison of pseudo-first order and pseudo-second order rate laws in the modeling of adsorption kinetics. *Chemical Engineering Journal*, *300*, 254–263. https://doi.org/10.1016/j.cej.2016.04.079

Standish, T., Chen, J., Jacklin, R., Jakupi, P., Ramamurthy, S., Zagidulin, D., Keech, P., & Shoesmith, D. (2016). Corrosion of copper-coated steel high level nuclear waste containers under permanent disposal conditions. *Electrochimica Acta*, *211*, 331–342. https://doi.org/10.1016/j.electacta.2016.05.135

Steinmetz, D. R. (2014). Texture evolution in processing of polystyrene-clay nanocomposites. https://www.researchgate.net/publication/28675168

Stepova, K. V, Maquarrie, D. J., & Krip, I. M. (2009). Modified bentonites as adsorbents of hydrogen sulfide gases. *Applied Clay Science 42*, 625–628. https://doi.org/10.1016/j.clay.2008.05.001

Strawn, D. G. (2021). Sorption Mechanisms of Chemicals in Soils. *Soil System*.

Stroes-gascoyne, S., Hamon, C. J., & Maak, P. (2011). Limits to the use of highly compacted bentonite as a deterrent for microbiologically influenced corrosion in a nuclear fuel waste repository. *Physics and Chemistry of the Earth*, *36*(17–18), 1630–1638. https://doi.org/10.1016/j.pce.2011.07.085

Stroes-Gascoyne, S., Hamon, C. J., Maak, P., & Russell, S. (2010). The effects of the physical properties of highly compacted smectitic clay (bentonite) on the culturability of indigenous microorganisms. *Applied Clay Science*, *47*(1–2), 155–162. https://doi.org/10.1016/j.clay.2008.06.010

Sun, Y., Li, Y., Xu, Y., Liang, X., & Wang, L. (2015). In situ stabilization remediation of cadmium (Cd) and lead (Pb) co-contaminated paddy soil using bentonite. *Applied Clay Science 106*, 200–206. https://doi.org/10.1016/j.clay.2014.12.031

Sun, W., & Fang, L. (2014). Swelling characteristics of Gaomiaozi bentonite and its prediction. *Journal of Rock Mechanics and Geotechnical Engineering*, 6(2), 113-118

Svensson, D., & Wikberg, P. (2017). *Experiments with bentonite and sulphide – results from experiments 2013 – 2016, SKB P-16-31, Swedish Nuclear Fuel and Waste Management Co* (Issue April).

Szczepanik, P., & Sawlowicz, Z. (2010). Fe-S mineralization in the Jurassic biogenic remains (Czestochowa, Poland). *Chemie Der Erde*, *70*(1), 77–87. https://doi.org/10.1016/j.chemer.2009.10.003

Tachi, Y., Shibutani, T., Sato, H., & Yui, M. (2001). Experimental and modeling studies on sorption and diffusion of radium in bentonite. *Journal of Contaminant Hydrology*, *47*(2–4), 171–186. https://doi.org/10.1016/S0169-7722(00)00147-9

Tachi, Y., & Yotsuji, K. (2014). Diffusion and sorption of Cs + , Na + , I À and HTO in compacted sodium montmorillonite as a function of porewater salinity : Integrated sorption and diffusion model. *Geochimica et Cosmochimica Acta*, *132*, 75–93. https://doi.org/10.1016/j.gca.2014.02.004

Tang, Q., Katsumi, T., Inui, T., & Li, Z. (2014). Membrane behavior of bentonite-amended compacted clay. *Soils and Foundations*, *54*(3), 329–344. https://doi.org/10.1016/j.sandf.2014.04.019

Taylor, J. K. (1981). *Quality assurance of chemical measurements*. *53*(14). https://doi.org/10.1021/ac00237a001

Tertre, E. (2006). *Surface chemistry of kaolinite and Na-montmorillonite in aqueous electrolyte solutions at 25 and 60 ° C : Experimental and modeling study*. *70*, 4579–4599. https://doi.org/10.1016/j.gca.2006.07.017

Torstenfelt, B., Allard, B., Johansson, W., & Ittner, T. (1983). Iron content and reducing capacity of granites and bentonite, KBS Tr 83-36. In *KBS Tr 83-36* (Issue April).

Tran, E. L., Teutsch, N., Klein-BenDavid, O., & Weisbrod, N. (2018). Uranium and Cesium sorption to bentonite colloids under carbonate-rich environments: Implications for radionuclide transport. *Science of the Total Environment*, *643*, 260–269. https://doi.org/10.1016/j.scitotenv.2018.06.162

Tsibranska, I., & Hristova, E. (2011). Comparison of different kinetic models for adsorption of heavy metals onto activated carbon from apricot stones. *43*(3), 370–377.

Uddin, F. (2018). Montmorillonite: An Introduction to Properties and Utilization. *Current Topics in the Utilization of Clay in Industrial and Medical Applications*, *September*. https://doi.org/10.5772/intechopen.77987

Uddin, M. K. (2017). A review on the adsorption of heavy metals by clay minerals, with special focus on the past decade. *Chemical Engineering Journal*, *308*, 438–462. https://doi.org/10.1016/j.cej.2016.09.029

USEPA. (2016). *Definition and Procedure for the Determination of the Method Detection Limit, Revision 2*. www.epa.gov

Usman, A. R. A., Kuzyakov, Y., & Stahr, K. (2010). *Effect of clay minerals on extractability of heavy metals and sewage sludge mineralization in soil*. *7540*(May). https://doi.org/10.1080/02757540410001665971

Vardeman, S. B. (2005). Measurement Theory for Engineers. In *Journal of Quality Technology* (Vol. 37, Issue 1). https://doi.org/10.1080/00224065.2005.11980305

Verma, P. K., Pathak, P., & Mohapatra, P. K. (2014). *Sorption of metal cations on suspended bentonite : effects of pH , ionic strength and complexing anions*. *102*(5), 401–409. https://doi.org/10.1515/ract-2014-2160

Vhahangwele, M., & Mugera, G. W. (2015). Journal of Environmental Chemical Engineering The potential of ball-milled South African bentonite clay for attenuation of heavy metals

from acidic wastewaters : Simultaneous. *Biochemical Pharmacology*, *3*(4), 2416–2425. https://doi.org/10.1016/j.jece.2015.08.016

Vilks, P. (2014). Sorption of Selected Radionuclides on Sedimentary Rocks in Saline Conditions - Updated Sorption Values. In *NWMO Technical Report* (Issue December).

Villar, M. V. (2007). Water retention of two natural compacted bentonites. *Clays and Clay Minerals*, *55*(3), 311–322. https://doi.org/10.1346/CCMN.2007.0550307

Vinšová, H., Jedináková-Křížová, V., Kolaříková, I., Adamcová, J., Přikryl, R., & Zeman, J. (2008). The influence of temperature and hydration on the sorption properties of bentonite. *Journal of Environmental Radioactivity*, *99*(2), 415–425. https://doi.org/10.1016/j.jenvrad.2007.11.003

Walker, A. (2018). Sorption study of Se (-II) onto illite, bentonite, and shale under high ionic strength conditions (Masters thesis, McMaster University).

Wang, P., Anderko, A., & Turner, D. R. (2001a). Thermodynamic Modeling of the Adsorption of Radionuclides on Selected Minerals . I : Cations. 4428–4443. https://doi.org/10.1021/ie000991p

Wang, P., Anderko, A., & Turner, D. R. (2001b). Thermodynamic Modeling of the Adsorption of Radionuclides on Selected Minerals . I I: Anions. 4428–4443. https://doi.org/10.1021/ie000991p

Wang, X., Wang, Z., Peak, D., Tang, Y., Feng, X., & Zhu, M. (2018). Quantication of Coexisting Inner- and Outer-Sphere Complexation of Sulfate on Hematite Surfaces. *ACS Earth and Space Chemistry*. https://doi.org/10.1021/acsearthspacechem.7b00154

Wen, X., Liang, Y., Bai, P., Luo, B., Fang, T., Yue, L., An, T., Song, W., & Zheng, S. (2017). First-principles calculations of the structural, elastic and thermodynamic properties of mackinawite (FeS) and pyrite (FeS2). *Physica B: Condensed Matter*, *525*, 119–126. https://doi.org/10.1016/j.physb.2017.09.007

Wersin, P., Alt-epping, P., Pekala, M., Pitkänen, P., & Snellman, M. (2017). Modelling sulfide fluxes and Cu canister corrosion rates in the engineered barrier system of a spent fuel repository. *Procedia Earth and Planetary Science*, *17*(iii), 722–725. https://doi.org/10.1016/j.proeps.2016.12.183

Wersin, P., Alt-Epping, P., Pitkänen, P., Román-Ross, G., Trinchero, P., Molinero, J., Smith, P., Snellman, M., Filby, A., & Kiczka, M. (2014a). Sulphide Fluxes and Concentrations in the Spent Nuclear Fuel Repository at Olkiluoto. In *Posiva Report 2014-01* (Vol. 31, Issue January).

Wersin, P., Curti, E., & Appelo, C. A. J. (2004). *Modelling bentonite – water interactions at high solid / liquid ratios : swelling and diffuse double layer effects*. *26*, 249–257. https://doi.org/10.1016/j.clay.2003.12.010

Wieland, E., Wanner, H., & Albinsson, Y. (1994). *A surface chemical model of the bentonite-water interface and its implications for modelling the near field chemistry in a repository for spent fuel*. *July*.

Wigger, C., & Van Loon, L. R. (2017). Importance of interlayer equivalent pores for anion diffusion in clay-rich sedimentary rocks. *Environmental Science and Technology*, *51*(4), 1998–2006. https://doi.org/10.1021/acs.est.6b03781

Wu, J., Li, B., Liao, J., Feng, Y., Zhang, D., Zhao, J., Wen, W., Yang, Y., & Liu, N. (2009). Behavior and analysis of Cesium adsorption on montmorillonite mineral. *Journal of Environmental Radioactivity*, *100*(10), 914–920. https://doi.org/10.1016/j.jenvrad.2009.06.024

Xu, D., Tan, X. L., Chen, C. L., & Wang, X. K. (2008a). Adsorption of Pb(II) from aqueous solution to MX-80 bentonite: Effect of pH, ionic strength, foreign ions and temperature. *Applied Clay Science*, *41*(1–2), 37–46. https://doi.org/10.1016/j.clay.2007.09.004

Yang, S., Li, J., Lu, Y., Chen, Y., & Wang, X. (2009). Sorption of Ni(II) on GMZ bentonite: Effects of pH, ionic strength, foreign ions, humic acid and temperature. *Applied Radiation and Isotopes*, *67*(9), 1600–1608. https://doi.org/10.1016/j.apradiso.2009.03.118

Yang, Y., Du, Y., Reddy, K. R., & Fan, R. (2017). Phosphate-amended sand / Ca-bentonite mixtures as slurry trench wall back fi lls : Assessment of workability , compressibility and hydraulic conductivity. *142*, 120–127. *Applied Clay Science* https://doi.org/10.1016/j.clay.2016.10.040

Yang, Y., Reddy, K. R., Du, Y., & Fan, R. (2019). Applied Clay Science Retention of Pb and Cr (VI) onto slurry trench vertical cutoff wall backfill containing phosphate dispersant amended Ca-bentonite. *Applied Clay Science*, *168*(December 2018), 355–365. https://doi.org/10.1016/j.clay.2018.11.023

Yu, J. W., & Neretnieks, I. (1997). Diffusion and sorption properties of radionuclides in compacted bentonite (No. SKB-TR--97-12). *Swedish Nuclear Fuel and Waste Management Co.*.

Zafar, S., Khalid, N., Daud, M., & Mirza, M. L. (2015). Kinetic studies of the adsorption of thorium ions onto rice husk from aqueous media: Linear and nonlinear approach. *The Nucleus*, *52*(1), 14-19.

Zbair, M., Anfar, Z., Ahsaine, H. A., & Khallok, H. (2019). Kinetics, equilibrium, statistical surface modeling and cost analysis of paraquat removal from aqueous solution using carbonated jujube seed. 1084–1094. https://doi.org/10.1039/c8ra09337g

Zhao, D. L., Feng, S. J., Chen, C. L., Chen, S. H., Xu, D., & Wang, X. K. (2008). Adsorption of thorium (IV) on MX-80 bentonite : Effect of pH , ionic strength and temperature. *41*, 17–23. https://doi.org/10.1016/j.clay.2007.09.012

APPENDICES

APPENDIX A

A.1 Standard operating procedures (SOPs)

A.1.1 Deoxygenation of water

All the samples and blanks used for each experiment under this study were prepared with deionized Milli Q water. Before deoxygenation, the water was boiled for around 15 minutes. After cooling, the water was deoxygenated by purging nitrogen (N_2) gas from a compressed gas cylinder (i.e., containing purified N_2 with oxygen level <0.1 mg/L). The water was kept for deoxygenation for 40 to 60 minutes or until the dissolved oxygen level came below 1 mg/L (Butler et al., 1994; Chowdhury et al., 2024).

A.1.2 Bisulfide analysis by methylene blue (MB) method (4500-S^{2-} D)

The MB method was carried out using a spectrophotometer (Hach DR 3900, Hach) set at a wavelength of 665 nm. Before analyzing the samples (i.e., containing sulfide), a method blank (i.e., containing no sulfide) was analyzed to "zero" the spectrophotometer. The method blank was prepared by filling a spectrophotometer cell with 10 ml of deoxygenated deionized water and subsequent addition of 0.5ml sulfide reagent 1 and 0.5 ml sulfide reagent 2. Similarly, sample cells were prepared by filling 10 ml of solution (i.e., containing bentonite with HS^-; only bentonite or only HS^-) with subsequent mixing of 0.5ml sulfide reagent 1 and 0.5 ml sulfide reagent 2. After adding the reagents, initially a pink color was developed, which turned blue if sulfide was present. The spectrophotometer was set at "zero" by placing the method blank cell in the cell holder. After that, each sample cell was kept in the holder, and the absorbance reading was recorded. Using the calibration curve (as shown in Figure 3.4, Chapter 3), the bisulfide concentrations in the samples were determined (APHA, 2017).

A.1.3 Determining method detection limit (MDL)

To calculate the MDL, 10 samples of 0.1 mg/L HS^- solutions were analyzed using the MB method, as stated in Section A.1.2. After the standard deviation (S) of the replicate analyses was calculated, the MDL was determined using the following formula:

$$MDL = [t(n - 1), \propto = 0.01] * [S]$$

where, $[t(n - 1), \propto = 0.01)]$ = the student's t value appropriate for a 99% confidence level and a standard deviation estimate with the appropriate degrees of freedom. $t(n - 1) = 2.821$ for 10 replicates and degree of freedom 9.

A.2 Effect of contact time and temperature on sorption%

Figure A.1 presents the resulting sensitivities in sorption% of HS^- onto bentonite with contact time and temperature.

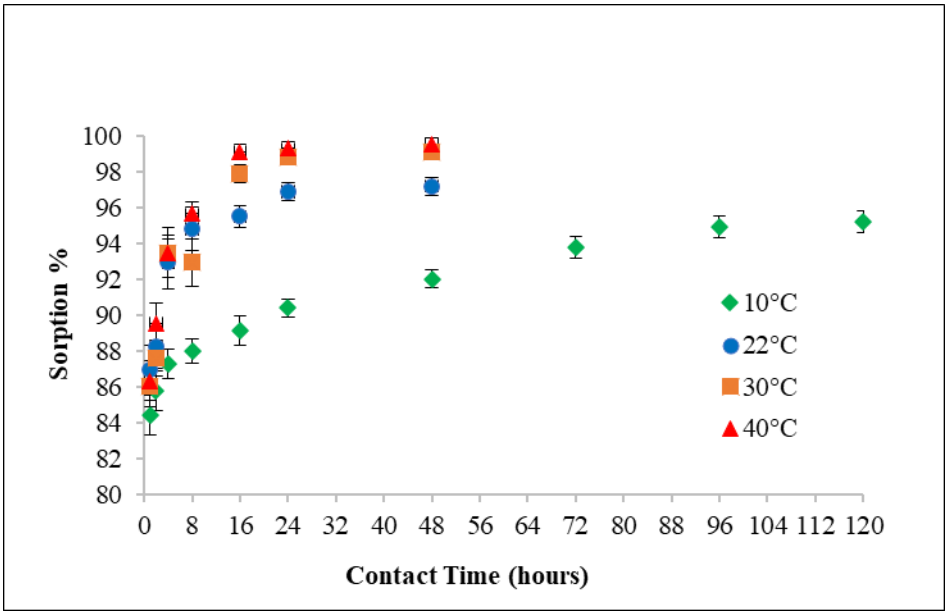

Figure A.1 Effect of contact time and temperature on sorption% related to HS^- sorption on bentonite (experimental conditions: L:S= 100; C_i= 5 mg L^{-1}, pH= 9.5). All data presented are the average of duplicate or triplicate tests, with error bars showing the standard deviation.

Figure A.1 suggests that 84-86% sorption of HS occurred within the first hour at all the studied temperatures. Similar sorption behaviour was observed for temperatures of 22, 30, and 40°C. At

these temperatures, the sorption% increased sharply until 8 hours, and then gradually approached equilibrium (i.e., with 97-99% sorption) in 24 hours at 22 and 30°C, and in 16 hours at 40°C. In contrast, slower sorption was observed at 10°C and it required much longer contact time (i.e., around 96 hours) to reach equilibrium at this lower temperature.

A.3 ANOVA analysis

A one-way ANOVA ("analysis of variance") was performed (using Microsoft Excel) to determine if there is a statistically significant difference between the corresponding means of the equilibrium sorption capacity values (Table A.1) obtained from Experiment Set 1 conducted at four different temperatures: 10, 22, 30 and 40°C.

Table A.2 presents the summary of the ANOVA test results.

Table A.1 Experimental data of equilibrium sorption capacity at the temperatures studied.

Equilibrium sorption capacity (q_e, mg kg^{-1})	Temperature (°C)			
	10	22	30	40
	443.5	446.9	455.8	456.5
	442.8	450.2	454.2	457.5
	441.2	447.8	454.3	455.8

Table A.2 ANOVA table for analysing statistical difference of the equilibrium sorption capacity values with temperature.

Anova: Single Factor							
SUMMARY							
Groups	*Count*	*Sum*	*Average*	*Variance*			
Column 1	3	1327.51	442.5033	1.361033			
Column 2	3	1344.9	448.3	2.91			
Column 3	3	1364.3	454.7667	0.803333			
Column 4	3	1369.8	456.6	0.73			
ANOVA							
Source of Variation	SS	df	MS	F	P-value	F crit	
Between Groups	372.5817	3	124.1939	85.581	2.03E-06		7.591
Within Groups	11.60873	8	1.451092				
Total	384.1904	11					

Notes: a. *SS (Sum of Squares):* the measurement of the variation around the mean
b. *df (Degree of Freedom*): (i) between groups: the number of groups minus 1; (ii) within groups: the total number of minus the number of groups
c. *MS (Mean Square)* is determined by dividing the sum of squared deviations (SS) by the degrees of freedom

F-Statistic or F-Ratio is the ratio of "between-group variation" to "within-group variation". If the F-Statistic is larger than F-Critical, then the variation between the groups is statistically significant.

d. *P-Value* is the probability to measure the indication against the null hypothesis. Lower P-values suggest stronger evidence against the null hypothesis.

As shown in Table A.2, the F-stat value (85.581) was found higher than the F-Critical value (7.59, at 99% level of confidence between the 2 degrees of freedom) and the P-value was found much lower than 0.01, which suggests that the variation in equilibrium sorption capacity with temperature is statistically significant (Kazerouni, 2009).

A.4 Linear kinetic model results

The resulting linear plots of the three kinetic models applied to the experimental data of Experiment set 1 are presented in Figure A.2 and the model parameter values are summarized in Table A.3.

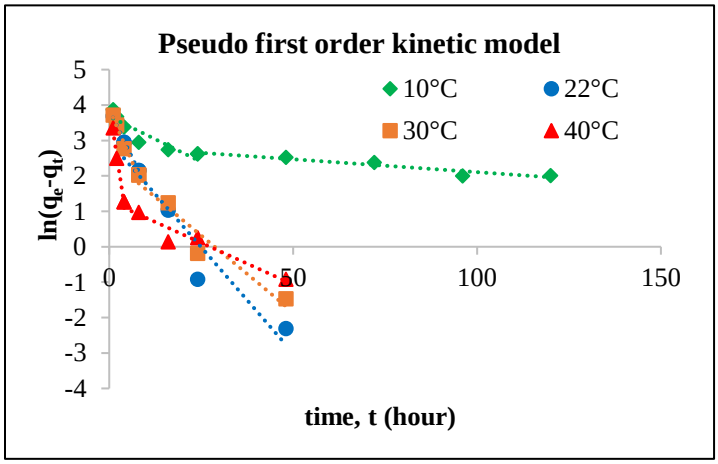

(a)

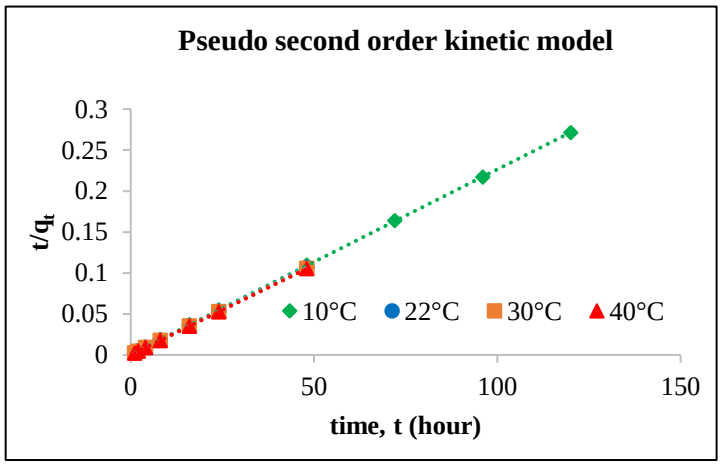

(b)

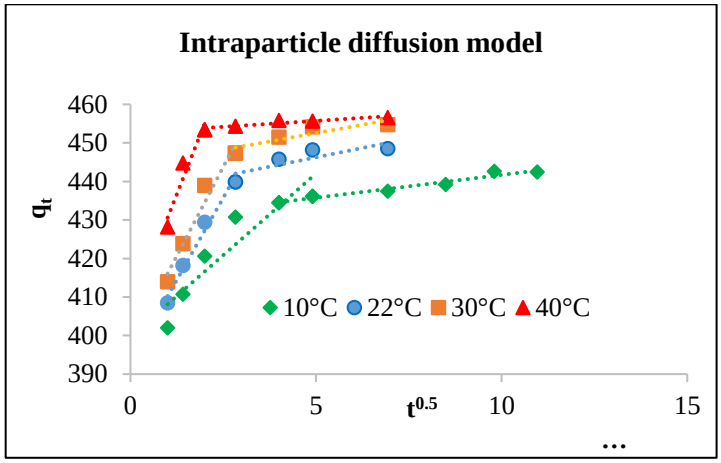

(c)

Figure A.2 Linear plots of Pseudo-first-order, Pseudo-second-order and Intraparticle diffusion models for HS^- sorption on bentonite (experimental set 1 conditions: L:S=100; Initial HS^- concentration = 5 mg L^{-1}, pH=9.5)

Table A.3. Parameter values obtained from linear fitting of kinetic models.

Model	Parameters	Temperature (°C)			
		10	22	30	40
Pseudo-first- order	k_{1a} (h^{-1})	0.051	0.216	0.241	0.684
	k_{1b} (h^{-1})	0.007	0.11	0.088	0.047
	q_{ea} (mg kg^{-1})	39.53	47.681	49.013	53.312
	q_{eb} (mg kg^{-1})	16.99	13.791	12.821	3.623
	R^2_a	0.831	0.996	0.981	0.993
	R^2_b	0.914	0.921	0.935	0.930
Pseudo-second- order	k_2 (kg mg^{-1} h^{-1})	0.008	0.015	0.016	0.042
	q_e (mg kg^{-1})	442.88	450.05	456.162	457.051
	q_e (mg kg^{-1}) (experimental)	442.538	448.512	454.781	455.756
	R^2	0.999	0.999	0.999	0.999
Intraparticle diffusion model	$k_{inp,a}$ (mg kg^{-1} $h^{1/2}$)	8.471	17.023	18.486	24.537
	$k_{inp,b}$ (mg kg^{-1} $h^{1/2}$)	1.168	1.943	1.728	0.621
	$C_{inp,a}$ (mg kg^{-1})	399.69	393.19	397.572	406.034
	$C_{inp,b}$ (mg kg^{-1})	430	436.54	443.913	452.623
	$R^2_{int,a}$	0.8624	0.980	0.955	0.925
	$R^2_{int,b}$	0.954	0.803	0.795	0.869

Notes: Subscripts "a" and "b" are used to denote the parameters obtained from the first and second linear portions of the graphs (Figure A.2(a) and (c)), respectively.

As shown in Figure A.2 (a), when the data was plotted assuming PFO kinetics, two linear sections with different rate constants were seen (see Table A.3), which suggests two-step sorption of HS^- onto bentonite. In all cases, the initial rate constants (k_{1a}) (0.051-0.684 h^{-1}) were found to be higher than the later rate constants (k_{2b}) (0.007-0.11 h^{-1}). That is, sorption initially proceeded faster. Then, as the bentonite sorption sites became increasingly full due to random orientation of sorbed molecules, the process became slower, resulting in a different rate (Li et al., 2007). In addition, k_{1a} values were found to increase with increasing temperature, i.e., increased temperature accelerated the initial sorption process. However, the k_{2b} values did not show such a trend. Furthermore, as reported by others in literature, (e.g., (Crini et al., 2007; López et al., 2019), the equilibrium sorption capacity (q_e) values determined from the model (39.531-53.312 mg kg^{-1}) were much lower than the experimentally obtained values (440.5±1.71 to 455.8±0.85 mg kg^{-1}). Such discrepancy in the parameters thus indicates that the linearized PFO model does not satisfactorily describe the HS^- sorption process on bentonite, regardless of reasonable regression coefficients ($R^2 > 0.8$).

In this study, the linearized PSO model showed better fit (with regression coefficients $R^2 \approx 1$) to the experimental data than PFO model at all temperatures studied (Figure A.2 (b) and Table A.3). This model could describe the whole sorption processes with one rate constant (k_2) and as expected from experimental results (discussed in Section 4.3.1). An increasing trend in rate constants (k_2) values (from 0.008 to 0.042 kg mg^{-1} h^{-1}) was observed with increasing temperature from 10 to 40˚C, respectively. Moreover, the model derived q_e values were found to be close to the experimentally determined q_e values – as the PSO model well-described sorption dynamics over the full ranges of the parameters used in the experiment (see Table A.3). This finding suggests that the sorption of HS^- on bentonite followed pseudo-second-order kinetics and the rate appears to have been controlled by a chemisorption process (Boparai et al., 2011; Crini et al., 2007b; Ho & Mckay, 1999; Senthilkumaar et al., 2006).

Figure A.2 (c) demonstrates that similar to the PFO model, the IPD model exhibited two linear sections with two different intra-particle diffusion rate constants (i.e., $k_{inp,a}$ and $k_{inp,b}$, see Table A.3). As expected, the first stage rate constant ($k_{inp,a}$) was found much higher than second stage

rate constants ($k_{inp,b}$), which indicates faster sorption in the initial stage. However, the large C_{inp} values observed in both stages suggest that intraparticle diffusion was not the only rate limiting step, but some other sorption mechanisms likely occurred simultaneously (Crini et al., 2007; Li et al., 2007; Tsibranska & Hristova, 2011).

Overall, like the non-linear plots, as discussed in Section 4.3.2, linearized model results in Figure A.2 reveal that the PSO model best described HS^- sorption on bentonite, which indicates that chemisorption appears to be the principal rate-limiting process. However, although higher R^2 was observed in the linear fit of the models, the results may encompass method bias due to linearization. Therefore, only the non-linear plots are reported in the main manuscript.

A.5 Goodness of fit

To evaluate the fit of each model used in Chapter 4, the chi-squared (χ^2) values were calculated alongside the coefficients of determination (R^2) as per following equations:

$$X^2 = \sum \frac{\left(q_{e,exp} - q_{e,cal}\right)^2}{q_{e,cal}} \tag{A.1}$$

$$R^2 = 1 - \frac{\sum\left(q_{e,exp} - q_{e,cal}\right)^2}{\sum\left(q_{e,exp} - q_{e,mean}\right)^2} \tag{A.2}$$

Where, $q_{e,exp}$ (mg/g) is the sorption capacity at equilibrium obtained from experiment; $q_{e,cal}$ (mg/g) is the is the sorption capacity at equilibrium achieved from the model using the Solver add-in, and $q_{e,mean}$ (mg/g) is the mean of the $q_{e,exp}$ values.

A.6 Effects of L:S and initial HS- concentration on sorption%

Figure A.3 presents the resulting sensitivities in sorption% of HS^- onto bentonite with L:S and initial HS^- concentration.

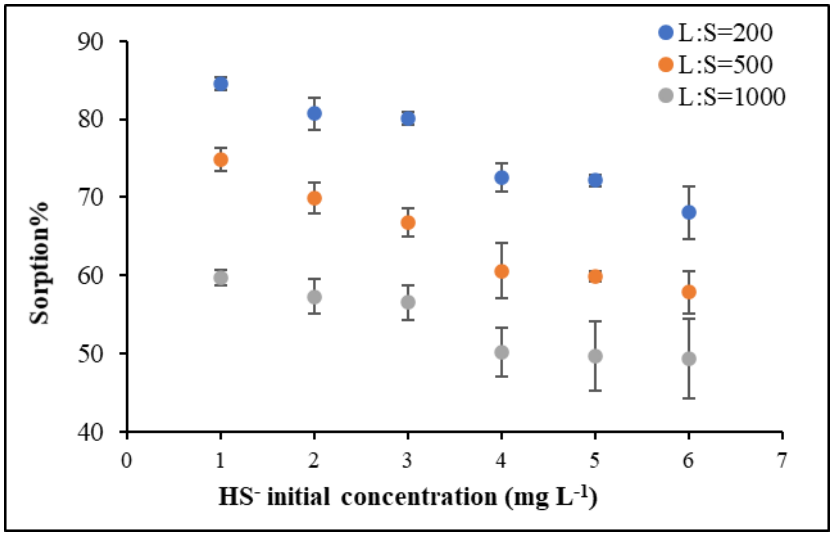

Figure A.3 Effect of L:S and initial HS^- concentration on sorption% of HS^- on bentonite (condition: pH= 9.5; temperature= 22±2°C, contact time: 28-30 hours). All data presented are the average of duplicate or triplicate tests, with error bars showing the standard deviation.

Figure A.3 indicates that sorption% decreased with increasing HS^- concentration for all L:S ratios, which indicates a progressive saturation of the available bentonite sorption sites with higher HS^- concentrations. Moreover, higher sorption% (85-68%) was observed at lower L:S ratio (i.e., 200) than at 500 (75-58%) and at 1000 (60-50%). This is expected because, as the L:S ratio increased, the mass fraction of solid (and associated sorption sites) decreased, thereby reducing the sorption%. Under the combined effect of both L:S and initial HS^- concentration considered in Experiment set 2, the maximum sorption% was observed at around 85% (at L:S of 200 and HS^- initial concentration of 1 mg L^{-1}).

APPENDIX B

B.1 Batch experiments for exploring the effects of temperature, pH and ionic strength

Table B.4 Batch experiments for exploring the effects of temperature, pH and ionic strength.

Experiment no.	**Variable experimental conditions**				**No. of samples and blanks**				**Constant experimental conditions**
	Temperature (°C)	Experiment Blanks	pH		Experiment Blanks	Experiment Blanks		Total sample analyzed	
			Before	after		without bisulfide	without bentonite		
1	40	1 M	9±0.12	8.7±0.12	5*3=15	5	5	25	▪ L:S=1000 ▪ Contact time= 30-100 hrs ▪ HS^- initial conc ==3 mgL^{-1}
			9.5±0.15	9.2±0.15					
			109.5±0.15	9.8±0.15					
			10.5±0.17	10.35±0.17					
			11±0.13	10.8±0.13					
2	40	0.1 M	9±0.14	8.9±0.12	5*3=15	5	5	25	
			9.5±0.16	9.3±0.13					
			10±0.15	9.8±0.15					
			10.5±0.17	10.33±0.17					
			11±0.12	10.9±0.13					
3	40	0.01 M	9±0.14	8.4±0.12	5*3=15	5	5	25	
			9.5±0.16	9.1±0.13					
			10±0.15	9.65±0.15					
			10.5±0.17	10.23±0.17					
			11±0.12	10.7±0.13					
4	25	1 M	9±0.12	8.6±0.42	5*3=15	5	5	25	
			9.5±0.15	9.2±0.15					
			10±0.15	9.8±0.15					
			10.5±0.17	10.35±0.16					
			11±0.15	10.8±0.13					

Experiment no.	Variable experimental conditions				No. of samples and blanks				Constant experimental conditions
	Temperature (°C)	Experiment Blanks	pH		Experiment Blanks	Experiment Blanks		Total sample analyzed	
			Before	after		without bisulfide	without bentonite		
5	25	0.1 M	9±0.17	8.9±0.12	5*3=15	5	5	25	▪ L:S=1000 ▪Contact time= 30-100 hrs ▪HS^- initial conc. = 3 mgL^{-1}
			9.5±0.25	9.2±0.15					
			109.5±0.15	9.8±0.15					
			10.5±0.17	10.35±0.17					
			11±0.13	10.8±0.13					
6	25	0.01 M	9±0.14	8.9±0.12	5*3=15	5	5	25	
			9.5±0.16	9.3±0.13					
			10±0.15	9.8±0.15					
			10.5±0.17	10.33±0.17					
			11±0.12	10.9±0.13					
7	10	1M	9±0.14	8.4±0.12	5*3=15	5	5	25	
			9.5±0.16	9.1±0.13					
			10±0.15	9.65±0.15					
			10.5±0.17	10.23±0.17					
			11±0.12	10.7±0.13					
8	10	0.1 M	9±0.14	8.4±0.12	5*3=15	5	5	25	
			9.5±0.16	9.1±0.13					
			10±0.15	9.8±0.15					
			10.5±0.17	10.33±0.17					
			11±0.12	10.9±0.13					
9	10	0.01 M	9±0.14	8.9±0.12	5*3=15	5	5	25	
			9.5±0.16	9.3±0.13					
			10±0.15	9.8±0.15					
			10.5±0.17	10.33±0.17					
			11±0.12	10.9±0.13					

B.2 SEM-EDS analyses

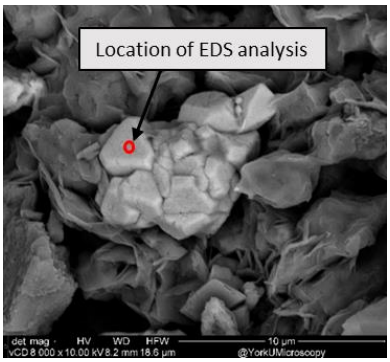

EDS point analysis results

Elements	Weight %	Atomic %
C K	9.02	19.27
O K	21.47	34.43
Al K	2.68	2.55
Si K	3.35	3.06
S K	33.89	27.11
Fe K	29.59	13.59

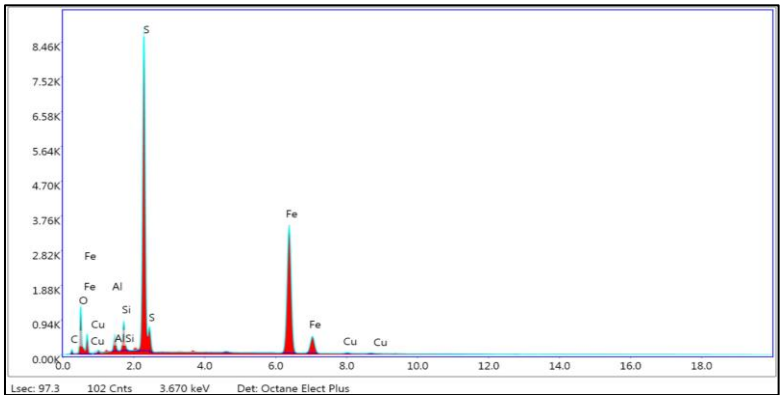

(a)

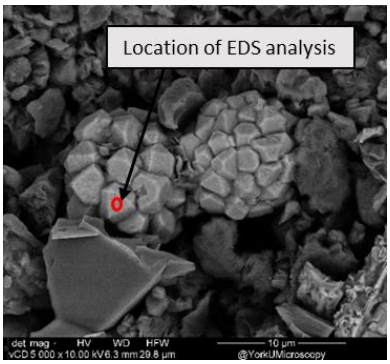

EDS point analysis results

Elements	Weight %	Atomic %
C K	19.96	38.56
O K	15.68	22.73
Al K	2.50	2.15
Si K	1.06	0.88
Zr L	0.96	0.24
S K	34.36	21.86
Mn K	0.31	0.13
Fe K	25.17	10.46

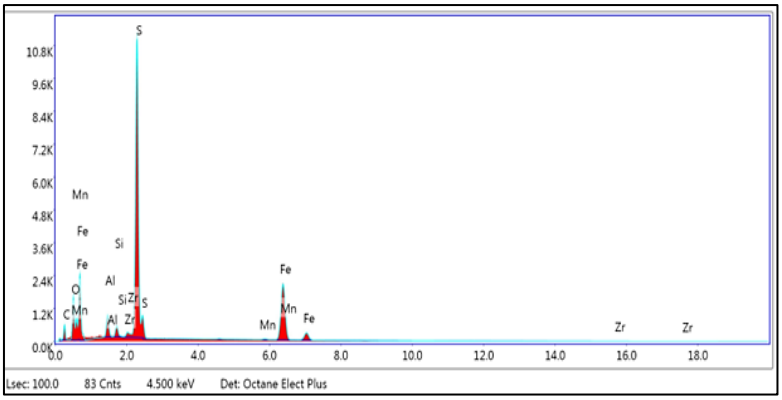

(b)

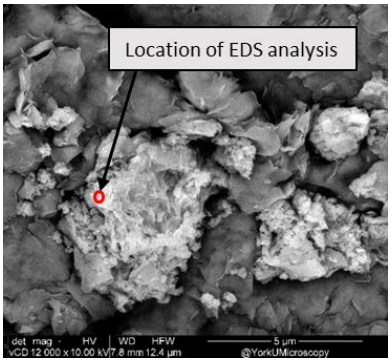

EDS point analysis results

Elements	Weight %	Atomic %
O K	40.84	59.14
Na K	2.08	2.1
Mg K	2.39	2.26
Al K	9.68	8.31
Si K	14.2	11.71
S K	8.83	6.98
Cl K	3.16	2.06
K K	0.39	0.23
Ca K	0.82	0.47
Fe K	17.62	7.31

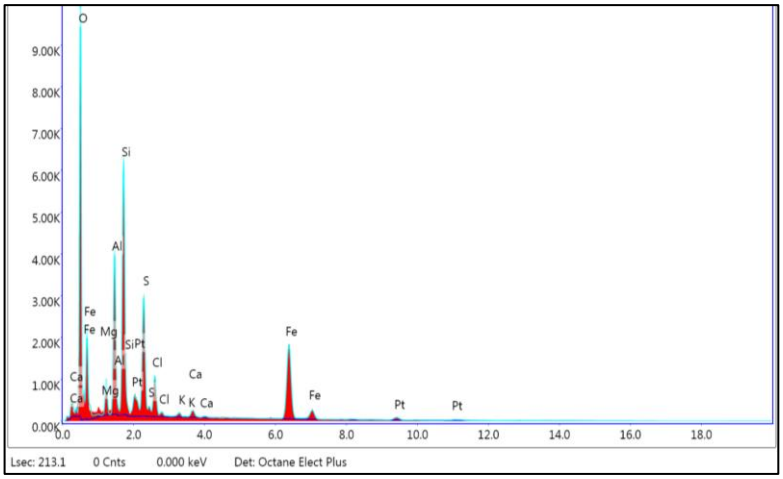

(c)

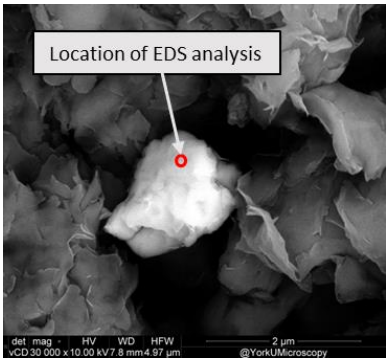

EDS point analysis results		
Element	Weight %	Atomic %
C K	0.01	0.02
O K	49.33	63.14
NaK	0.15	0.14
MgK	1.03	0.87
AlK	16.93	12.85
SiK	28.81	21.01
S K	27.2	17.6
K K	0.34	0.18
CaK	1.23	0.63
FeK	15.6	5.8

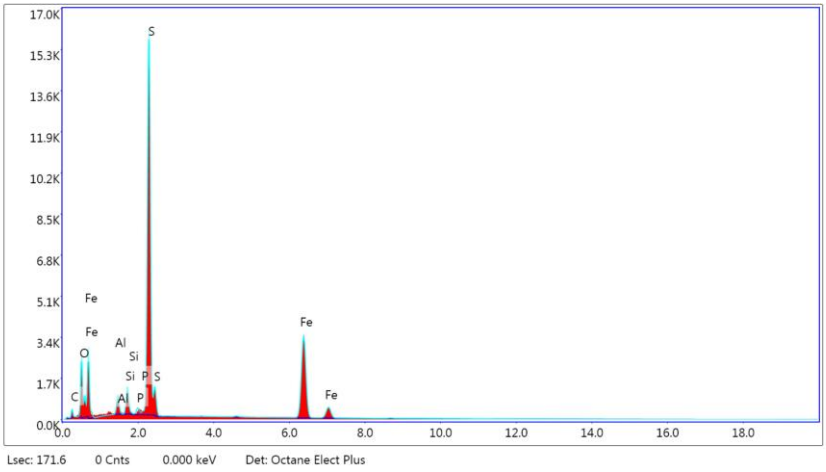

(d)

Figure B.4 SEM (back-scattered) images and EDS point analyses results of (a) blank sample (only bentonite, no HS^-); (b), (c), & (d) test sample (with L:S=1000, initial HS^- concentration 6 mgL^{-1})

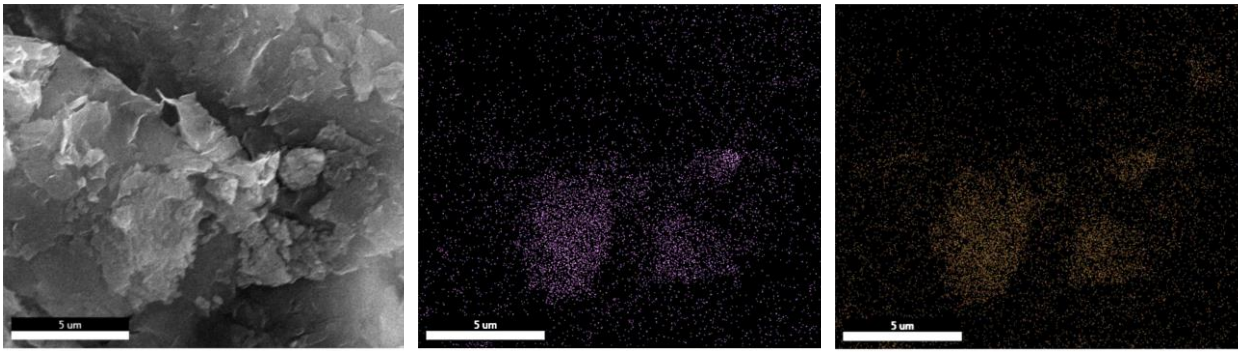

(a) (b) (c)

Figure B.5 EDS mapping of test sample (with L:S=1000, initial HS^- concentration 6 ppm) (a) topographic view from SEM image (b) distribution of S (c) distribution of Fe

APPENDIX C

C.1 Theory of surface complexation model (SCM)

Surface complexation model (SCM) approaches are based on the conception that surface complex formation with surface sites at mineral-water interfaces is similar to aqueous complex formation in the bulk solution. In addition to a permanent negative charge at the layer surfaces, the clay minerals like bentonite are known to carry variable charge at the edge surfaces due to ionisation of surface OH groups as a function of the solution pH (Wieland et al., 1994). This pH-dependent charge of the minerals is described in the SCM by the protonation and deprotonation reactions, or acid base reactions as follows:

$$\equiv SOH^0 + H^+ = \equiv SOH_2^+ \qquad K_+^{int}$$

$$\equiv SOH^0 = \equiv SO^- + H^+ \qquad K_-^{int}$$

In the equations $\equiv SOH^{2+}$, $\equiv SO^-$ and $\equiv SOH^0$, denote positively, negatively and neutrally charged surface sites respectively. The equilibrium constants for these reactions, K_+^{int} and K_-^{int}, known as intrinsic surface acidity constants are inherent to the solids, and are stated as

$$K_+^{int} = \frac{(\equiv SOH_2^+)}{(\equiv SOH^0)\, a_{H_S^+}}$$

$$K_+^{int} = \frac{(\equiv SO_2^-)\, a_{H_S^+}}{(\equiv SOH^0)}$$

where the terms in parentheses indicate surface species concentrations and $a_{H_S^+}$ refers to the activity of H^+ at the surface. Given this variably charged surface sites, the sorption of contaminants (both cations and anions) can take place through the formation of surface complexes. For instance, the surface complex reaction of a cation C^{n+} and an anion A^{z-} can be represented by the reactions as follows (P. Wang et al., 2001a):

Cation:

$$\equiv SOH^0 + C^{n+} \rightarrow \equiv SOC^{(n-1)+} + H^+$$

$$K_C^{int} = \frac{(\equiv SOC^{(n-1)+})\, a_{H_S^+}}{(\equiv SOH^0) a_{C_S^{n+}}}$$

Anion:

$$\equiv SOH + A^{Z-} + H^+ \rightarrow \equiv SOH_2 - A^{(z+1)-}$$

$$K_A^{int} = \frac{(\equiv SOH_2 - A^{(z+1)-})}{(\equiv SOH^0) a_{A_S^{z-}}\, a_{H_S^+}}$$

K_C^{int} and K_A^{int} are the equilibrium constants, known as the binding constants. The terms $a_{C_S^{n+}}$, $a_{A_S^{z-}}$ and $a_{H_S^+}$ indicate the activity of the cation (C^{n+}), anion (A^{Z-}) and H^+ species respectively. In the SCM conception, the activity of an aqueous species at the charged surface is corelated to that in the bulk solution by a Boltzmann relation. For example, for a cation (C^{n+}), the relation of the activity at surface ($a_{C_S^{n+}}$) with that in the bulk solution ($a_{C_b^{n+}}$) can be expressed as follows:

$$a_{C_S^{n+}} = a_{C_b^{n+}} [\exp\left(-\frac{\psi F}{RT}\right)]^n$$

where ψ refers to the electrostatic potential at the surface; T is temperature in Kelvin; and F and R indicate the Faraday constant (96485 C /mol) and ideal gas constant (8.3145 J K^{-1} mol^{-1}), respectively. Thus, a general expression of the mass law equations of the reactions (1), (2), (3), and (4) can be expressed as:

$$K^{int} = K^{app} [\exp\left(-\frac{\psi F}{RT}\right)]^{-\Delta z}$$

where Δz indicates the change in surface charge caused by the formation of a surface complex, and K^{app} denotes the apparent equilibrium constant as it includes the surface charge effects. The equations suggest that the SCM approach should integrate the aqueous activity coefficient model to account for the aqueous speciation of the system and the sorption equilibrium at the mineral-water interface. Thus, the SCM is capable of predicting and interpreting complex sorption behavior via incorporating the changes in system chemistry (such as pH and ionic strength of the solution).

C.2 Model calibration results

Table C.5 Model calibration results

% of total Fe-site	log K (25°C) outer-sphere	Ionic strength of NaCl	R^2	RMSE*	Compliance with expected trend of pH and ionic strength effect
10	16.5±0.5	0.01M	0.93	*1.87E-06*	Yes
		0.1 M	*0.92*	*5.82E-06*	
		1M	*0.92*	*4.87E-06*	
20	16.7±0.3	0.01M	0.96	*1.87E-06*	Yes
		0.1 M	*0.92*	*3.85E-06*	
		1M	*0.92*	*2.87E-06*	
30	17.5±0.5	0.01M	0.93	*9.82E-05*	No
		0.1 M	*0.76*	*9.84E-05*	
		1M	*0.68*	*7.78E-05*	
40	18.5±0.5	0.01M	*0.95*	*1.87E-06*	No
		0.1 M	0.76	*2.87E-05*	
		1M	0.64	*1.87E-05*	
50	18.7±0.3	0.01M	0.94	*1.87E-06*	No
		0.1 M	0.58	*5.87E-05*	
		1M	0.56	*9.87E-05*	
60	18.8±0.4	0.01M	0.97	*1.47E-06*	No
		0.1 M	0.57	*6.87E-05*	
		1M	0.58	*5.97E-05*	
70	18.9±0.2	0.01M	0.94	*1.87E-06*	No
		0.1 M	0.54	*5.87E-05*	
		1M	0.55	*3.87E-05*	
80	18.9±0.2	0.01M	0.97	*1.87E-06*	No
		0.1 M	0.54	*9.77E-05*	
		1M	0.55	*8.85E-05*	
90	18.9±0.1	0.01M	0.96	*1.87E-06*	No
		0.1 M	0.54	*7.81E-05*	
		1M	0.55	*5.67E-05*	
100	18.9±0.1	0.01M	0.96	*4.87E-06*	No
		0.1 M	0.54	*6.87E-05*	
		1M	0.55	*5.97E-05*	

*Root mean square error (RMSE) = $\sqrt{\frac{\sum_i^N x_i - \hat{x_i}}{N}}$

Where, N= total number of data points, x_i = actually observed value; $\hat{x_i}$ = predicted value

C.3 Model simulation results

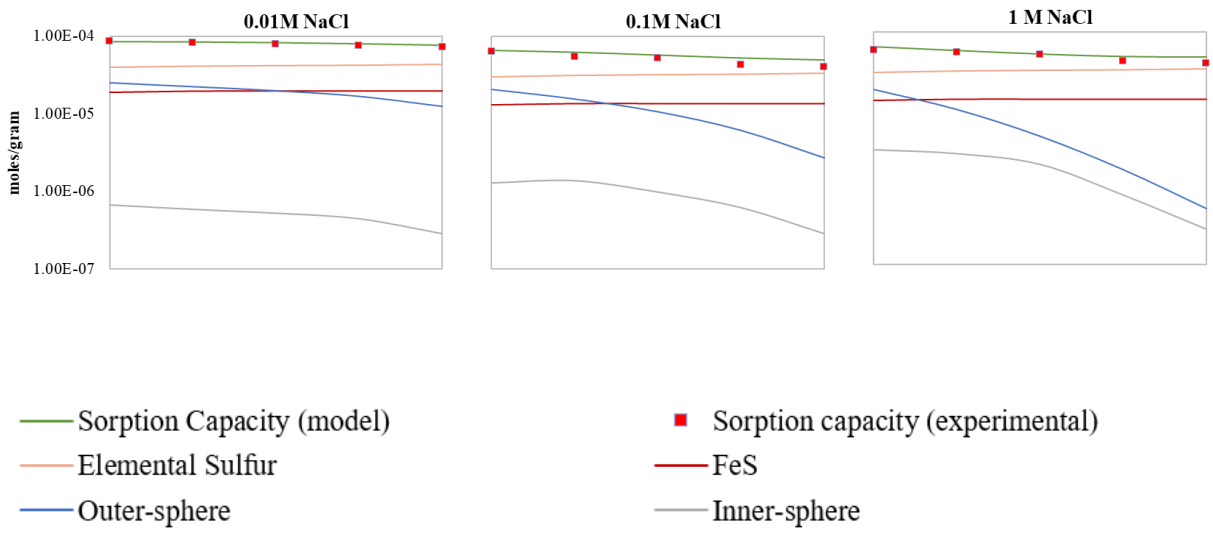

Figure C.6 Model Simulation results at 40°C

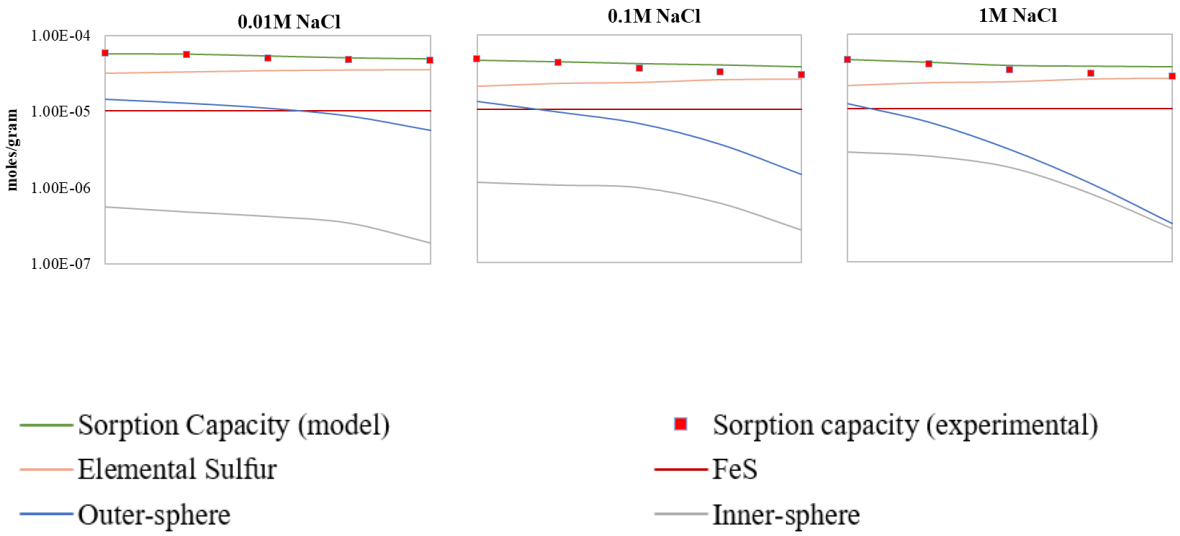

Figure C.7 Model Simulation results at 10°C